Inaugural-Dissertation zur Erlangung der Doktorwürde
der Tierärztlichen Fakultät der Ludwig-Maximilians-Universität
München

Renal alterations in *Pou3f3*^{L423P} mutant mice

von Alexandra Rieger
aus Starnberg

München 2018

Aus dem Zentrum für Klinische Tiermedizin der
Tierärztlichen Fakultät der Ludwig-Maximilians-Universität München
Institut für Tierpathologie

Arbeit angefertigt unter der Leitung von:

Univ.-Prof. Dr. Rüdiger Wanke

Mitbetreuung durch:

Priv.-Doz. Dr. Andreas Parzefall (geb. Blutke)

Gedruckt mit Genehmigung der Tierärztlichen Fakultät
der Ludwig-Maximilians-Universität München

Dekan:	Univ.-Prof. Dr. Reinhard K. Straubinger, Ph.D.
Berichterstatter:	Univ.-Prof. Dr. Rüdiger Wanke
Korreferent/en:	Univ.-Prof. Dr. Markus Meißner

Tag der Promotion: 27. Juli 2018

Meinen Großeltern

TABLE OF CONTENTS

[The page numbers indicated in the table of contents refer to the consecutively numbered pages of the entire document, found at the end of the pages and are not to be confused with the page numbers of the original publication.]

List of Abbreviations

CKD	Chronic progressive kidney diseases
BMP	Bone morphogenetic protein
BrdU	Bromdesoxyuridin
BUN	Blood urea nitrogen
CD	Collecting duct
CRISPR	Clustered regulatory interspaced short palindromic reapeats
DNA	Deoxyribonucleic acid
DN	Diabetic nephropathy
DOHaD	Developmental origins of health and disease
dpc	Days post conception
DT	Distal tubule
E	Embryonic day
ECM	Extracellular matrix
EGF	Epidermal growth factor
ENU	N-ethyl-N-nitrosourea
ESRD	End-stage renal disease
FGF	Fibroblast growth factor
FGFR	Fibroblast growth factor receptors
GBM	Glomerular basement membrane
GDNF	Glial cell line-derived neurotrophic factor
GFR	Glomerular filtration rate
GPI	Glycosylphosphatidylinositol
HNF	Hepatocyte nuclear factor
IM	Intermediate mesoderm
IUGR	Intrauterine growth restriction
KCC4	K^+/Cl^- cotransporter
kDa	Kilodalton
LIF	Leukemia inhibitory factor
MD	Macula densa
MET	Mesenchymal-to-epithelial transition
MM	Metanephric mesenchyme
ND	Nephric duct
NKCC2	Na^+-K^+-$2Cl^-$ -cotransporter
pn	Post natum
POU3F3	POU domain class 3 transcription factor 3
qRT-PCR	Quantitative reverse transcriptase polymerase chain reaction
RAAS	Renin-angiotensin-aldosterone-system
RAR	Retinoic acid receptors
RNA	Ribonucleic acid
ROMK	Renal outer medullary potassium channel
TAL	Thick ascending limb of loop of Henle
TALEN	Transcription activator-like effector nucleases

TDL	Thin descending limb of loop of Henle
TGFβ	Transforming growth factor beta
TUNEL	Terminal deoxynucleotidyl transferase dUTP nick end labeling
UB	Ureteric bud
UMOD	Uromodulin, Tamm-Horsfall glycoprotein
VEGF	Vascular endothelial growth factor
WT1	Wilms tumor protein
ZFN	Zinc-finger endonucleases

1. Introduction

With the completion of the “Human Genome Project” in 2004, the post-sequencing era began, and scientists now were presented with the challenge to unravel every gene’s function (Wiemann et al., 2004). Since experimental approaches in humans are limited due to technical and ethical reasons, animal models became important elements of biomedical research (Bockamp et al., 2002, Macchiarini et al., 2005). By using forward and reverse genetic approaches, various diverse murine models for experimental research purposes were already generated. Nevertheless, there is still a huge ‘phenotype gap’, that is the void between the available mouse mutant resource and the entire range of possible phenotypes. Closing this gap is necessary to fully elucidate genotype-phenotype correlations that hopefully lead to the discovery of novel strategies in prevention, diagnosis and therapy of human disease (Brown and Peters, 1996). Especially in the field of kidney diseases experimental animal models are urgently required. The incidences and prevalences of chronic progressive kidney diseases (CKD), especially occurring in the course of metabolic disorders, e.g., diabetic nephropathy (DN), are steadily rising and already represent a major health problem worldwide (Ritz, 2006, Jha et al., 2013). To this day, the complex pathogenetic processes of CKDs are not entirely understood. In particular, the relevant risk factors and conditions, that promote their development, have only in part been identified yet. In the past years, however, several different studies provided evidence for an existing causative link between a low nephron endowment, that is the number of nephrons per kidney after the completion of nephrogenesis, and the occurrence of hypertension and chronic kidney diseases later in life (Bertram et al., 2011).

Pou3f3^{L423P} mutant mice, recently derived from the phenotype-driven Munich ethylnitrosourea (ENU) Mouse Mutagenesis Project harbor a recessive mutation in the transcription factor Pou3f3-gene. Initial phenotypic analysis revealed that adult homozygous *Pou3f3*^{L423P} mutants of both sexes display increased plasma urea levels and smaller kidney weights as compared to heterozygous *Pou3f3*^{L423P} mutants and non-mutant controls, possibly indicating renal dysfunction (Kumar et al., 2016).

The present study used functional, as well as qualitative and quantitative morphological analyses to characterize the renal phenotype of *Pou3f3*^{L423P} mutant mice in order to gain further insight into the role of the transcription factor Pou3f3 in kidney development and function, and to examine the suitability of *Pou3f3*^{L423P} mutant mice as model organisms for nephrological research.

2. Scientific Background

2.1. Genetic modification in the mouse

The main challenge of the post sequencing era still remains in unraveling every gene's function and the complex interactions of different genes in different tissues within the living organism (Wiemann et al., 2004). Among the many different animal models used for that purpose nowadays, the laboratory mouse regularly continues to be the model of choice (Rosenthal and Brown, 2007). Mice are easy to handle, maintain and transport, they reproduce quickly and their short lifespan makes it possible to study all stages of life within an adequate time frame. Furthermore, the availability of inbred strains facilitates the accuracy and reproducibility of experiments by reducing phenotypical variability owed to genetic differences (2001, Silver, 1995). This fact, in combination with the ability to modify the murine genome in a plethora of ways, makes mice the ideal candidates to mimic human disease states and study gene actions (Kile and Hilton, 2005, Acevedo-Arozena et al., 2008, Ericsson et al., 2013). Over the past years, many different methods of genetic modification have been established. Basically, these methods can be classified in two categories. For one, there is a "gene driven" approach, where a selected candidate (endogenous or heterogenous) gene is overexpressed or otherwise modified, e.g., by use of homologous recombination in embryo-derived stem cells or gene-trap strategies, resulting in the production of a knock-out or knock-in organism ("reverse genetics") (Thomas and Capecchi, 1987, Evans et al., 1997). Well established methods of genetic modification in mice comprise pronuclear DNA microinjection, sperm-mediated as well as lentiviral gene transfer techniques, and somatic cell nuclear transfer ("cloning") (Auerbach, 2004, Lavitrano et al., 2006, Pfeifer and Hofmann, 2009, Wilmut et al., 2015). Furthermore, several novel genome engineering techniques emerged, that allow a broad range of alterations at specific DNA locations. Among these are chimeric nucleases, such as zinc-finger endonucleases (ZFN) and transcription activator-like effector nucleases (TALEN), consisting of a DNA-binding molecule, that is programmable and sequence-specific and linked to an unspecific DNA cleavage domain, as well as CRISPR (clustered regulatory interspaced short palindromic repeats)/CRISPR-associated (Cas) systems, which facilitate RNA-guided DNA modification. In particular, the CRISPR-Cas technology presents an efficient and easily available tool for customized DNA alterations (Gaj et al., 2013). Altogether, the established genetic engineering methods allow the in-detail assessment of hypotheses

regarding the function of specific genes, as well as the meticulous dissection of designated molecular pathways. However, presumptions about these gene functions and pathways need to be made in advance and the resulting phenotype is rarely predictable and therefore, does not always mirror the respective human disorder or condition (Russ et al., 2002).

This issue is addressed by a completely different, complementary strategy, known as the “phenotype driven” approach. By using physical (ionizing radiation like gamma rays or X-rays) or chemical methods (e. g., procarbazine, N-ethyl-N-nitrosourea (ENU), chlorambucil), random mutations are generated. In the first instance the resulting mutant offspring (i.e.,“founders”) are screened for interesting phenotypes (“forward genetics”). In subsequent analyses, the mutation causative for the observed phenotype is identified. That way yet unknown gene functions and pathways can be unraveled without previously needed knowledge about the genetic basis of distinct disease processes (Russell et al., 1979, Rathkolb et al., 2000, Nguyen et al., 2011).

Ionizing radiation and chlorambucil tend to cause large DNA deletions involving several genes, making it difficult to identify the affected locus. Therefore, ENU with its preference to induce point mutations became the most favoured mutagen (Balling, 2001).

2.1.1. N-ethyl-N-nitrosourea (ENU) mutagenesis

N-ethyl-N-nitrosourea (ENU) has long been known as the most potent germline mutagen in mice (Russell et al., 1979, Weber et al., 2000). As a monofunctional alkylating agent, ENU has the property of transferring an ethyl group to reactive oxygen or nitrogen sites of the DNA. This leads to a DNA mismatch during replication (Noveroske et al., 2000), mainly inducing point mutations by single base-pair substitutions (A-T to T-A transversions and A-T to G-C transitions). The predominant results are missense mutations (64%), however, nonsense mutations (10%) and splicing errors (26%) can be found as well (Shibuya and Morimoto, 1993, Justice et al., 1999).

ENU is usually administered to adult male mice by a sequence of intraperitoneal injections and mostly affects premeiotic spermatogonial stem cells. Hereby, the optimal dose and administration regime vary according to the strain of mouse being used (Weber et al., 2000). Since the actions of ENU are dose-dependent, increased dos-

es might cause higher mutation rates. However, the toxic and carcinogenic effects of ENU increase concomitantly, eventually leading to decreased viability and fertility.
Treatment regimens with fractionated administration of a total ENU dosage of 250 – 300 mg/kg were shown to yield better results regarding survival and fertility recovery rates than those with one single dose of 150 – 200 mg/kg (Cordes, 2005). These optimized treatment regimens can reach mutation rates of up to 1,5-6 x 10^{-3} per locus, that is one mutation every 1 to 2,5 Mb (Hitotsumachi et al., 1985, Aigner et al., 2008). Every gamete of an ENU-treated male harbours up to 1000 mutations, eventually giving rise to about 20 functional mutations (Hitotsumachi et al., 1985, Augustin et al., 2005). Most of the time, these mutations lead to hypomorphic alleles (partial loss of function), they can, however, also result in nullimorphic alleles (complete loss of function), or even alleles with a gain of function (hyper-, neo-, antimorphic) (Noveroske et al., 2000). This is an additional advantage of ENU mutagenesis, as it bears the potential of creating an allelic series that allows for investigation of a genes different activity levels and therefore mapping of functional domains (Barbaric and Dear, 2007). Allelic series are usually established in region-specific screens, that focus on mutations in a particular chromosomal segment (Kile and Hilton, 2005). Genome-wide screening strategies on the contrary aim for identifying candidate genes all over the genome, thus being very suitable for studying genetic diseases that involve different genetic and biochemical pathways (Kile and Hilton, 2005, Fox, 2007). In the last two decades, several large-scale ENU mouse mutagenesis projects have been established world-wide, allowing the systematic and efficient generation and establishment of numerous mutant mouse lines (Aigner et al., 2008, Nguyen et al., 2011).

2.1.2. The Munich ENU mouse mutagenesis project

As a part of the “German Human Genome Project”, the Munich ENU mouse mutagenesis project is a large-scale, genome-wide, phenotype-driven approach to generate, detect and define new mutant mouse lines by ENU mutagenesis, which are relevant for human inherited diseases (Hrabé de Angelis and Balling, 1998).
Ten week old male mice on a C3HeB/FeJ (C3H) inbred genetic background are injected intraperitoneally with ENU at a dose of 90 mg/kg three times in weekly intervals (Hrabé de Angelis et al., 2000). After the treatment mice undergo an approximately 10 week long period of sterility, which is seen as indicator for a successful treatment (Russell et al., 1979). Subsequently the ENU-treated male mice are mated

to C3H wild-type females. The resulting first generation (G1) is screened for dominant mutations, indicated by obviously aberrant phenotypes. Subsequently, miscellaneous back- and side-crosses are carried out to define the mutations inheritance and to reveal recessive mutations in G3 animals (Hrabé de Angelis et al., 2000, Aigner et al., 2008). Moreover, non-causative mutations will be eliminated by approximately 50% per generation, i.e., after 5 backcrosses, mouse mutants only possess one mutation on the average (Aigner et al., 2008). Depending upon the presence of dominant and recessive mutations, G1 and G3 animals undergo phenotyping, which includes, but is not limited to, clinical chemistry, behavior, dysmorphology, neurology, immunology, pathology and molecular expression profiling analyses (Hrabé de Angelis et al., 2000, Balling, 2001). Since ENU mutagenesis does not allow the use of molecular markers, identification of the mutated gene is done by linkage analysis using an outcross-backcross panel. Heterozygous mutants (C3H background) are mated to wild-type mice of another inbred strain such as BALB/c or C57Bl/6. From the resulting G1 offspring, male hybrids displaying the phenotype are then again mated to wild-type females of the second inbred strain. DNA analysis using a panel of genome-wide single-nucleotide polymorphisms (SNPs) or microsatellites, which are polymorphic for the two utilized inbred strains, is then carried out on samples from phenotypically mutant and phenotypically non-mutant G2 offspring (Lindblad-Toh et al., 2000).

Genotypic distinction yields determination of the chromosomal region in question, which is heterozygous in phenotypic G2 mutant mice and homozygous for the C57BL/6J genotype of the second inbred strain in phenotypic G2 non-mutant mice. For mapping of the causative mutation to a specific chromosomal region only 50 phenotypic mutant G2 animals are needed. With the determination of the number of scored meioses and number of loci that exhibit combination of recombinant alleles, validation of the hypothesis regarding the linkage of two loci is realizable by chi-squared (χ^2) testing. Candidate gene selection and sequencing is therefore, based on linkage analysis in combination with the availability of the mouse genome sequence (Silver, 1995, Green, 1997, Balling, 2001).

2.1.3. Establishment of the mutant mouse line Pou3f3^{L423P}

The mouse line Pou3f3^{L423P} was recently derived from the Munich ENU mutagenesis project within a special screen conducted to reveal kidney disease models. Hereby, elevated plasma urea levels (cut-off values: >70 mg/dl for males and >65 mg/dl for females) were used as a marker for impaired kidney function (Aigner et al., 2007). Initially, the line was referred to as HST011 (UREHR2), after identification of the causative mutation, the name was specified as Pou3f3^{L423P}.

Pou3f3^{L423P} mutant mice harbor a recessive mutation in the transcription factor *Pou3f3* gene, affecting the highly conserved homeodomain of the protein. Sequence analysis revealed a T→ C transition at nt 1268 (ENSMUST00000054883), leading to a missense mutation, namely an amino acid exchange from leucine to prolin at codon 423. Homozygous mutant mice of both sexes are viable and fertile. In comparison to non-mutant littermates, they display a reduced body size and body weight, whereas other grossly evident phenotype alterations were not detectable (Kumar et al., 2016). Systemic phenotyping, following a standard protocol, which involves a wide array of parameters was performed in the German Mouse Clinic using homozygous *Pou3f3*^{L423P} mutants and non-mutant controls of both sexes. Apart from increased plasma urea levels and reduced body and kidney weights, *Pou3f3*^{L423P} mutants of both sexes display certain metabolic changes associated with renal dysfunction such as increased serum levels of creatinine, chloride and potassium, a slightly microcytic, erythropenic anemia, as well as decreased bone mineral density and content. Besides, mutant mice display increased locomotor activity, but a decreased rearing activity. This, however, is most likely due to deficits in balance, since the vestibular organ of *Pou3f3*^{L423P} mutants shows an abnormal diameter and curvature of the superior semi-circular canal. Regarding the inner ear, the hearing sensitivity of mutant animals also seems impaired (Kumar et al., 2016). For a detailed analysis of the phenotype of *Pou3f3*^{L423P} mutant mice, the interested reader is referred to the publication of Kumar et al. (2016).

2.2. Kidney structure and embryonic development

2.2.1. Morphological and functional segmentation of the nephron

The functional unit of the kidney is the nephron, which shows a characteristically segmented pattern. It consists of the renal corpuscle with the glomerular tuft and the Bowman's capsule, where the blood is filtered into a tubular system, consisting of a proximal and distal part, linked by the loop of Henle with its thin descending (TDL) and thick ascending limb (TAL). In the tubular system, the filtrate is modified by reabsorption, secretion and concentration processes until it is finally delivered to the collecting ducts for elimination (Kriz and Koepsell, 1974). The glomerular filtration barrier is composed of three layers, the fenestrated glomerular capillary endothelium, the glomerular basement membrane (GBM), and the podocyte slit diaphragm and provides substantial resistance to the hydrodynamic flow. When intact, the glomerular filter and its charge and size selectivity only allows particles smaller than approximately 69 kDa and preferably non- or positively charged molecules to pass. Therefore, it prevents the loss of albumin with a molecular weight of around 63- 69 kDA. After filtration, the primary urine is isosmotic with the blood plasma. It continues to the proximal tubule, which is composed of a convoluted and straight part. The main function of this nephron segment consists of the reabsorption of filtered solutes. To enlarge the resorptive capacity, its lining cuboidal epithelial cells carry a luminal microvilli brush border and possess numerous mitochondria that provide energy for active transport systems (Taal et al., 2012). Of significance is the basolateral Na^+/K^+-ATPase that facilitates the reabsorption of sodium. Water follows passively along the concentration gradient. Furthermore, the generated sodium gradient drives several co-transport channels for the reabsorption of glucose, amino acids and inorganic phosphate. Potassium and urea leave the lumen via simple diffusion and paracellular solvent drag. In addition, the proximal tubule is also important for the secretion of organic ions including ammonium and creatinine (Cunningham and Klein, 2013). The following intermediate tubule i.e. the thin descending limb of Henle's loop (TDL) is defined by its passive permeability and spatial configuration in the renal medulla, which are both essential for water reabsorption. In mammals, there are short and long looped nephrons. The ones situated in the superficial or midcortical zones of the kidney generally possess short loops of Henle, whereas juxtamedullary nephrons hold long loops of Henle, which descend down into the inner medullary zone and play a major role for the urine concentration ability (Kriz and Koepsell, 1974). The de-

scending thin limb has a low permeability for ions and urea, but is highly permeable for water. By presence of a high solute concentration in the surrounding renal medulla, this allows for osmosis and thus a substantial increase in urine concentration. The thin ascending limb, in contrast, is not permeable for water anymore but for ions, which as a consequence of the highly osmotic urine then follow along the concentration gradient from the tubular lumen into the medullary interstitium. This renders the interstitium near the papilla hyperosmotic and the passing urine hypoosmotic. The function of the ensuing straight part of the distal tubule, also known as thick ascending limb (TAL) of the loop of Henle is vital for creating and maintaining a hypertonic medullary interstitium, which provides the basis for the renal urine concentration mechanism via the countercurrent multiplier system. In the TAL, sodium, potassium and chloride ions are actively reabsorbed by the Na^+-K^+-$2Cl^-$ -cotransporter (NKCC2), which is exclusively expressed in this segment. At the same time the TAL is impermeable to water. Via K^+-channels such as ROMK, potassium ions passively travel back into the tubular lumen, creating a positive electron potential. As a consequence, divalent cations such as Mg^{2+} and Ca^{2+} are absorbed via paracellular transport (Mount, 2014). Salt reabsorption is actively driven by the basolateral Na^+/K^+-ATPase, which transports Na^+ into the interstitial fluid. Cl^- ions follow along their chemical gradient through CLC chloride channels. In the TAL at least two types of CL-transporters, CLC-K1 and CLC-K2 are coexpressed. Moreover, the K^+/Cl^- cotransporter (KCC4) allows for electroneutral K^+- dependent passing of Cl^- ions into the interstitium (Mount, 2014). The TAL also plays an important role for acid-base balance by excreting ammonium and reabsorbing up to 15% of filtered bicarbonate. This is mainly facilitated by the Na^+/H^+-exchanger (NH3) (Mount, 2014). Furthermore the TAL together with the early convoluted part of the distal tubule are the origin of the abundant urinary glycoprotein (Uromodulin), also called Tamm-Horsfall protein (Pollak and Arbel, 1969, Pennica et al., 1987). The macula densa (MD), a cluster of specialized cells constituting the juxtaglomerular wall of the TAL at the point, where it meets the vascular pole of its parent glomerulus is critically involved in the regulation of the glomerular blood flow and thereby glomerular filtration rate (GFR). Depending on the intratubular sodium chloride concentration, the macula densa cells control the release of renin from juxtaglomerular cells and hereby regulate the tubular reabsorption of water and sodium via the renin-angiotensin-aldosterone-system (RAAS) (Burg, 1982, Mount, 2014).

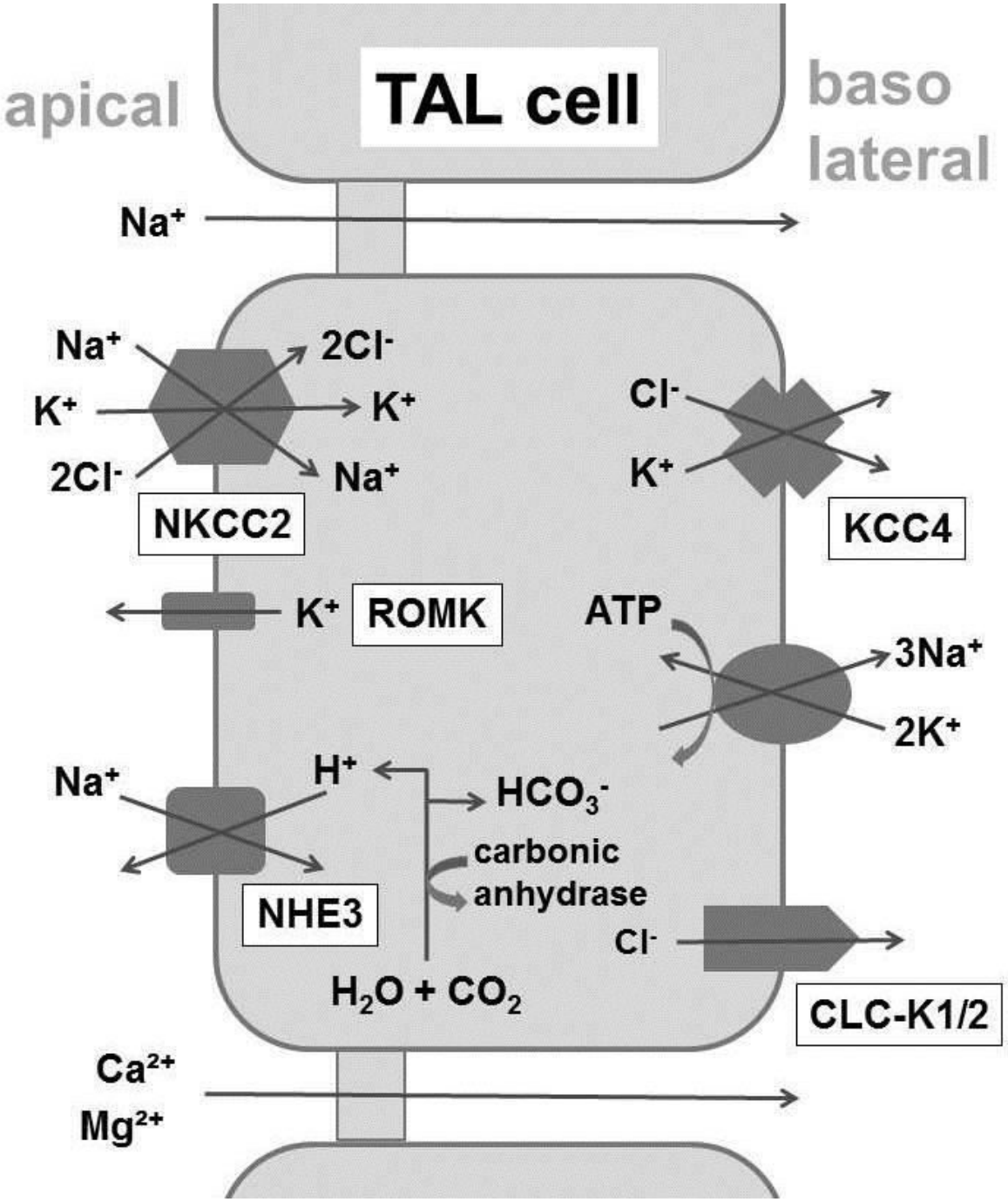

Figure 1) Selected transport pathways within the TAL

Involved in transepithelial Na^+Cl^- transport are e.g. NKCC2 (Na^+-K^+-$2Cl^-$ cotransporter), K^+-channels such as ROMK (renal outer medullary potassium channel), KCC4 (K^+/Cl^- cotransporter) and CLC-K1/2 (Cl^- channels). The NHE3 (Na^+/H^+-exchanger) is a key component of bicarbonate reabsorption (based on Mount, 2014).

Following the loop of Henle, the distal convoluted tubule is the last segment of the tubular system before the filtrate reaches the collecting duct system and is excreted as urine. Just as its proximal counterpart, the distal convoluted tubule modifies uri-

nary pH through the exchange of bicarbonate and protons. Upon that, it creates a Na^+ concentration gradient via the basolaterally situated Na^+-K^+-ATPase. This causes sodium to leave the lumen via simple diffusion or via a $Na^{+/}Cl^-$ co transporter or a Na^+/H^+ antiporter, creating a negative electric potential all along the distal convoluted tubule. Consequently passive Na^+ reabsorption is inhibited. Therefore the Na^+-H^+-antiporter increases the secretion of H^+ ions, creating an intracellular alkalosis and an accumulation of K^+ ions in the tubular lumen. Contrary to the permanent electrolyte resorption in the proximal tubule, the distal tubule and the collecting duct respond to systemic signals, mainly hormones, such as aldosterone, angiotensin II, and antidiuretic hormone. This is urgently required to maintain homeostasis despite altered dietary intake or extra renal loss of salts and water (Reilly and Ellison, 2000, Cunningham and Klein, 2013).

2.2.2. Embryonic and postnatal development of the murine kidney

Mammalian nephrogenesis comprises the sequential formation of three pairs of kidneys, which arise from the intermediate mesoderm in cranio-caudal direction along the embryonic axis, recapitulating the phylogeny of the excretory system in the process (Horster et al., 1999). In spatial and temporal sequence, the rudimental pronephros evolves, followed by the temporarily functioning mesonephros and finally the permanent metanephros. Although there are significant differences in their complexity, they share the nephron as a basic structural unit (Desgrange and Cereghini, 2015). In mice, pronephric development begins at embryonic day (E) 8 (McCrory, 1972). Starting from the cranial part of the intermediate mesoderm, a subset of cells begins to aggregate and after undergoing mesenchymal-to-epithelial transition, an epithelial tube, the (pro)nephric duct begins to form. It keeps growing in caudal direction along the embryonic trunk until at E11 it reaches and fuses with the ventral portion of the cloaca (Hoar, 1976). At its origin, a species-specific number of paired tubules arise from the nephrogenic cord, one end opening into the coelom, the other into the nephric duct. As no further differentiation takes place, the development of the pronephros is aborted and also the cranial parts of the nephric duct undergo apoptosis (Davidson, 2008). The pronephros is mostly an atavistic structure, however, its evolutionary preservation is explained by the emergence of the (pro)nephric duct, whose caudal parts remain as the nephric (Wolffian) duct and eventually give rise to the permanent kidney (Moody, 2007). With the regression of the pronephric struc-

tures at E9, the formation of up to 18 paired mesonephric tubules starts. A clear distinction can be made between the cranial and the caudal sets, as only the first 4-6 are connected to the nephric duct and fully developed. In spite of their simple design (no loop of Henle or juxtaglomerular apparatus are formed) these nephrons are able to produce scant amounts of urine. After all, the mesonephroi atrophy and degenerate from cranial to caudal at E14 (Vetter and Gibley, 1966, Sainio et al., 1997a). In males, some mesonephric tubules remain and form the vas deferens, epididymis and seminal vesicles. In females, they completely regress. Nevertheless the presence of the cranial parts of the nephric duct are required for the correct development of the Müllerian duct, which gives rise to the oviducts, uterine horns and parts of the vagina (Orvis and Behringer, 2007). The development of the enduring mammalian kidney begins with the formation of the metanephric mesenchyme from the posterior end of the intermediate mesoderm at around E10.5 (Dressler, 2006). For a short period of time, meso- and metanephros exist in parallel.

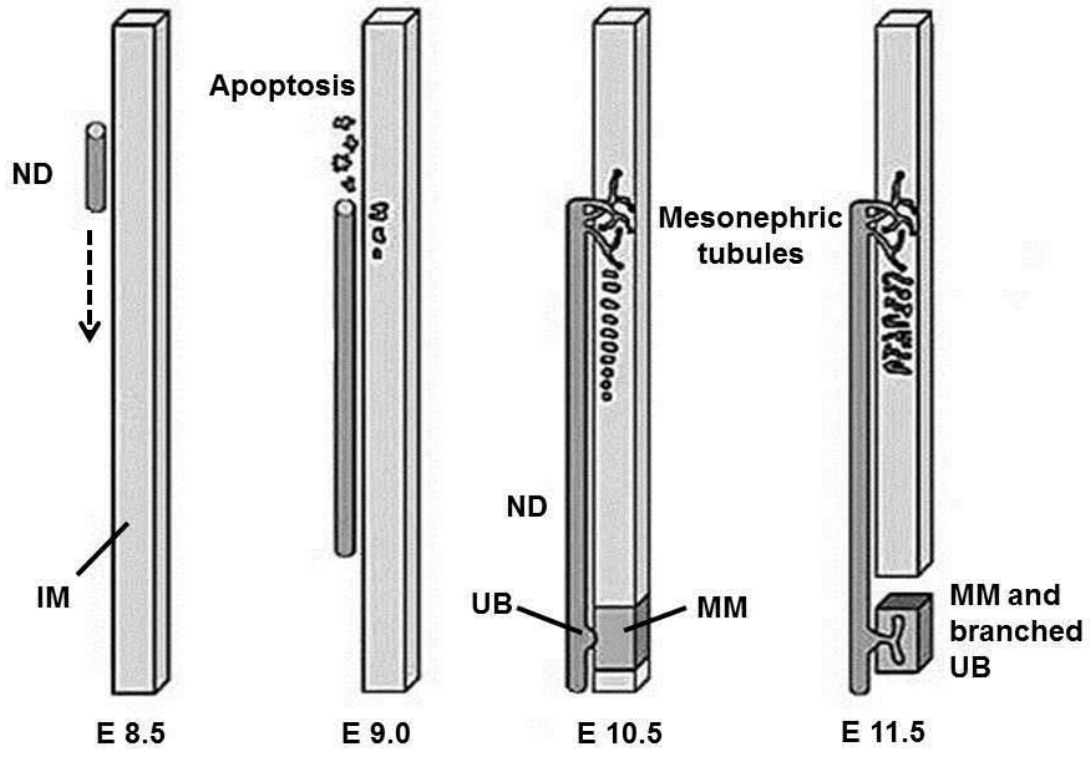

Figure 2) Schematic overview of embryonal kidney development

Mouse kidney development begins at about embryonic day (E) 8.5 with the formation of the (pro)nephric duct (ND) from the intermediate mesoderm (IM). Rostral parts undergo apoptosis while it elongates caudally to reach the cloaca. In extending along the trunk the ND induces mesonephric tubule formation the adjacent IM. Around E10.5 the ureteric bud (UB) grows out of the ND into the metanephric mesenchyme (MM), a specialized population of IM cells. Reciprocal inductive interactions between the UB and the MM induce branching of the UB (adapted from Davidson et al., 2008, with permission).

The metanephric mesenchyme induces the outgrowth of the ureteric bud from the caudal end of the nephric duct. Subsequently the ureteric bud invades the metanephric mesenchyme at E11 and a series of reciprocal inductive interactions between these two primordial tissues triggers various morphogenetic differentiation events. Once the ureteric bud has entered the metanephric mesenchyme, it starts to grow and branch repeatedly in a dichotomous way, leading to the formation of the ureteric tree, which eventually becomes the urinary collecting duct system and the renal pelvis. The metanephric mesenchyme on the other hand develops into the nephrons, stroma, and most likely endothelia (Saxen and Sariola, 1987). Nephron formation begins with the epithelial cells at the ends of the ureteric bud prompting the surrounding mesenchyme cells to condensate, forming the induced mesenchyme or cap mesenchyme. The cap mesenchyme consists of several cell layers that are morphologically distinguishable from the more peripherally situated uninduced mesenchyme. Successively, a subset of cap mesenchyme
cells that is located right underneath the terminal ureteric tree branches further cumulates. The resulting pretubular aggregates rapidly proliferate to form a tightly adhering cluster of approximately 30 cells, which sequentially undergoes mesenchymal-to-epithelial transition and forms a cyst-like structure, the renal vesicle at E 12.5 (Bard et al., 2001). Through a series of differentiating events, involving symmetry interruption and invagination, the renal vesicle firstly transforms into a comma-shaped body, followed by an S-shaped body. The lower limb of the S-shaped body ultimately develops into the renal corpuscle, whereby the inner cell lining differentiates into the visceral epithelial cells (podocytes) and the outer cell lining into the parietal epithelial cells of the Bowman's capsule. Angioblasts finally invade the lower cleft and contribute to the formation of the glomerular tuft (Eremina et al., 2003). As the central part of the S-shaped body proliferates, the emerging proximal and distal tubule differentiate and the middle part between them starts growing down into the medullary zone to shape/constitute the loop of Henle (Neiss, 1982). Finally the upper limb of the S-shaped body turns into the distal convoluted tubule and fuses with the collecting duct (Saxén, 1987).

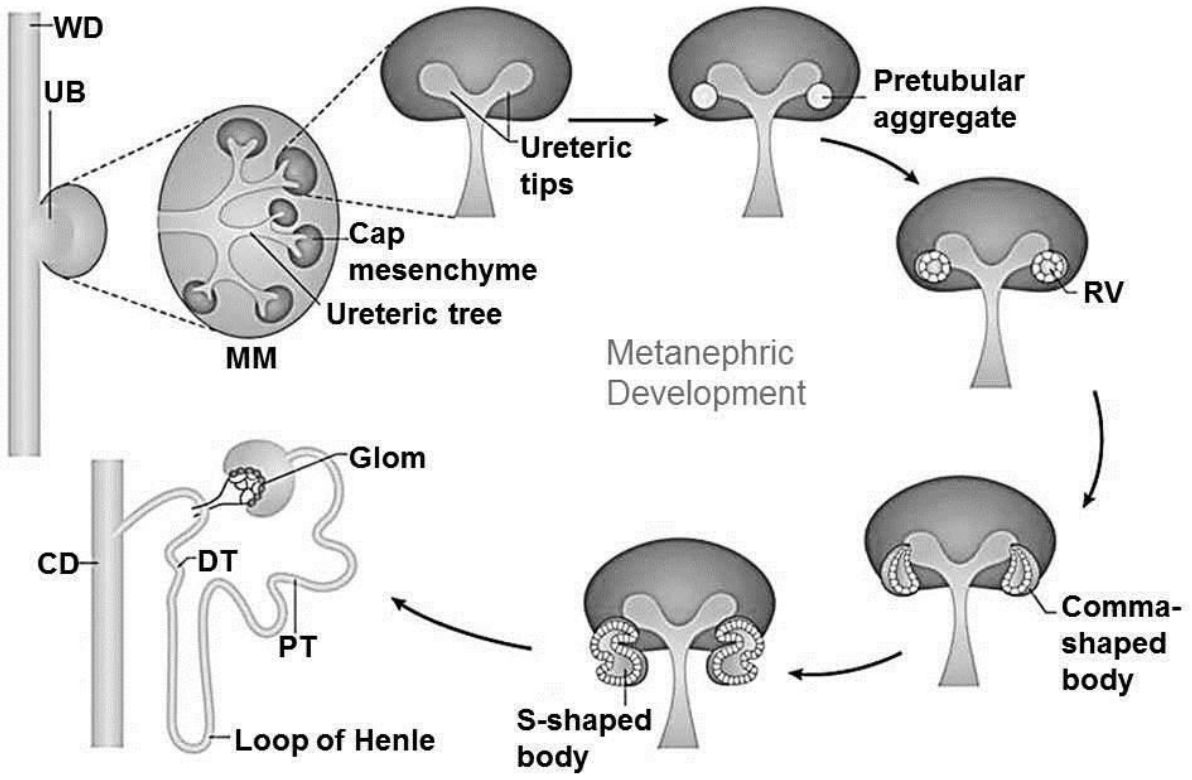

Figure 3) Schematic illustration of the morphological stages of metanephric development

Signals from the ureteric bud (UB) induce the formation of the cap mesenchyme within the metanephric mesenchyme (MM). The subsequently developing pretubular aggregate undergoes mesenchymal-to-epithelial transition and forms the renal vesicle, which then differentiates into the comma- and the s-shaped body. The cleft of the S-shaped body is colonized by endothelial cell precursors that eventually help to form the renal corpuscle together with the distal limb of the of the s-shaped body. The proximal limb fuses with the ureteric duct that eventually will form into the collecting ducts, and after a series of transformative events it differentiates into the nephrons tubule system. CD, collecting duct; DT, distal tubule; MM, metanephric mesenchyme; RV, renal vesicle; UB, ureteric bud; WD, Wolffian (nephric) duct (adapted from Bertram et al., 2016, with permission).

2.2.3. Molecular regulation of embryonic kidney development

Embryonic kidney development is a very complex process that requires the expression of innumerable regulatory genes, which govern the precise temporarily and spatially coordinated interaction of several networks of transcription and growth factors, their receptors and many other signaling molecules to warrant the physiological course of events in the developing kidney.

2.2.3.1. Specification of the metanephric mesenchyme and formation of the nephric duct

The first essential step in the course of kidney development consists of specification of the nephrogenic cord, i.e., the regions of intermediate mesoderm, the transient and permanent kidney structures originate from. Several genes that are involved in initial patterning processes in the course of pro- and mesonephric development also play important roles in the formation of the metanephric mesenchyme. Gene expression in kidney progenitor cells includes *Odd-skipped related 1* (*Odd1*) (James et al., 2006), *Eyes-absent 1* (*Eya1*) (Kalatzis et al., 1998), *Hox11 paralogous members a,c and d* (Wellik et al., 2002), *paired-box transcription factor 2 (Pax2)* (Dressler et al., 1990, Torres et al., 1995), *Wilms tumor 1* (*Wt1*) (Kreidberg et al., 1993), *Sine oculis family members* (*Six*) *1, 2 and 4* (Xu et al., 2003), *Spalt-Like Transcription Factor 1* (*Sall1*) (Nishinakamura et al., 2001) and *Glial cell line-derived neurotrophic factor* (*Gdnf*) (Moore et al., 1996, Pichel et al., 1996a, Pichel et al., 1996b, Sanchez et al., 1996). Metanephric mesoderm specification in particular is coordinated involving tripartite *Eya-Hox-Pax* and *Eya-Six-Pax* complexes. The coexpression of *Eya1*, *Hox11* and *Pax2* positively regulates *Gdnf* and *Six2* expression (Brodbeck and Englert, 2004, Gong et al., 2007). Loss of function of any of the genes mentioned above results in incomplete formation of the intermediate mesoderm, whereby absence of the earliest markers *Odd1* and *Eya1* leads to complete renal agenesis (James et al., 2006, Xu et al., 1999). Renal agenesis also occurs if there is a loss of the *LIM class homeodomain transcription factor* LHX1 (aka LIM1), which is essential for the formation of the nephric duct (Tsang et al., 2000). Likewise, activated by *Odd1* and *Lhx1*, the *Pax2* and *Pax8* are critical for nephric lineage specification (Torres et al., 1995, Mansouri et al., 1998). The presumed redundancy of their function at the early stages of kidney development was endorsed in *Pax2/8* double-mutant embryos, which show no signs

of nephric duct formation or expression of other nephric duct markers like *Ret proto-oncogene (c-Ret)* at all (Bouchard et al., 2002).

2.2.3.2. Outgrowth of the ureteric bud and branching morphogenesis

The emergence of the ureteric bud and subsequent branching morphogenesis are regulated by many different stimulating and inhibiting signaling networks. Growth and branching of ureteric bud tips is promoted by factors released by metanephric mesenchyme cells. In contrast, cells alongside the ureteric bud stems (epithelial nephron progenitors and stromal cells) promote elongation, but oppress branching (Sweeney et al., 2008). These reciprocal interactions create a tight link between epithelial and mesenchymal compartments and guarantee for a balanced development of the ureteric tree. Hereby a signaling pathway of the transforming growth factor beta (TGF–β) superfamily, the glial cell line-derived neurotrophic factor (GDNF) pathway occupies a central role. Stimulated by growth factors, GDNF is secreted by the metanephric mesenchyme at E 10.5 (Gong et al., 2007, Reidy and Rosenblum, 2009). Its action is mediated through the c-RET receptor tyrosine kinase and the GPI-linked co-receptor GFRα1, both expressed by the nephric duct. GDNF triggers RET-positive cells from the nephric duct to grow outwards in the direction of the GDNF signal. Deficiency of either GDNF, c-RET or GFRα1 leads to a failure in ureteric bud formation (Pichel et al., 1996a, Moore et al., 1996, Sainio et al., 1997b, Davies and Fisher, 2002). GDNF/c-Ret signaling is modified by multiple factors. To prevent the formation of ectopic ureteric buds for example, it is important that the signal is localized to the region of anticipated ureteric bud outgrowth. By restricting *Gdnf* expression in the anterior parts of the nephrogenic cord, the forkhead transcription factor FOXC1 and the ROBO2/SLIT2 receptor ligand pair are able to prevent the formation of supernumerary ectopic ureteric buds (Kume et al., 2000, Grieshammer et al., 2004). Another known inhibitor of GDNF is the bone morphogenetic protein 4 (BMP4). It is secreted by stromal cells that surround the nephric duct and antagonize ureteric bud outgrowth, whereby its exact working mechanism remains elusive. BMP4 in turn can be inhibited by the gene product of *Gremlin1* (*Grem1*), which is locally secreted around the emerging ureteric bud to maintain *Gdnf* expression (Michos et al., 2007). GDNF/c-Ret as well as Bmp4/Gremlin signaling are not only essential for primary ureteric bud outgrowth but also for ureteric bud branching. In the course of branching morphogenesis the expression of *c-Ret* is restricted to the ureteric tree tips and that of *Gdnf*

to the surrounding mesenchyme, allowing branching only to occur at the end of the tips (Costantini and Shakya, 2006). Activation of Ret signals is mediated via several pathways including ERK MAP kinase, PLC γ and PI3K (Fisher et al., 2001, Watanabe and Costantini, 2004, Ihermann-Hella et al., 2014). Moreover, several ureteric bud tip target genes are upregulated by GDNF/c-Ret signaling including *Etv4*, *Etv5*, *Met*, *Mmp, Spry1* and *Wnt11* (Pepicelli et al., 1997, Basson et al., 2005, Lu et al., 2009).

Sprouty1 (*Spr1*) encodes for a cytoplasmic membrane-associated protein that belongs to a group of receptor tyrosine kinase signaling inhibitors. It is expressed in the ureteric bud and the metanephric mesenchyme and as part of a negative feedback loop prevents excessive GDNF/c-Ret signaling, which would result in formation of ectopic ureteric buds. Furthermore *Spry1* helps to coordinate branching morphogenesis by regulating the synergistic interactions of GDNF/c-RET and the secreted glycoprotein WNT11 (Majumdar et al., 2003, Mason et al., 2006, Basson et al., 2006).

Wilms' tumor-1 (WT1), a zinc finger protein that can act as a transcription factor as well as a RNA binding protein, has manifold roles in nephrogenesis (Hohenstein and Hastie, 2006). It has also been proposed to regulate GDNF/c-Ret signaling, although the exact interactions yet remain unclear. It was suggested that it helps GDNF levels to exceed a critical threshold required for ureteric bud outgrowth. Also, it may regulate expression of Vascular Endothelial Growth Factor A (VEGF-A), which then stimulates angioblasts to release a yet unknown signal that induces the expression of *Gdnf* and *Pax2* (Donovan et al., 1999, Gao et al., 2005).

Early metanephric development also relies on signaling via Fibroblast Growth Factor Receptors (FGFR) 1 and 2, which at around E 10.5 are expressed in the metanephric mesenchyme as well as the ureteric bud. In a conditional knockout mouse model it was shown that combined deficiency of *Fgfr1/2* leads to renal agenesis. The ureteric bud initially forms, but subsequently fails to grow and branch. Concordantly, the metanephric mesenchyme is hypoproliferative with increased rates of apoptosis. In the metanephric mesenchyme expression of *Eya1* and *Six1* is still present, albeit it lacks expression of *Pax2, Six2* and *Sall1*. Therefore it is indicated that FGF signaling lies downstream of *Eya1* and *Six1*, and upstream of *Pax2, Six2* and *Spalt-Like Transcription Factor 1* (*Sall1)* (Poladia et al., 2006b). This was endorsed by studies in *Sall1*-mutants. Sall1 is one of four gene family members that encode for homologues of the Drosophila homeotic gene *Spalt*, a multi zinc finger transcription factor with activating

and repressing properties (Nishinakamura et al., 2001, Kanda et al., 2014). Renal defects in *Sall1*-mutants include failed outgrowth of the ureteric bud and increased apoptotic rates in the metanephric mesenchyme at E11.5 (Nishinakamura et al., 2001). The absence of *Sall 1* expression in both *Six1* and *Fgfr1/2* mutants indicates that the *Eya1-Six1* complex and FGF signaling are necessary for *Sall1* expression in the metanephric mesenchyme (Davies and Fisher, 2002, Poladia et al., 2006b).

Besides, branching morphogenesis also requires several other molecules of the extracellular matrix (ECM) (Davies and Fisher, 2002). The basal lamina surrounding the ureteric bud is composed of collagen type IV, laminin and different proteoglycans (Saxen and Sariola, 1987, Ekblom et al., 1990). These proteoglycans, particularly heparan sulfate are able to bind growth factors such as FGFs with their glycosaminoglycan side chains. Thereby they modulate their activity and for example are able to initiate branching (Coutts and Gallagher, 1995). Transmembrane proteins such as integrins α3 and α8 also have been shown to promote branching (Muller et al., 1997, Davies and Fisher, 2002).

2.2.3.3. Survival and proliferation of the metanephric mesenchyme

The default fate of the metanephric mesenchyme is apoptosis (Coles et al., 1993). To maintain cell survival, the ureteric bud secretes several soluble factors, inter alia TGF α, Epidermal Growth Factor (EGF), the metalloprotease inhibitor TIMP2 and several different BMPs (Coles et al., 1993, Di Marco et al., 1989, Lyons et al., 1995, Bernardini et al., 2001). During the course of kidney development the metanephric mesenchyme needs to grow continuously. This is partly facilitated by BMP4, which is secreted by the emerging tubules and stromal cells. Therefore the loss of mesenchymal cells to epithelial transition induces the remaining metanephric mesenchyme cells to multiply (Miyazaki et al., 2000). It was suggested that also BMP7 and FGF2 synergistically prevent the mesenchyme from apoptosis (Dudley et al., 1999). In that, BMP7 is presumably more involved in promoting stromogenic than nephrogenic progenitors (Dudley et al., 1995). FGF2 not only has anti-apoptotic properties itself, but also upregulates of *Wt1* expression, which contributes to metanephric mesenchyme cell survival as well (Perantoni et al., 1995).

While the nephron precursor cells in the cap mesenchyme are characterized by *Six2* expression, stromogenic progenitors surrounding the cap mesenchyme express the winged helix transcription factor *Foxd1* (Hatini et al., 1996, Levinson et al., 2005,

Kobayashi et al., 2008). Stromal cells are essential for the epithelial development, not only by supporting the emerging nephrons in a mechanical way, but also as an important source of modulatory signals (Davies and Fisher, 2002). Apart from the above mentioned BMPs, there is evidence for the existence of stromal derived-factors that regulate the correct c-Ret expression upon ureteric bud branching morphogenesis in response to retinoic acid signaling (Batourina et al., 2001). In mice that are deficient of retinoic acid receptors (RAR) α and β2, in the embryonic kidney both expressed by stromal cells, ureteric bud branching is greatly impaired and expression of *c-Ret* is downregulated (Mendelsohn et al., 1999).

2.2.3.4. Metanephric nephron formation

In both meso- and metanephros the induction of nephron formation is facilitated by *Wnt9b*, coding for a member of the secreted Wnt signaling proteins (Carroll et al., 2005). WNT9B is produced and released from the ureteric bud branches, and considered the primary paracrine signal for pre-tubular aggregate formation (Carroll et al., 2005). In concert with several other factors, including the FGF2, transforming growth factor (TGFβ2) and the Leukemia inhibitory factor (LIF) WNT9B stimulates via the canonical β-catenin signaling pathway the expression of several early nephron markers in the metanephric mesenchyme surrounding the ureteric bud (Perantoni et al., 1995, Barasch et al., 1999, Plisov et al., 2001). At the same time, WNT9B also promotes *Six2* expression in the cap mesenchyme to maintain a self-renewing nephron progenitor cell population (Karner et al., 2011). In the pretubular aggregates *Wnt9b* serves as initial activator, stimulating the expression of *Pax8*, *Fgf8* and *Wnt4* (Grieshammer et al., 2005, Davidson, 2008). WNT4, acting in an autocrine fashion, then is required to maintain the expression levels and promote mesenchymal-to-epithelial transition with subsequent formation of the renal vesicle (Stark et al., 1994, Kispert et al., 1998, El-Dahr et al., 2008).

The following terminal differentiation process constitutes another critical step in nephrogenesis. It involves the downregulation of embryonic genes and the simultaneous acquisition or upregulation of distinct functional genes that characterize the final specialized cell type the epithelial progenitors eventually turn into (El-Dahr et al., 2008). The exact interactions and mechanisms thereof still need to be fully elucidated. However, several of the involved transcription factors and signaling networks have been identified. Some of them, e.g. the p53 gene family, are involved in promot-

ing the epithelial differentiation fate overall, while others govern the highly specific segmentation of the nephron (El-Dahr et al., 2008, Heliot et al., 2013). Once the renal vesicle has formed, the proximal domain, i.e. the part that is furthest from the ureteric bud, is characterized by high expression levels of *Wt1* (Kreidberg et al., 1993). To allow glomerular podocyte development, *Wt1* directly represses *Pax2* activity (Ryan et al., 1995). Otherwise *Pax2* and *Pax8*, acting downstream of *Wnt4,* induce the expression of *Lhx1 (Narlis et al., 2007). Lhx1* a key regulator of the early stages of proximal-distal nephron patterning (Kobayashi et al., 2005). Its expression is also advanced by WNT4 directly, probably in concert with FGF8 (Grieshammer et al., 2005). Lhx1 induces the expression of POU domain class 3 transcription factor 3 (*Pou3f3, Brn1*) and Notch ligand *Dll1* (Nakai et al., 2003). While *Lhx1* and *Pou3f3* are required to specify the more distal segments of the nephron, including the loop of Henle and the distal convoluted tubule, Notch ligands *Dll1* and *Jag1* and the pathway modulator *Lfng* contribute to the development of the proximal tubule segments via Notch2 signaling (Nakai et al., 2003, Cheng et al., 2007, Desgrange and Cereghini, 2015). By also controlling the mentioned Notch components as well as the Iroquois homeodomain transcription factor (*Irx*) family members 1 and 2, the Hepatocyte nuclear factor-1 β (HNF1B) governs intermedio-proximal nephron segment identity (Heliot et al., 2013).

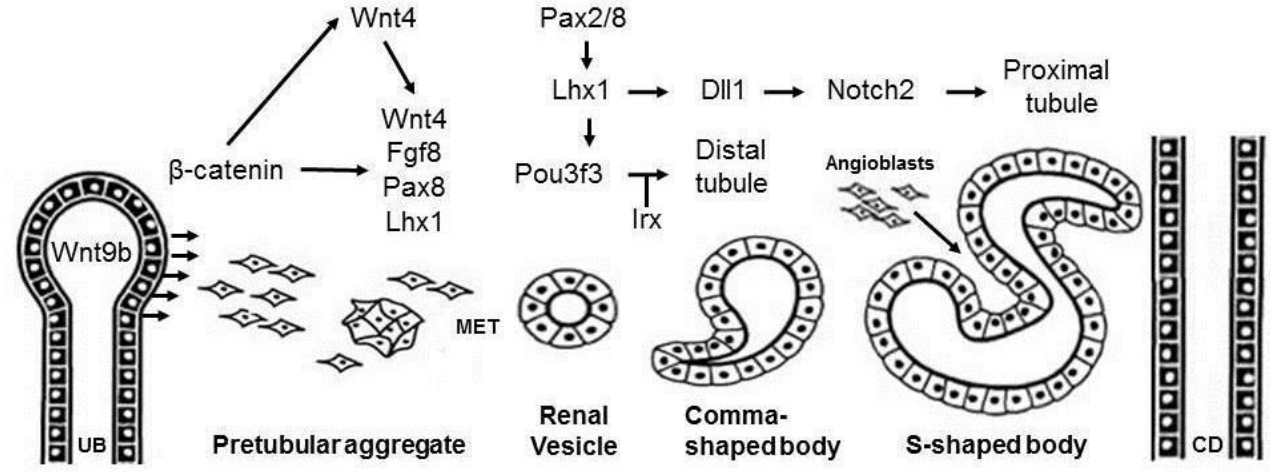

Figure 4) Transcriptional networks in terminal nephron differentiation.

CD, collecting duct; MET, mesenchymal-to-epithelial transition; UB, ureteric bud. See text for details (based on Horster et al., 1990, Davidson, 2008 and El-Dahr et al., 2008).

2.3. The importance of nephron endowment

In the last decades, the number of nephrons in the kidney has emerged as an important parameter of renal structure and an important indicator of renal health (Moritz et al., 2008). Up to the present day, most textbooks state that a human kidney contains approximately 1 million nephrons. This number does in fact come close to the average mean of the population, however, there appear to be tremendous inter-individual differences. One of the most comprehensive studies, performed on autopsied kidneys from over 400 subjects of five racial groups, indeed yielded an overall 12.8 fold variation. Nephron (glomerular) numbers of individual kidneys ranged from 210,332 to 2,702,079 with an overall mean of 910,902 (Hoy et al., 2010a, Hoy et al., 2010b). Several other studies go along with these findings by showing relatively similar mean values but large ranges of nephron numbers in kidneys of individuals with no signs of renal disease (Nyengaard and Bendtsen, 1992, Merlet-Benichou et al., 1999). Several factors, including different methods applied for counting of nephrons (refer to section 2.5), might contribute to the high variability of nephron numbers in humans. Age-related decline in nephron numbers certainly plays a role, however, these wide variations have been shown to be already largely present at birth (Hinchliffe et al., 1992, Nyengaard and Bendtsen, 1992, Zhang et al., 2008). Hence, they are not only the result of a glomerular loss due to acute and chronic renal insults throughout life, but determined developmentally. The awareness of possible implications thereof was awakened in the late 1990s, when two hypotheses emerged. The Barker hypothesis, now known as the developmental origins of health and disease (DOHaD), represents the concept that many diseases with onset in adulthood have their origin during fetal development (Hales and Barker, 1992). In utero insults prompting the fetus to make adaptions that ensure short-term survival, may eventually increase the risk to develop particular diseases in the long-term, therefore factors altering developmental processes during gestation or shortly after birth can have lifelong consequences for the health of the individual. Concordantly in 1988, Brenner et al. proposed that a congenital low nephron number explains why a couple of patients are susceptible to hypertension and renal disease, whereas others under similar circumstances seem relatively insusceptible to the development of disease. It was proposed that a nephron deficit and its concomitant reduction in surface filtration area lead to a compensatory glomerular hyperfiltration, which is associated with glomerular hypertension and hypertrophy. Initially these adaptive changes help to maintain

an overall normal glomerular filtration rate (GFR). In the long run, however, they may result in secondary changes, e.g., glomerulosclerosis that can lead to further nephron loss, proteinuria and systemic hypertension (Brenner et al., 1988). Among the most appreciated concepts regarding the pathogenesis of progressive glomerulosclerotic lesions following an unspecified first insult are glomerular hyperfiltration (Brenner, 1983), glomerular hypertrophy (Fogo and Ichikawa, 1989) and the impairment of the glomerular permselectivity with subsequent development of tubular and interstitial alterations (Remuzzi and Bertani, 1990). None of these concepts by itself, however, is able to explain the differences in development of CKDs in different animal models (Fogo et al., 1988, Yoshida et al., 1988).

Low nephron endowment alone is unlikely to be the only factor initiating the development of chronic kidney disease (CKD), but nowadays it is seen as a first hit, a risk factor that renders the kidney more susceptible for following secondary hits such as diabetes or obesity (Nenov et al., 2000). Irrelevant of the initial underlying cause, CKDs have the tendency to progress to end-stage renal disease (ESRD) with need for kidney replacement therapy i.e. dialysis or transplantation (Fogo, 2006). Conceivably, this progression is accelerated when the number of present and functioning nephrons in the kidney is already decreased at onset of disease. A plethora of factors has impact on metanephric development and thereby determination of nephron endowment. Apart from genetic polymorphisms (regarding e.g. *Pax2*, *Osr1*, *c-Ret*), a large range of perturbances to the feto-maternal environment has been identified to alter nephron number (Moritz et al., 2008, Walker and Bertram, 2011). Among them are placental insufficiency and maternal glucocorticoid exposure as well as undernutrition (Moritz et al., 2008). Maternal undernutrition can either mean a deficit in total calorie intake or a deficit in distinct dietary components like protein (Hoppe et al., 2007, Wlodek et al., 2007, Singh et al., 2007b, Langley-Evans et al., 1999, Moritz et al., 2009). However, maternal deficiencies in micronutrients like iron or vitamin A and D have also been shown to affect total nephron number in the offspring (Lelievre-Pegorier et al., 1998, Maka et al., 2008).

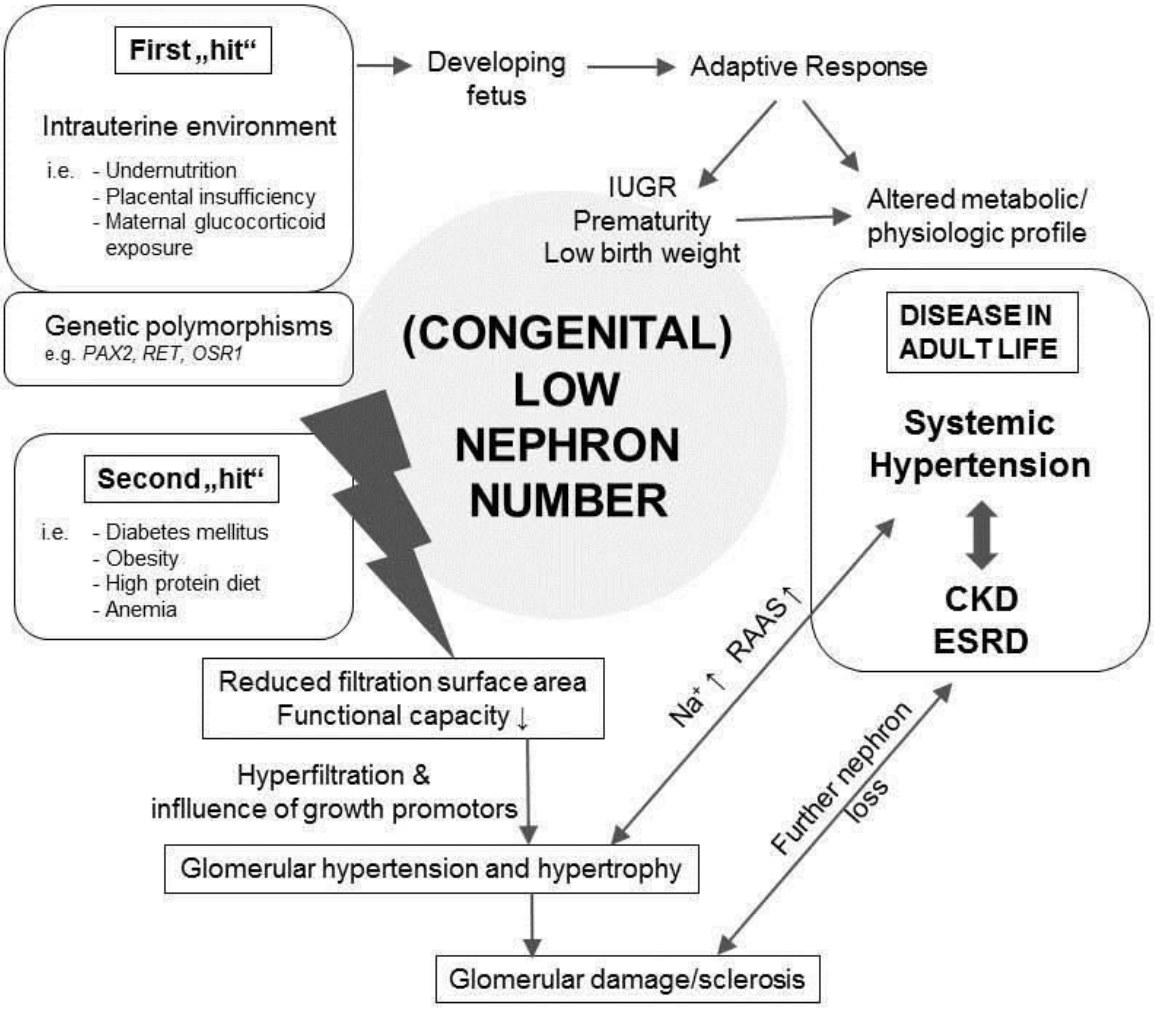

Figure 5) Causes and consequences of low nephron numbers.

Apart from genetic polymorphisms, several other factors mainly relating to the intrauterine environment contribute to a congenitally low nephron endowment. Thereby, these so called “first hits” render the kidney more susceptible for disease development later in life in case a “second hit” follows. Once the vicious cycle of nephron loss and compensatory mechanisms is initated, progression towards renal failure is the consequence. CKD, chronic kidney disease; ESRD, end-stage renal disease; IUGR, intrauterine growth restriction; RAAS, Renin-Angiotensin-Aldosterone-System (based on data from Fogo and Ichikawa, 1989, and Luyckx et al., 2013).

2.3.1. Interspecies differences in completion of nephron(no)genesis and nephron numbers

A lot of our knowledge about kidney development has been derived from studies in comparative animal models. Hence it is important to take species-specific differences into account, especially when putting results of experimental studies into a clinical context. One aspect of particular relevance is the completion of nephrogenesis (see Table 1). In humans, even though nephron maturation continues for a while after

birth, kidney development, i.e., nephronogenesis is basically completed at week 36 of gestation, whereas in rodents nephronogenesis lasts until at least 1 week postnatally (Zhong et al., 2012, Cullen-McEwen et al., 2016). Therefore, it is not only dependent upon *in utero* conditions, but also influenced by the postnatal environment. Under experimental conditions, most of these external factors can be controlled, however, another major aspect in which the human and the kidney of other mammalian species differ, is the total number of nephrons formed. Due to long-term inbreeding the differences in nephron endowment seen between individual animals of the commonly used rodent strains are in general very small (Moritz et al., 2008). Therefore it stands in direct contrast to the human condition.

Species	Period of meta-nephrogenesis	Length of pregnancy	Nephrons per kidney [x10³]	References
Human	5 – 36 weeks	40 weeks	210 – 2702	(Hoy et al., 2010a)
Sheep	30 – 130 days	150 days	200 – 800	(Zohdi et al., 2007, Galinsky et al., 2011, Wintour et al., 2003, Bains et al., 1996)
Spiny Mouse	19 – 37 days	40 days	7	(Dickinson et al., 2005)
Mouse	11 dpc – pn 5-7 d	20 days	10 – 14	(Sims-Lucas et al., 2009, Cullen-McEwen et al., 2001, David et al., 2010, Walker et al., 2012)
Rat	12 dpc – pn 8-10 d	22 days	25 – 35	(Cullen-McEwen et al., 2011, Black et al., 2002, Zimanyi et al., 2002, Bertram et al., 1992)
Pig	20 dpc – pn 21-25 d	112 days	812 – 2306	(Lodrup et al., 2008a, Lodrup et al., 2008b, van Vuuren et al., 2012)

Table 1) Timing of metanephrogenesis and average number of nephrons formed in different mammalian species.

All cited studies used unbiased stereology for the determination of nephron numbers; dpc, days post conceptum; pn, post natum (modified from Moritz et al., 2008, and Cullen-McEwen et al., 2016).

2.3.2. Animal models of low nephron numbers

As described in section 2.3., nephron endowment is determined by both, environmental and genetic factors. Accordingly, a number of strategies to generate animal models with reduced nephron numbers exist. Probably the most straightforward approach is the performance of a surgical reduction in renal mass, e.g., an unilateral nephrectomy. Obviously, this yields a 50% reduction in nephrons, however, the effects on the cardiovascular system and the remaining kidney depend on the point of time the procedure is performed. Is the kidney removed right after birth, there is an association with the development of hypertension, whereas removal during adulthood yields no further negative effects (Woods, 1999, Woods et al., 2001, Ryba, 2011). This has been shown to be true also in a recently established ovine model for of low nephron endowment, in which an unilateral nephrectomy is performed in a sheep fetus around day 100 of gestation, i.e. before the end of metanephrogenesis (Moritz et al., 2005).

Another strategy to create *a priori* low nephron numbers is to make use of known perturbations during pregnancy that result in a low birth weight or intrauterine growth restriction (IUGR), which has been shown to be associated with reduced nephron count (Luyckx and Brenner, 2005). Among these experimental manipulations are, e.g., maternal undernutrition, achieved by either a calorie restriction (global undernutrition) or a diet low in specific components such as protein, vitamin A or iron or by selectively depriving the fetus of nutrients by creating a placental insufficiency by uterine vessel ligation (Moritz et al., 2008).

Another experimental method that is not associated with reduced birth weights, but leads to offspring with hypertension and reduced nephron numbers is maternal glucocorticoid administration during the critical early stages of renal development. In rats, dexamethasone exposure around day 14-15 of gestation, leads to significantly reduced, i.e., 30% lower nephron numbers after birth as well as an altered gene expression profile with reduced levels of GDNF, TGF-ß1 and BMP-4, indicating interference with nephron formation during branching morphogenesis (Singh et al., 2007a, Singh et al., 2007b). Additionally, there are several models of genetically modified mice that exhibit reduced nephron counts. Apart from models for unilateral renal agenesis (Mesrobian, 1998, Wang et al., 2015), a few single gene deficiencies were found to be associated with alterations in nephron numbers. Benz et al. (2011) examined the kidneys of mice heterozygously deficient in the glial cell line-derived

neurotrophic growth factor (GDNF+/-). They examined 26 week-old animals of both sexes and compared them to sex- and age-matched wild-type controls. GDNF is a key molecule in signaling of branching morphogenesis of the ureteric bud. Therefore, GDNF deletion leads to reduced induction of branching and formation of nephrons (Costantini, 2010). Unbiased stereological investigations showed that GDNF+/- mice display a reduction in nephron number of approximately 30%, as compared to the wildtype animals (Benz et al., 2011). Furthermore, in these animals the mean glomerular volume was significantly higher. The glomerula of GDNF+/- animals also showed a proliferation of endothelial and mesangial cells, with a significant reduction in the podocyte density. Electron microscopically, a markedly thickened glomerular basement membrane was detectable. Blood pressure in GDNF+/- mice was not elevated with a regular diet. However, being fed a high salt diet, GDNF+/- mice became hypertensive (Schlote et al., 2013).

Mice with a homozygous *Fgfr2* deficiency of the ureteric bud, represent another genetically modified model of reduced nephron numbers (Poladia et al., 2006a). Compared to control animals, these mice exhibited 24% lower nephron numbers, and morphological kidney alterations consistent with renal disease (thickening and hypercellularity of the glomerular tuft, thickening of the capsule of Bowman, proteinaceous tubular casts), and increased serum levels of BUN. Additionally, the reduction in nephron numbers was associated with a significant increase of the systolic blood pressure by 20 mmHg and left-ventricular myocardial hypertrophy.

2.4. POU domain transcription factors

Transcription factors are able to regulate gene expression in a time and cell type specific manner by either activating or inhibiting the transcription of one or more genes. They possess specific DNA binding sites, that allow them to interact sequence specific with the DNA (Latchman, 1997).

Structural characteristic of all POU domain transcription factor family members is the eponymous POU domain. It was named after the first transcription factors in which it was identified: Pit-1, a pituitary-specific transcription factor, Oct-1/Oct-2, members of a transcription factor group, that bind to a specific ubiquitous octamer regulatory element and Unc-86, a transcription factor that plays an essential role in the neurogenesis of the nematode *Caenorhabditis elegans*. Pit-1 as well as Oct-1 and Oct-2 are mammalian specific, however, regarding the POU domain there is sequence homology to Unc-86 as well (Herr et al., 1988). Part of the POU domain consists of an evolutionary highly conserved DNA-binding motif, the homeodomain (Sturm et al., 1988). It has been shown that members of the homeodomain protein superfamily are critically involved in the regulation of key processes in embryonic development (Gehring et al., 1994, Mitchell and Tjian, 1989). Besides the POU-type homeodomain (POU_H) at the C terminus of the DNA binding motif, there is the POU specific domain (POU_S) at the N terminus.

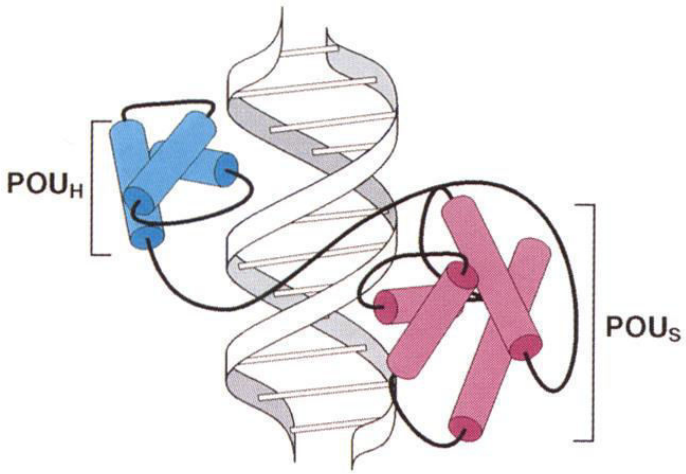

Figure 6) Schematic illustration of the POU domain

The POU-specific (POU_S) and POU homeodomains (POU_H) bind to opposite faces of the DNA and have a tail-to-tail orientation (adapted from Ryan and Rosenfeld, 1997, with permission).

Both sub-domains are connected by a variable linker region (Sturm and Herr, 1988). This bipartite arrangement allows taking on a variety of confirmations, thus facilitating the versatility in binding core DNA elements with different orientation and spacing. By using various coactivators, contingent upon binding to the DNA as a monomer or as a dimer, POU domain transcription factors can modulate the expression of distinct genes with spatio-temporal specificity. This also explains the fact that they often share crucial roles in the early stages of embryonic development, during lineage progression and when terminal cell differentiation takes place (Ryan and Rosenfeld, 1997, Phillips and Luisi, 2000).

2.4.1. Class III POU domain proteins

According to the amino acid sequence of the POU domain, POU proteins have been classified into at least six different groups (Wegner et al., 1993). Four intronless mammalian class III POU genes have been established, which are predominantly expressed during development of the central nervous system: *Brn-1*, *Brn-2*, *Brn-4* and *Tst-1/Oct-6/SCIP* (He et al., 1989). All four of them are related with one another, as they show a high sequence homology (Hara et al., 1992).

POU Transcription Factor (aliases)	Tissue expression pattern
Brn-1 (Otf-8, POU3F3)	all levels of CNS in embryo and adult – more restricted expression in adult; intestine, kidney
Brn-2 (Otf-7, N-Oct-3, POU3F2)	all levels of CNS in embryo and adult – more restricted expression in adult
Brn-4 (RHS2, N-Oct-4, POU3F4, Oft-9)	all levels of CNS in embryo and adult, pancreas, Rathke's pouch, whiskers, otic vesicle
XLPOU 2	Spemann's organizer (embryonal signaling center), mesoderm in gastrula, neuroectoderm, neural plate, notochord, brain
Tst-1/Oct-6/SCIP (Oft-6, POU3F1)	all levels of CNS, oligodendrocyte precursors, Schwann cells, testes, skin

Table 2) Summary of expression patterns of mammalian Class 3 POU domain proteins.

CNS, central nervous system (adapted from Ryan and Rosenfeld, 1997, with permission).

2.4.2. POU Domain Class 3 Transcription Factor 3 (POU3F3, BRN1)

Pou3f3 is an intronless gene and abundant in guanine and cytosine throughout the entire coding region. The mammalian gene encodes characteristic alanine, glycine and proline repeats. They are well conserved between mice and humans regarding both position and number (Sumiyama et al., 1996). *Pou3f3* and the closely related *Pou3f2* (*Brn2*) are both expressed in the developing nervous system (He et al., 1989). There they inhibit redundant functions in the production and radial migration of postmitotic upper-layer neurons (McEvilly et al., 2002, Sugitani et al., 2002). Deficiency of both, *Brn1* and *Brn2* eventually results in laminar inversion of the neocortex. Only deletion of *Brn2* yielded no detectable abnormalities in cortical development, while *Brn1* knockouts showed a substantial derangement of cells in the cortical layers with a delayed radial migration of the layer III and IV neurons (McEvilly et al., 2002). While *Brn2* expression is restricted to the brain, *Brn1* is also expressed in the developing kidney (He et al., 1989). So far, two *Pou3f3* knockout mouse lines have been established via homologous recombination. In both lines hemizygous knockouts did not exhibit any phenotypic alterations, whereas homozygous knockouts all died perinatally (McEvilly et al., 2002, Nakai et al., 2003). Apart from histological abnormalities, i.e., the significant cellular disorganization in the hippocampal region and adjacent transitional cortical areas of the brain, one-day-old homozygous *Pou3f3* knockout mice also exhibit abnormalities in the developing kidney, which were suspected to cause the perinatal deaths (McEvilly et al., 2002, Sugitani et al., 2002). To confirm this fact, Nakai et al. (2003) examined the kidneys of hemi- and homozygous *Brn1* knockouts. While hemizygous *Brn1* knockout mice were virtually indistinguishable from their wildtype littermates, homozygous *Brn1* knockout mice showed a striking reduction of 20% in kidney weight and elevated BUN (blood urea nitrogen) and potassium levels in the serum. Further histological examination using H&E and PAS stained kidney sections yielded a reduction in the number of Henle's loops with a concomitant prominence of interstitial cells, whereas collecting ducts and cortices with glomeruli appeared to have developed normally.

To assess the expression of *Brn1* during mouse kidney development an anti-BRN1 antibody was used. Immunoreactivity was first detected within the renal vesicle, and subsequently in particular in regions of the S-shaped body, that were supposed to develop into the Henle loop, the Macula densa and the distal convoluted tubule. Dur-

ing the following developmental stages, immunoreactivity within these areas continued to be positive, however, in the mature loop of Henle it was restricted to the thick ascending limb (TAL) (Nakai et al., 2003). BrdU labeling and TUNEL assay suggested, that the obvious reduction in Henle loops in newborn *Brn1* deficient mice was due to a reduced cell proliferation and a premature induction of the caspase cascade, leading to an early onset of apoptosis during the primitive loop stage of Henle loop development (Nakai et al., 2003). Although hemizygous *Brn1* knockout mice showed no histologically or clinically detectable abnormalities in kidney development and function, the expression levels of several TAL-related genes, including *Umod, Ptger3, Nkcc2, Kcnj1* and *Bsnd* were significantly reduced (Nakai et al., 2003).

2.5. Quantitative morphological phenotyping of genetically modified animal models

Since changes in function generally correlate with changes in morphology, histological examination is an essential part in phenotyping of genetically manipulated organisms. For studying effects of genetic manipulations, it is particularly critical to recognize not only qualitative morphological alterations, such as inflammatory or degenerative changes, but also differences regarding the basic constitution of the studied structure and its components. Evaluated parameters hereby might be volume, surface area, length or number of structures in a given reference space, such as a cell or tissue (Weibel, 1979c, Howard and Reed, 2004, Lucocq, 2007, West, 2012). Being highly adapt to pattern recognition, the human visual system apparently lacks the ability to recognize small changes regarding spatial characteristics like sizes or numerical densities of structures (Wanke, 2002, Boyce et al., 2010, Wanke, 2017). In fact, changes in the numerical densities of, e.g., cell section profiles in a respective reference compartment such as a tissue section can only be perceived, once the difference between the compared probes reaches approximately 25-40% (de Groot et al., 2005, Haschek et al., 2013). This yields the danger of missing subtle, yet potentially pivotal morphological changes that might indicate early pathological changes. Therefore, researchers urgently rely on different methods that allow the precise and objective quantification of structures in all sorts of reference spaces like organs, tissues, cells or even cellular subcompartments. To perform a direct measurement, however, it is necessary to view the structure of interest as a whole and together with its entire reference compartment. In general this is not possible due to the non-transparency, size or three-dimensional complexity of the desired structure. Three-dimensional imaging can be achieved by tissue clearing techniques, such as the so-called CLARITY method (Azaripour et al., 2016) which uses different chemicals to replace tissue lipids by acrylamide-based hydrogels, resulting in an almost complete translucency of the tissue (Chung et al., 2013). However, most studies rely on the use of classical tissue slices. A consequence thereof is a loss of dimensionality that inevitably leads to a loss of spatial information - objects turn into section profiles, areas into lines, and lines into points. Furthermore, it is absolutely essential to keep in mind that the actual number of particles in a reference space cannot be obtained from the number of sectioned particle profiles, since there is an unpredictable varia-

tion depending upon the size and shape as well as the spatial orientation of the respective particles (Howard and Reed, 2004, Boyce et al., 2010, West, 2012).
Artifacts related to tissue processing like shrinkage due to embedding, or unprecise information about the section thickness (Matenaers et al., 2018), together with the use of inappropriate sampling techniques further complicate it to obtain unbiased information from histological tissue sections and make a lot of scientists shy away from the implementation of quantitative morphological methods in their repertoire (Weibel et al., 1966). This is very unfortunate, since the application of stereological methods enables the generation of a large amount of significant data with a high degree of objectivity. The possibility to assess tissue quantitatively, ultimately broadens the traditional descriptive use of microscopy. According to Weibel, stereology comprises “a body of mathematical methods relating three-dimensional parameters defining the structure to two-dimensional measurements obtainable on sections of the structure“ (Weibel, 1979c). In other words, by applying principles of stochastic geometry and statistics, stereology enables researchers to obtain information about three-dimensional structures from two-dimensional sections (Nyengaard, 1999, Madsen, 1999). Hereby, the nature of the obtained information can either be qualitative or quantitative, but it is always three-dimensional. The term “morphometry” in contrast, refers to all methods used to measure morphological structures. Hence morphometrical analyses are always quantitative, but don’t have to be three-dimensional (Weibel et al., 1967). Quantitative stereological analyses can be divided into model-based and design-based methods. Model-based stereology uses geometric properties of the studied objects and mathematical approximations based on assumptions like spatial homogeneity. This is often appropriate in material or geological sciences. In life sciences, however, they are generally biased, as the investigated objects, in this case biological structures, do not entirely comply with the geometrical model. Therefore, even though they allow obtaining data quickly and uncomplicatedly, they mostly need to be largely viewed as outdated (Baddeley and Jensen, 2005, West, 2012). The new gold standard is set by design-based methods like the “disector”, a renowned principle to estimate number and size of even arbitrarily shaped particles (Sterio, 1984). No prior knowledge about these particles is necessary, no presumptions need to be made here, precision and unbiasedness only rely on choosing an adequate sampling strategy and method of investigation (Gundersen et al., 1988a, Gundersen et al., 1988b). During all steps of sampling uniform random sampling pro-

cedures should be applied. This guarantees that the partial quantity chosen for investigation is statistically representative (Gundersen and Jensen, 1987, Howard and Reed, 2004). It is imperative that the whole reference compartment containing the structure of interest is available for sampling and moreover, that the total volume thereof can be accurately determined, since absolute parameters like total volumes, surface areas, lengths, and object numbers are in general obtained by calculation from their corresponding relative parameters (volume-, surface-, length-, or numerical densities of the structures of interest within their reference compartments) (Tschanz et al., 2014).

For details on the methodology of quantitative stereological analyses, the reader is referred to standard textbooks (Weibel, 1979b, Howard and Reed, 1998, Haschek et al., 2013), a steadily growing number of excellent reviews and publications (Weibel, 1979a, Nyengaard, 1999, Dorph-Petersen et al., 2001, Albl et al., 2016, Blutke et al., 2016, Matenaers et al., 2018), and, also to the descriptions provided in the methods section of the publication in the present thesis (see pages 38-40).

3. Research Article

Missense Mutation of POU Domain Class 3 Transcription Factor 3 in *Pou3f3*^{L423P} Mice Causes Reduced Nephron Number and Impaired Development of the Thick Ascending Limb of the Loop of Henle*

Alexandra Rieger, Elisabeth Kemter, Sudhir Kumar, Bastian Popper,
Bernhard Aigner, Eckhard Wolf, Rüdiger Wanke, Andreas Blutke

PLoS One. 2016 Jul 15;11(7):e0158977.

Impact factor (2016): 3.23

*Parts of this study were previously presented at meetings as posters and oral presentations and the abstracts were published in peer reviewed journals and conference proceedings:

A. Rieger, R. Wanke, A. Blutke (2013). Morphologische, morphometrische sowie quantitativ stereologische Charakterisierung des renalen Phänotyps der Mauslinie *Pou3f3*^{L423P}. Poster presentation at the 56th annual conference of the pathology division of the German Veterinary Medical Society, March 4 – 6, 2013 in Fulda, Germany. [Abstract published in Tierärztliche Praxis (K) 3/2013 A39].

A. Rieger, R. Wanke, A. Blutke (2013). *Pou3f3*^{L423P} mutant mice - A new model for low nephron numbers? Poster presentation at the 5th Annual Meeting of the German Society of Nephrology, October 5-8, 2013 in Berlin, Germany. [Abstract published in the conference proceedings: Abstract-USB-Stick Kongress für Nephrologie 2013 - 5. Annual Meeting of the German Society of Nephrology, ISSN 1863-2262].

A. Rieger, R. Wanke, A. Blutke (2014). Die Rolle des Transkriptionsfaktors POU3F3 in der Nephronogenese. Oral presentation at the 57th annual conference of the pathology division of the German Veterinary Medical Society, March 7-9, 2014 in Fulda, Germany. [Abstract published in Tierärztliche Praxis (K) 2/2014 A19].

A. Rieger, B. Popper, R. Wanke, A. Blutke (2014). Mutante Mäuse der Mauslinie *Pou3f3*^{L423P} als Modell für *a priori* niedrige Nephronzahlen? Oral presentation at the meeting „Junge Niere“ May 9-10, 2014 in Munich, Germany. [Abstract published in Nieren- und Hochdruckkrankheiten, Jahrgang 43, Nr. 4/2014, S. 192–199].

PLOS ONE

RESEARCH ARTICLE

Missense Mutation of POU Domain Class 3 Transcription Factor 3 in *Pou3f3*^{L423P} Mice Causes Reduced Nephron Number and Impaired Development of the Thick Ascending Limb of the Loop of Henle

Alexandra Rieger[1], Elisabeth Kemter[2], Sudhir Kumar[2], Bastian Popper[3], Bernhard Aigner[2], Eckhard Wolf[2,4], Rüdiger Wanke[1], Andreas Blutke[1]*

1 Institute of Veterinary Pathology at the Centre for Clinical Veterinary Medicine, Ludwig-Maximilians-Universität München, Munich, Germany, **2** Chair for Molecular Animal Breeding and Biotechnology and Laboratory for Functional Genome Analysis, Gene Center, Ludwig-Maximilians-Universität München, Munich, Germany, **3** Department of Anatomy and Cell Biology, Biomedical Center, Ludwig-Maximilians-Universität München, Munich, Germany, **4** German Center for Diabetes Research (DZD), Helmholtz Zentrum München, Neuherberg, Germany

* blutke@patho.vetmed.uni-muenchen.de

Citation: Rieger A, Kemter E, Kumar S, Popper B, Aigner B, Wolf E, et al. (2016) Missense Mutation of POU Domain Class 3 Transcription Factor 3 in *Pou3f3*^{L423P} Mice Causes Reduced Nephron Number and Impaired Development of the Thick Ascending Limb of the Loop of Henle. PLoS ONE 11(7): e0158977. doi:10.1371/journal.pone.0158977

Editor: Shree Ram Singh, National Cancer Institute, UNITED STATES

Received: April 19, 2016

Accepted: June 25, 2016

Published: July 15, 2016

Data Availability Statement: All relevant data are within the paper.

Funding: AR recieved a PhD scholarship from the Hanns-Seidel-Stiftung e. V., Munich, Germany.

Competing Interests: The authors have declared that no competing interests exist.

Abstract

During nephrogenesis, POU domain class 3 transcription factor 3 (POU3F3 *aka* BRN1) is critically involved in development of distinct nephron segments, including the thick ascending limb of the loop of Henle (TAL). Deficiency of POU3F3 in knock-out mice leads to underdevelopment of the TAL, lack of differentiation of TAL cells, and perinatal death due to renal failure. *Pou3f3*^{L423P} mutant mice, which were established in the Munich ENU Mouse Mutagenesis Project, carry a recessive point mutation in the homeobox domain of POU3F3. Homozygous *Pou3f3*^{L423P} mutants are viable and fertile. The present study used functional, as well as qualitative and quantitative morphological analyses to characterize the renal phenotype of juvenile (12 days) and aged (60 weeks) homo- and heterozygous *Pou3f3*^{L423P} mutant mice and age-matched wild-type controls. In both age groups, homozygous mutants *vs*. control mice displayed significantly smaller kidney volumes, decreased nephron numbers and mean glomerular volumes, smaller TAL volumes, as well as lower volume densities of the TAL in the kidney. No histological or ultrastructural lesions of TAL cells or glomerular cells were observed in homozygous mutant mice. Aged homozygous mutants displayed increased serum urea concentrations and reduced specific urine gravity, but no evidence of glomerular dysfunction. These results confirm the role of POU3F3 in development and function of the TAL and provide new evidence for its involvement in regulation of the nephron number in the kidney. Therefore, *Pou3f3*^{L423P} mutant mice represent a valuable research model for further analyses of POU3F3 functions, or for nephrological studies examining the role of congenital low nephron numbers.

Introduction

Members of the POU domain transcription factor family are crucially involved in the regulation of a variety of developmental processes in diverse organs and tissues [1]. Amongst others, the transcription factor POU3F3 (BRN1) plays an important role in the embryonic development of the brain and the kidney, where it participates in regulation of cerebro-cortical neuron migration [2,3] and renal distal tubule formation [4–7]. In the developing brain, POU3F3 acts in concert with another POU domain transcription factor, POU3F2 (BRN2), and loss of function of either one can partially be compensated by the other [2]. However, in the developing kidney only POU3F3 is expressed, largely restricted to parts of the nephron that develop into the thick ascending limb (TAL) and the macula densa (MD) of the loop of Henle and the distal tubule [5].

In the mature kidney, the TAL is functionally important for the urinary concentrating mechanism via the countercurrent multiplier system, the regulation of the extracellular fluid volume and pH, as well as for the homeostasis of calcium and magnesium, and of bicarbonate and ammonium. For this, the TAL is equipped with several, partially energy dependent, specialized ion transporters, such as NKCC2, ROMK, NHE3, CLC-K1/2 and KCC4 [8]. The TAL is also the origin of the abundant urine glycoprotein uromodulin (UMOD), also known as Tamm-Horsfall protein [9,10]. The MD in the juxtaglomerular wall of the distal TAL is crucially involved in regulation of the glomerular blood flow and the glomerular filtration rate (GFR). In response to the intra-tubular sodium chloride concentration, the MD controls the release of renin from juxtaglomerular cells, thereby regulating the renin–angiotensin–aldosterone system (RAAS) dependent tubular reabsorption of sodium and water in the kidneys [11].

In 2003, Nakai and colleagues reported generation of *Pou3f3* knock-out mice [5]. Homozygous knock-outs displayed increased plasma urea and potassium levels and renal hypoplasia with severe malformations of distinct tubular nephron segments. In particular, elongation and differentiation of the TAL and development of MD cells were impaired, and homozygous *Pou3f3* knock-out mice died within 24 hours after birth due to renal failure [5].

Mammalian nephrogenesis is a complex process involving the spatially and timely coordinated interaction of several transcription and growth factors, from initial interaction of the metanephric mesenchyme and the ureteric bud (i.e., nephron induction), to the final formation of the different tubular segments of the mature nephron and the collecting duct (CD) system (i.e., nephron differentiation or nephron patterning) [4,6,7]. In mice, nephron endowment is completed by postnatal day 7–10 [12–14]. The transcription factor POU3F3 is involved in control of this complex nephron patterning, however its role is yet not completely understood, and analysis of POU3F3 function in postnatal renal development in knock-out mice is limited by the neonatal death of the animals.

Recently, we reported generation and phenotypical characterization of a *Pou3f3* mutant mouse line on C3H genetic background in the Munich ethyl-N-nitrosourea (ENU) mouse mutagenesis project [15,16]. These *Pou3f3*^{L423P} mutant mice harbor a recessive T→C point mutation, leading to an amino acid exchange from leucine to proline in the conserved homeobox domain of the protein at amino acid position 423 [16]. In contrast to *Pou3f3* knock-out mice, hetero- and homozygous *Pou3f3*^{L423P} mutant mice are viable and fertile. They display increased plasma urea levels, reduced body and kidney weights, as well as neurological deficits, impaired hearing, malformation of the semicircular canals of the vestibular organ, and several metabolic changes associated with renal dysfunction [16].

In the present study, the renal phenotype of juvenile and aged homo- and heterozygous *Pou3f3*^{L423P} mutant mice was characterized in detail using comprehensive quantitative morphological and functional analyses. State-of-the-art design-based quantitative stereological

methods were applied to identify the effects of the *Pou3f3* mutation on development, growth, and cellular composition of different nephron segments, including the TAL and glomeruli. The results of these analyses provide new insights into the role of POU3F3 in pre- and postnatal kidney development and provide the basis for using *Pou3f3*^{L423P} mutant mice as an animal model in nephrological research.

Materials and Methods

Ethics statement and animal housing

All experiments were approved by the responsible animal welfare authority (Regierung von Oberbayern) and were carried out in accordance with the German Animal Protection Law, conforming to international guidelines on the ethical use of animals.

Mice

Pou3f3^{L423P} mutant mice were originally generated in the Munich ENU mouse mutagenesis project and maintained on the genetic background of C3HeB/FeJ inbred mice [16]. All mice investigated in the present study were kept under specified pathogen-free conditions in a closed barrier system on a 12:12 hour light-dark cycle and had free access to a standard rodent diet (V1534; Ssniff, Soest, Germany) and drinking water [16]. Genotyping of mice was performed by allele-specific PCR restriction fragment length polymorphism (RFLP) analysis, as described previously [16]. Mice were examined at 12 days of age and at 60 weeks of age. If not stated otherwise, the following numbers of mice were analyzed at 12 days of age: non-mutant control mice (CON), male: n = 6, female: n = 11; heterozygous *Pou3f3*^{L423P}-mutant mice (HET), male: n = 15, female: n = 15; homozygous *Pou3f3*^{L423P}-mutant mice (HOM), male: n = 7, female: n = 5; and at 60 weeks of age: CON, male and female: n = 7; HET, male: n = 8, female: n = 7; HOM, male and female: n = 6.

Blood pressure, serum, and urine analyses

Blood pressure was noninvasively measured by regular tail cuff plethysmography (CODA System, Kent Scientific, Torrington, CT) in 60-week-old mice, as previously described [17]. To this, mice were trained daily to accustom them to the blood pressure measuring procedure over a period of two weeks (at least four times per week). Blood pressure data were averaged from valid readings of ten consecutive measurements per mouse. Spot urine samples from 12-day-old mice and from 60-week-old mice, and serum from tail vein blood specimen from 60-week-old mice were collected and stored at -80°C until assayed. The serum concentrations of urea and sodium were determined using a COBRAS INTEGRA® 400 plus analyzer (Roche Diagnostics, Germany). Serum cystatin C concentrations were measured by an enzyme linked immunosorbent assay (Mouse Cystatin C ELISA-kit RD291009200R, BioVendor GmbH, Germany).

Urine albumin concentrations were determined in spot urine samples of 12-day-old and of 60-week-old mice using the mouse albumin ELISA-kit Bethyl E90-134 (Bethyl, USA). Additionally, the specific gravity of the urine and the urinary creatinine concentrations were determined in spot urine samples of 60-week-old mice. Urine creatinine concentrations were measured using a Hitachi automated analyzer (Merck, Germany). Subsequently, urine albumin-to-creatinine ratios (UACR) were calculated from corresponding urine albumin and creatinine concentrations. The specific gravity of the urine samples was determined by refractometry (MHRS-10-ATC, Müller Optronic, Germany).

For SDS-PAGE urine protein analysis, individual spot urine samples of non-mutant control mice (male: n = 6, female: n = 11), heterozygous *Pou3f3*^{L423P}-mutant mice (male: n = 15, female: n = 15), and homozygous *Pou3f3*^{L423P}-mutant mice (male: n = 7, female: n = 5) were diluted to a creatinine content of 1.5 mg/dl. Urine proteins were temperature denatured (Thermoblock TB1, Biometra, Germany) and separated using 12% SDS-PAGE gels (Protean III, Bio-Rad, Munich, Germany) together with a broad molecular weight standard (Bio-Rad) and a mouse albumin standard (Biotrend, Cologne, Germany), as previously described [17]. In all gels, individual urine samples of male and female homozygous and heterozygous *Pou3f3*^{L423P}-mutant mice and non-mutant controls were loaded. After electrophoresis, the gels were stained with Coomassie blue.

Body and kidney weight, kidney processing, histology and electron microscopy

After determination of body weight at 12 days and at 60 weeks of age, respectively, mice were killed by cervico-cranial dislocation. After removal of the left kidney, mice were perfused with neutrally buffered 2.5% glutaraldehyde solution through the heart, as previously described [17,18]. After in situ immersion fixation in 2.5% glutaraldehyde solution, the right kidney was carefully separated from adjacent tissues and blotted dry. The kidneys were weighed to the nearest mg and cut perpendicular to the longitudinal axis in ~1 mm thick slices, using a precision tissue slicing device [19]. The slices of the left kidney were fixed in neutrally buffered 4% formaldehyde solution and routinely embedded in paraffin for immunohistochemical analyses.

The slices of the right, perfusion-fixed kidney (6.9 ± 0.5 slices in 12-day-old mice and 11.5 ± 0.9 slices in 60-week-old mice) were routinely processed and embedded in plastic for light microscopy and transmission electron microscopy (TEM) as previously described [20,21]. For TEM, three 1 mm^3 samples of the renal cortex per animal were selected by systematic random sampling [22], postfixed in 1% osmium tetroxide and embedded in Epon-resin. From each Epon block, ten consecutive 0.5 μm thick semi-thin sections were cut and stained with toluidine blue O and safranin. Ultrathin sections (70–80 nm) were cut, contrasted with uranyl citrate and lead citrate and examined with a TEM (EM10, Zeiss, Eching, Germany). The remaining kidney slices were embedded in plastic, containing hydroxymethylmethacrylate and methylmethacrylate (GMA/MMA, Sigma-Aldrich Laborchemikalien GmbH, Seelze, Germany), as described previously [20]. For qualitative and quantitative morphological analyses, plastic sections with a nominal section thickness of 1.0 μm were cut on a Reichert-Jung 2050 rotary microtome (Leica, Wetzlar, Germany) and stained with hematoxylin and eosin, periodic acid Schiff (PAS), and periodic acid silver methenamine (PASM). For quantitative stereological analyses, ~100 consecutive sections with a nominal section thickness of 1 μm were additionally cut from each GMA/MMA block per case. From each section series, every 20th section was systematically randomly selected (5 ± 1 sections per case) and stained with PAS.

Immunohistochemistry

Immunohistochemical analyses were performed on sections of paraffin embedded kidney tissue. The following primary antibodies were used: rabbit polyclonal anti human uromodulin antibody (H-135; sc-20631, Santa Cruz Biotechnology, Heidelberg, Germany, dilution 1:1000) [23], monoclonal rat anti mouse uromodulin IgG antibody (MAB5175, R&D Systems, Abingdon, UK, dilution 1:250), polyclonal rabbit anti mouse AQP2 IgG antibody (A7310, Sigma-Aldrich, Munich, Germany, dilution 1:450) and guinea pig anti mouse BRN1 IgG antibody (gp56, by courtesy of Prof. Dr. Wegner, Institute of Biochemistry, Emil Fischer Center, University Erlangen-Nuremberg, Germany, dilution 1:600). As secondary antibodies, biotinylated

goat anti rabbit IgG antibody (BA-1000, Vector, Peterborough, UK, dilution 1:200), horseradish peroxidase labeled goat anti rabbit IgG antibody (P0448, DAKO, Hamburg, Germany, dilution 1:150), horseradish peroxidase labeled rabbit anti guinea pig IgG antibody (P0141, DAKO, Hamburg, Germany, dilution 1:150), and alkaline phosphatase labeled goat anti rat IgG antibody (112-055-167, Jackson ImmunoResearch, Newmarket, UK, dilution 1:300) were used. Immunoreactivity was visualized using 3,3-diaminobenzidine tetrahydrochloride dihydrate (DAB) or a combination of nitro blue tetrazolium chloride (NBT) and 5-bromo-4-chloro-3-indolyl phosphate (BCIP). Kidney sections stained with buffer instead of the primary antibody were used as negative control.

Quantitative-stereological investigations of the kidney

Plastic resin-embedded samples of kidney tissue were used for quantitative stereological analyses, using design-based stereological methods, such as the physical disector and point counting [24,25], essentially carried out as described previously in detail [26]. Quantitative stereological estimates were corrected for embedding-related tissue shrinkage.

Total volumes of the kidney, renal zones, glomeruli. The kidney volume was obtained by dividing the weight of the glutaraldehyde-fixed right kidney by the density of perfusion-fixed murine kidney tissue (1.05 g/cm^3) [27]. The cross-sectional areas of the kidney (Kid) as well as the cortex and the medulla (Med) of the kidney [28,29], were planimetrically determined in micrographs of PASM-PAS stained GMA/MMA kidney sections (9 ± 2 per case), using a Videoplan^{TM} image analysis system (Zeiss-Kontron, Eching, Germany). The volume fractions of the cortex ($V_{V(Cortex/Kid)}$) and the medulla ($V_{V(Med/Kid)}$) were calculated according to the principle of Delesse [24]. The absolute volumes of the individual renal zones ($V_{(Cortex, Kid)}$, $V_{(Med, Kid)}$) were calculated by multiplication of the volume fractions of the respective zones in the kidney with the total kidney volume. The fractional volume of the glomeruli in the cortex ($V_{V(Glom/Kid)}$) was determined by point counting (1029 ± 115 points per case) [30] in systematically randomly selected areas [22] of PASM-PAS stained GMA/MMA sections, as principally described earlier [21]. The absolute volume of the glomeruli in the perfusion-fixed (right) kidney ($V_{(Glom, Kid)}$) was calculated from the volume fraction of the glomeruli in the cortex and the absolute cortex volume. The volume fractions of the TAL in the kidney ($V_{V(TAL/Kid)}$) were determined by point counting (3713 ± 1646 points per case) in systematically randomly selected areas of paraffin embedded kidney sections immunostained for uromodulin (UMOD, section 2.6). The absolute volume of the TAL in the kidney ($V_{(TAL, Kid)}$) was calculated from the volume fraction of the TAL cells in the kidney and the absolute volume of the kidney.

Mean glomerular volume and total number of glomeruli. The mean glomerular volume ($\bar{v}_{(Glom)}$) and the total number of nephrons (glomeruli) in the right kidney ($N_{(Glom, Kid)}$) were estimated, using the physical disector method [24,25], in combination with systematic point counting, as described in previous publications of our group [17,21,27]. Per case, 5 ± 1 PAS stained GMA/MMA section pairs with 20 μm distance (disector height) were systematically randomly selected. Using an automated stereology system (VIS-Visiopharm Integrator System^{TM} Version 3.4.1.0 with newCAST^{TM} software, Visiopharm A/S, Denmark), corresponding locations of the renal cortex were then systematically randomly sampled at 40x final magnification in both sections, automatically congruently aligned, and digitally superimposed with unbiased counting frames (344017 μm^2 area) and 9 x 9 point test grids. The sectional area of cortical kidney tissue present within each sampled counting frame ($A_{(Cortex)}$) was determined by point counting. In the subsequent disector analyses, 67 ± 18 Q^- (glomeruli) were counted per case. The numerical volume density of glomeruli in the renal cortex of the right kidney was calculated as: $N_{V(Glom/Kid)} = (\Sigma Q^-_{(Glom)}/h \times \Sigma A_{(Cortex)}) \times$

f_s^3 with f_s = linear tissue shrinkage factor for GMA/MMA-embedded murine kidney tissue (0.91) [31]. The number of glomeruli in the right kidney $N_{(Glom, Kid)}$ was then calculated as the product of $N_{V(Glom/Kid)}$ and $V_{(Cortex, Kid)}$. Subsequently, the mean glomerular volume was estimated as $\bar{v}_{(Glom)} = V_{V(Glom/Kid)} / N_{V(Glom, Kid)}$.

To validate the precise disector heights used for calculation of the numerical volume densities of glomeruli in the kidney and glomerular cells in the glomeruli, the thicknesses of GMA/MMA and Epon sections were controlled, using an orthogonal resectioning technique, as previously described [21,27]. Since the measured thickness of GMA/MMA sections and Epon sections was 1.028 ± 0.031 and 0.501 ± 0.005, respectively, a section thickness of 1.0 μm for GMA/MMA sections and 0.5 μm for Epon sections was consistently used for the calculation of the disector volumes.

Number and volumes of glomerular cells. The mean numbers of distinct glomerular cell types per glomerulus (C: all glomerular cells; Pod: podocytes, M-E: mesangial and endothelial cells), and the mean podocyte volume were unbiasedly determined, applying the physical disector method [24,25], principally as described above. For this, the numerical volume density of glomerular cells in the glomerulus was unbiasedly determined in consecutive serial semi-thin sections of Epon-embedded cortical kidney tissue samples: per section series, 2–3 pairs of sections with 1.5 μm distance were systematically randomly sampled [24]. Per case, the corresponding profiles of 10 ± 1 systematically randomly sampled glomeruli were photographed at 400x magnification in both sections of a section pair, using a Leica DFC 320 camera (Leica, Germany) connected to a microscope (Orthoplan, Leitz, Germany). Images including a size ruler were printed and overlaid with a plastic transparency with 576 equally spaced test points. The areas of the glomerular cross-sections ($A_{(Glom)}$) were planimetrically measured, using a Videoplan image analysis system (Zeiss-Kontron, Germany). The volume fraction of podocytes per glomerulus $V_{V(Pod/Glom)}$ was estimated from the fraction of points hitting podocyte section profiles, and points hitting the corresponding glomerular cross-section profile [24]. On the average, 681 ± 206 points were counted per case. All glomerular cell nuclei profiles (C, Pod, M-E) sampled within a glomerular cross-section in the first (reference) section, which were not present in the corresponding glomerular section profile in the second (look-up) section, were counted (Q^-). The operation was then repeated by interchanging the roles of the look-up section and the reference section, increasing the efficiency of cell nuclei counting by factor two. On the average, 250 ± 47 glomerular cell (C) nuclei (Q^-) were counted per case (Pod: 72 ± 9; M-E: 181 ± 39). The numerical volume density of glomerular cells in the glomerulus ($N_{V(C/Glom)}$, $N_{V(Pod/Glom)}$, $N_{V(M-E/Glom)}$) was calculated from the number of Q^- counted per cell type and the respective disector volume, defined by the cumulative areas of analyzed glomerular section profiles and the distance (disector height = 1.5 μm) between the examined section pairs: $N_{V(X/Glom)} = (\Sigma Q^-_{(X)} / h \times \Sigma A_{(Glom)}) \times f_s^3$ with X = C, or Pod, or M-E; h = disector height (1.5 μm) and f_s = linear tissue shrinkage factor for Epon-embedded murine kidney tissue (0.95) [17]. The mean number of cells per glomerulus ($N_{(C, Glom)}$) and of podocytes per glomerulus ($N_{(Pod, Glom)}$) was calculated by multiplying the numerical volume density of the respective glomerular cells in the glomerulus with the mean glomerular volume. The mean podocyte volume ($\bar{v}_{(Pod)}$) was calculated dividing $V_{V(Pod/Glom)}$ by $N_{V(Pod/Glom)}$.

Volume of the mesangium and glomerular capillaries. The volume densities of capillaries, and of the mesangium within the glomeruli ($V_{V(Cap/Glom)}$ and $V_{V(Mes/Glom)}$) were determined by point counting (fraction of points hitting capillary section profiles, or the mesangial area in PAS stained sections, respectively, and points hitting the glomerular section profile) in 51 ± 6 systematically randomly sampled glomerular profiles in PAS stained GMA/MMA sections at 200x magnification. Per case, 932 ± 256 points were counted. The mean mesangial and capillary volumes per glomerulus ($V_{(Mes, Glom)}$ and $V_{(Cap, Glom)}$) were calculated as the product of the

respective volume density in the glomerulus and the mean glomerular volume ($\bar{v}_{(Glom)}$). The total volume of glomerular capillaries in the kidneys was calculated as $V_{(Glom\text{-}cap,\ Kid)} = V_{V(Cap/Glom)} \times V_{(Glom,\ Kid)}$.

Length of glomerular capillaries. The mean length of the capillaries per glomerulus ($L_{(Cap,\ Glom)}$) was determined in the same glomerular profiles sampled in the serial semi-thin Epon sections used for estimation of glomerular cell numbers. The number of glomerular capillary section profiles ($\Sigma Q_{(Cap)} = 1261 \pm 122$ per case) present within the examined glomerular section profiles was counted. The cumulative glomerular tuft profile area of all examined glomerular section profiles ($\Sigma A_{(Glom)}$) was measured planimetrically, as described above. The length density of capillaries in the glomeruli was calculated as $L_{V(Cap/Glom)} = 2 \times Q_{A(Cap/Glom)} \times f_s^2$, with $Q_{A(Cap/Glom)} = \Sigma Q_{(Cap)}/\Sigma A_{(Glom)}$ and $f_s = 0.95$. $L_{(Cap,\ Glom)}$ was then obtained as: $L_{(Cap,\ Glom)} = L_{V(Cap/Glom)} \times \bar{v}_{(Glom)}$ [22,24]. The total length of the glomerular capillaries in the kidney ($L_{(Glom\text{-}cap,\ Kid)}$) was calculated as: $L_{(Glom\text{-}cap,\ Kid)} = L_{V(Cap,\ Glom)} \times V_{(Glom,\ Kid)}$.

Glomerular basement membrane (GBM) thickness and filtration slit frequency (FSF). The thickness of the GBM was determined by the orthogonal intercept method as described earlier [17,32,33]. Per case, eight glomeruli were sampled from semi-thin sections, as described earlier [34]. Ultrathin sections of these glomeruli were prepared for TEM, and peripheral glomerular capillary loops were photographed (9 ± 2 pictures per case) in a predetermined manner (by half turns of the stage handle). Photographs were developed to a final print magnification of 54324 x, and covered by a transparent 1.5-cm^2 grid. Where gridlines transected the GBM, the shortest distance between the endothelial cell membrane and the outer lining of the lamina rara externa underneath the cell membrane of the epithelial foot processes was measured, using a logarithmic ruler template with dimensions and midpoints, as described earlier in detail [33]. The true harmonic mean thickness ($T_{h(GBM)}$) of the GBM was estimated as: $T_{h(GBM)} = (8/3\pi) \times (10^6/M) \times l_{h(GBM)}$, with $l_{h(GBM)}$ (apparent harmonic mean GBM thickness) = ∑ Number of observations / ∑ (Midpoints x number of observations), and M = final print magnification. On the average, 1379 ± 264 (range: 938–2204) intercepts per animal were measured. The FSF was determined in the same electron micrographs, by counting the number of epithelial filtration slits divided by the length of the peripheral capillary wall at the epithelial interface, as described earlier [32]. On the average, 1890 ± 667 filtration slits (range: 922–3372) were counted per animal.

Renal POU3F3 mRNA and protein abundance

Quantitative RT-real time PCR (RT-qPCR) analyses. The renal *Pou3f3* mRNA expression abundances in 60-week-old mice were examined by RT-qPCR analyses (n = 7/7 (male/female) non-mutant controls, 8/6 heterozygous mutants, and 5/6 homozygous mutants). RNA-isolation was performed, using Trizol® (Invitrogen, CA, USA). The integrity of RNA was assessed by agarose gel electrophoresis. RNA quantity and purity were determined using a NanoDrop 1000 Spectrophotometer (Thermo Fisher Scientific, Germany). Following DNase digestion (Thermo Scientific dsDNase, Thermo Fisher Scientific, Germany), on the average 2.9 ± 0.4 μg of total RNA per case were reverse transcribed using the RNA to cDNA EcoDryTM Premix (Clontech, CA, USA). RT-qPCR analyses were performed on an Applied Biosystems StepOne Real-Time PCR System (Applied Biosystems, Germany) using Power SYBR® Green PCR Master Mix (Applied Biosystems, UK) and primers for amplification of mouse *Pou3f3* [35] (accession N°: NM_008900.2, forward primer: 5'-GGT ACC CAC CTG CGA GTA GA-3'; reverse primer: 5'-CAG CCT ACA GCT GGA AAA GG-3'; amplicon length: 127 bp), *uromodulin (Umod)* [36] (accession N°: NM_001278605.1, forward primer: 5'-gga aag cag aaa acc tgg tg-3'; reverse primer: 5'-gag aca ggg ctt cat aca-3'; amplicon length: 205 bp), and

glyceraldehyde-3-phosphate dehydrogenase (Gapdh) [37] (accession N°: NM_001289726.1, forward primer: 5'-TGT GTC CGT CGT GGA TCT GA-3'; reverse primer: 5'-CCT GCT TCA CCA CCT TCT TGA T-3'; amplicon length: 77 bp). Primer sequences were queried by NCBI Blast software and the comparability of amplification efficiencies of the single primers was confirmed by performance of RT-qPCR-based standard curve analyses. All RT-qPCR measurements were performed in duplicates and included no template controls and RT-minus controls (DNase-digested RNA). The expression abundances of *Pou3f3*, and *Umod* were calculated in relation to the expression of *Gapdh* as internal reference, as well as the abundance of *Pou3f3* in relation to *Umod* using the $2^{-\Delta CT}$ method [38]. The relative mRNA abundances were then normalized to the respective mean relative mRNA abundance of non-mutant control mice.

Western-blot analyses. Renal protein abundances of POU3F3 and GAPDH in 60-week-old mice were examined by Western-blot analyses (n = 6/6 (male/female) non-mutant controls, 6/6 heterozygous mutants, and 6/6 homozygous mutants). For protein extraction, kidney tissue samples were homogenized in protein extraction buffer (10 mm Na_2HPO_4 at pH 7.0; 0.2% (wt/vol) sodium dodecyl sulfate solution; 10% (vol/vol) glycerine; adjusted to pH 7.0), heated to 95°C for 5 minutes and cooled on ice for 5 minutes. After centrifugation (18,000 g, 5 min, 4°C), protein contents were quantified using the bicinchoninic acid method [39]. For Western-blot analyses, 30 micrograms of denatured protein were loaded per lane on 12% sodium dodecyl sulfate-polyacrylamide gels and separated by electrophoresis (SDS–PAGE) together with a prestained protein ladder (PageRuler, Thermo Scientific, Germany). After electrophoresis, separated proteins were blotted to polyvinylidene difluoride (PVDF) membranes (Thermo Fisher Scientific, Germany). For detection of POU3F3 and GAPDH, the following antibodies (diluted in 5% dry milk) were used after blocking of the membranes: Guinea pig-anti-Brn1 antibody, diluted 1:2500 [40]; and Rabbit-anti-GAPDH (D16H11) mAb (#51741, Cell Signaling, New England Biolabs GmbH, Germany), diluted 1:2000. Incubation with primary antibodies was carried out overnight at 4°C. After washing of the membranes, incubation with appropriate horseradish-peroxidase coupled secondary antibodies (HRP-goat anti-rabbit IgG (#7074), Cell Signaling, New England Biolabs GmbH, Germany), diluted 1:2000; Donkey anti-guinea pig IgG HRP conjugated (43R-ID039hrp, Fitzgerald Industries International Inc., Bioleague GmbH & Co.KG, Germany), diluted 1:5000) and final washing steps, bound antibodies were visualized using Amersham ECL Western blotting detection reagent and Amersham ECL Hyperfilms (GE Healthcare Life Sciences, Germany). After detection of POU3F3, the membranes were stripped in stripping buffer (37.5 ml of 250 mM TRIS buffer at pH 6.7; 30 ml of 10%; 82.5 ml H2O; 1050 µl ß-mercaptoethanol) for 40 minutes at 70°C and then used for detection of GAPDH.

Statistical analyses

All data are presented as means ± SD. To determine genotype effects data were analyzed by one-way ANOVA with Gabriel's post hoc tests. Gender specific differences were analyzed by comparison of male *vs*. female mice of identical genotypes by using an unpaired Student's t-test (IBM SPSS Statistics, Version 18). P-values <0.05 were considered significant. For all examined parameters, the exact p-values of all comparisons are provided in the Supporting Information (S1 and S2 Tables).

Results

Body weights, absolute and relative kidney weights, and kidney volumes

In juvenile mice of 12 days of age, the body weights of male and female homozygous *Pou3f3*^{L423P} mutant mice tended to be reduced as compared to heterozygous mutants and control mice (Fig 1),

reaching statistical significance in male homozygous vs. heterozygous mutants ($p<0.05$). Homozygous *Pou3f3*^{L423P}-mutant mice consistently displayed significantly lower absolute ($p<0.01$) and relative kidney weights ($p<0.05$) and kidney volumes ($p<0.01$) than heterozygous mutants or non-mutant control mice. However these parameters were not significantly different between heterozygous mutants and control mice (Table 1, Fig 1). At 60 weeks of age, the body weights of male homozygous *Pou3f3*^{L423P} mutant mice were significantly smaller, as compared to heterozygous mutants (male $p<0.01$) or non-mutant control mice (male $p<0.01$, female $p<0.01$). Furthermore

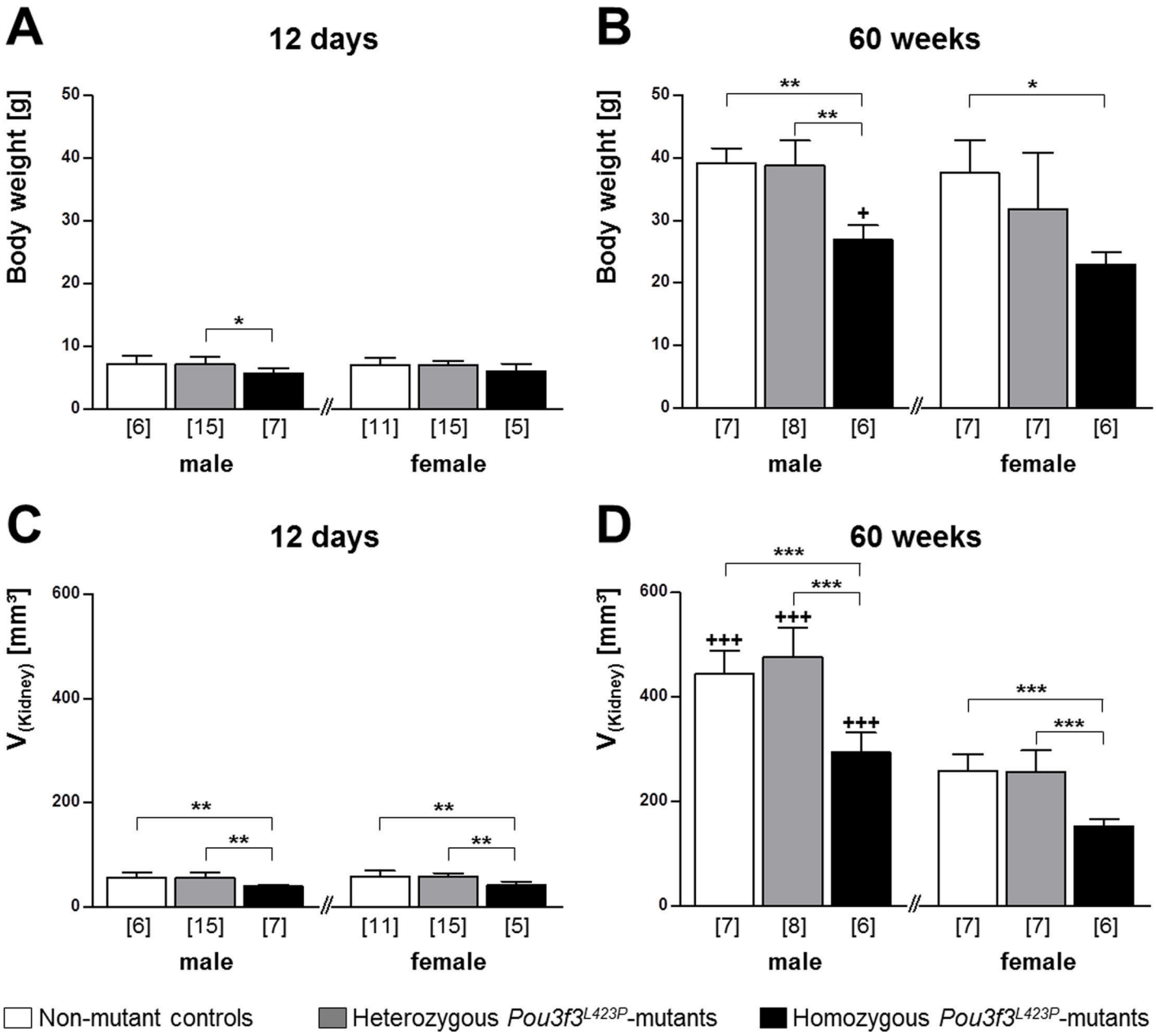

Fig 1. Body weight (A, B) and volume of the perfusion-fixed right kidney (C, D) of 12-day-old (A, C) and of 60-week-old (B, D) *Pou3f3*^{L423P} mutant mice and non-mutant control mice. The numbers of animals examined are given in parentheses. Data are means ± SD. Significant differences between homozygous and heterozygous mutants and non-mutant control mice are indicated by asterisks. *: $p < 0.05$, **: $p < 0.01$, ***: $p < 0.001$. Significant differences between male and female mice of identical genotypes are indicated by crosses. +: $p < 0.05$, ++: $p < 0.01$, +++: $p < 0.001$.

doi:10.1371/journal.pone.0158977.g001

Table 1. Absolute and relative kidney weights and urine albumin concentrations in homozygous (HOM) and heterozygous (HET) *Pou3f3*^{L423P} mutant mice and control (CON) mice at 12 days of age.

Parameter	Sex	CON *(6/11)*		HET *(15/15)*		HOM *(7/5)*		*Statistical significance**		
								CON vs. HET	*CON vs. HOM*	*HET vs. HOM*
Kidney weight [mg]	M	63	±11	60	±11	42	±3	*n.s.*	*p<0.01*	*p<0.01*
	F	62	±11	62	±8	46	±8	*n.s.*	*p<0.01*	*p<0.01*
Relative kidney weight [% of body weight]	M	1.8	±0.2	1.7	±0.1	1.5	±0.1	*n.s.*	*p<0.05*	*p<0.05*
	F	1.8	±0.1	1.8	±0.2	1.5	±0.1	*n.s.*	*p<0.05*	*p<0.05*
Urine albumin concentration [µg/ml]	M	25	±9	18	±6	18	±8	*n.s.*	*n.s.*	*n.s.*
	f	19	±3	21	±7	15	±4	*n.s.*	*n.s.*	*n.s.*

Numbers of animals examined are given in brackets (male/female). Data are means ± SD.

* 1-way ANOVA with Gabriel's post hoc test. *n.s.* not significant.

doi:10.1371/journal.pone.0158977.t001

the reduction of the absolute kidney weights, as well as the kidney volumes of homozygous *Pou3f3*^{L423P} mutant mice of both sexes was highly significant ($p<0.001$). In contrast, the body weights, absolute and relative kidney weights, and kidney volumes were not significantly different between heterozygous mutants and non-mutant control mice (Table 2, Fig 1).

Blood pressure, serum, and urine analyses

The mean blood pressures of 60-week-old homo- and heterozygous *Pou3f3*^{L423P} mutants and of non-mutant control mice of the same sex did not display statistically significant differences. Comparing male and female mice of identical genotypes, however, male non-mutant control mice displayed significantly higher ($p<0.05$) mean blood pressures than female mice (Fig 2).

For characterization of the renal function in 60-week-old mice, the serum concentrations of urea, sodium, and cystatin C, as well as the urine concentrations of albumin and creatinine, and the specific gravities of spot urine samples were determined. Homozygous mutants displayed

Table 2. Absolute and relative kidney weights, serum sodium levels, and urine albumin and creatinine concentrations in homozygous (HOM) and heterozygous (HET) *Pou3f3*^{L423P} mutant mice and control (CON) mice at 60 weeks of age.

Parameter	Sex	CON *(7/7)*		HET *(8/7)*		HOM *(6/6)*		*Statistical significance**		
								CON vs. HET	*CON vs. HOM*	*HET vs. HOM*
Kidney weight [mg]	m	365 ^{c}	±23	399 ^{b}	±55	229 ^{b}	±31	*n.s.*	*p<0.001*	*p<0.001*
	f	198 ^{c}	±23	219 ^{b}	±33	112 ^{b}	±11	*n.s.*	*p<0.001*	*p<0.001*
Relative kidney weight [% of body weight]	m	0.9 ^{c}	±0.1	1.0 ^{a}	±0.1	0.9 ^{b}	±0.1	*n.s.*	*n.s.*	*p<0.05*
	f	0.5 ^{c}	±0.1	0.7 ^{a}	±0.2	0.5 ^{b}	±0.0	*n.s.*	*n.s.*	*p<0.05*
Serum sodium concentration [mmol/l]	m	146	±5	146	±4	147	±4	*n.s.*	*n.s.*	*n.s.*
	f	141	±6	143	±1	144	±10	*n.s.*	*n.s.*	*n.s.*
Urine albumin concentration [µg/ml]	m	50	±20	57	±22	25	±24	*n.s.*	*n.s.*	*p<0.05*
	f	125	±81	38	±22	11	±8	*n.s.*	*p<0.01*	*n.s.*
Urine creatinine concentration [mg/ml]	m	0.21	±0.05	0.16	±0.05	0.14	±0.11	*n.s.*	*n.s.*	*n.s.*
	f	0.19	±0.04	0.16	±0.04	0.10	±0.03	*n.s.*	*p<0.05*	*n.s.*
UACR [µg/mg]	m	253.3	±67.0	337.8	±121.9	183.9	±48.6	*n.s.*	*n.s.*	*n.s.*
	f	642.4	±433.3	258.5	±140.1	114.9	±76.7	*n.s.*	*p<0.05*	*n.s.*

Numbers of animals examined are given in brackets (male/female). UACR: Urine albumin-to-creatinine ratio. Data are means ± SD.

*1-way ANOVA with Gabriel's post hoc test.

^{a,b,c}: Statistically significant differences (a: $p\leq0.05$, b: $p\leq0.01$, c: $p\leq0.001$) between male and female mice of the identical genotype; *n.s.* not significant.

doi:10.1371/journal.pone.0158977.t002

significantly, on average two-fold higher serum urea concentrations than non-mutant control mice and heterozygous mutants (male mice: $p<0.01$, female mice: $p<0.05$), whereas the serum urea levels between heterozygous mutants and control mice were not significantly different (Fig 2A).

The serum concentrations of sodium (Table 2) and of cystatin C (Fig 2B), an endogenous marker of glomerular filtration [41], were also not significantly different between the different groups of mice.

Urine analyses results revealed no evidence of albuminuria in *Pou3f3*^{L423P} mutant mice. At 12 days of age, the urine albumin concentrations were not significantly different between homo- and heterozygous Pou3f3^{L423P} mutants and control mice (Table 1). At 60 weeks of age, the urine albumin concentrations were even significantly lower in female homozygous mutants *vs*. non-mutant controls ($p<0.01$), as well as in male homo- *vs*. heterozygous mutants ($p<0.05$) (Table 2). Moreover, 60-week-old homozygous *Pou3f3*^{L423P} mutant mice also consistently displayed lower urine creatinine concentrations, urinary albumin-to-creatinine ratios, and urine specific gravities than heterozygous *Pou3f3*^{L423P} mutants and non-mutant control mice. Here, the specific urine gravity (Fig 2D) in homozygous mutants was significantly lower than in heterozygous mutants and control mice (male mice: $p<0.01$, female mice: $p<0.05$). as well, the urine creatinine concentrations and the urine albumin-to-creatinine ratios (UACR) (Table 2) of female homozygous mutants were also statistically significantly lower as compared to control mice ($p<0.05$). In contrast, the specific urine gravities (Fig 2D), the urine creatinine concentrations and the UACRs (Table 2) were not significantly different between heterozygous mutants and non-mutant controls mice (Fig 2). Corresponding to these quantitative findings, SDS-PAGE based urine protein analyses did also not demonstrate signs of albuminuria in homo- or heterozygous *Pou3f3*^{L423P} mutants (Fig 3).

Qualitative histological, immunohistochemical and ultrastructural kidney findings

Histological evaluation revealed an obvious decrease in the number of glomerular profiles in kidney sections of 60-week-old homozygous *Pou3f3*^{L423P} mutant mice, as compared to heterozygous mutants and non-mutant control mice. Moreover, the glomerular section profiles of homozygous *Pou3f3*^{L423P} mutants appeared strikingly smaller than in heterozygous *Pou3f3*^{L423P} mutants or control mice (Fig 4). In contrast, histological examination of kidney sections revealed no conspicuous differences between heterozygous *Pou3f3*^{L423P} mutants and control mice (Fig 4).

Apart from the apparently diminished size of glomeruli in 60-week-old homozygous *Pou3f3*^{L423P} mutants, which was more prominent than in 12-day-old mutant mice, no qualitative histopathological or ultrastructural glomerular alterations were present in either homo- or heterozygous mutants at 12-days and at 60-weeks of age (Figs 4 and 5). Histological and ultrastructural analysis also showed no conspicuous morphological alterations of the epithelial cells of the thick ascending limb (TAL) of the loop of Henle of 12-day-old, or of 60-week-old homo- and heterozygous *Pou3f3*^{L423P} mutant mice (Figs 4 and 5).

The abundance pattern of POU3F3 in different nephron segments and tubular compartments of homozygous *Pou3f3*^{L423P} mutant mice and non-mutant controls, were demonstrated by immunohistochemical detection of POU3F3, and co-localization with the TAL marker uromodulin (UMOD), and the CD marker aquaporin 2 (AQP2). Immunohistochemical detection of UMOD in the kidneys of non-mutant controls revealed a diffuse homogeneous cytoplasmic and distinct apical membrane staining pattern in epithelial cells of the TAL. In contrast, homozygous *Pou3f3*^{L423P} mutant mice of 12 days of age (data not shown) and of 60 weeks of age

showed a less dense immunohistochemical UMOD staining pattern of individual TAL section profiles in the kidney, as compared to age and sex-matched heterozygous mutants and non-mutant control mice (Fig 6).

Immunohistochemical detection of POU3F3 revealed a nuclear staining pattern in epithelial cells of the TAL, the MD, and the CDs in homo- and heterozygous mutants and non-mutant control mice (Fig 6), as demonstrated by co-localization with the TAL marker UMOD and the

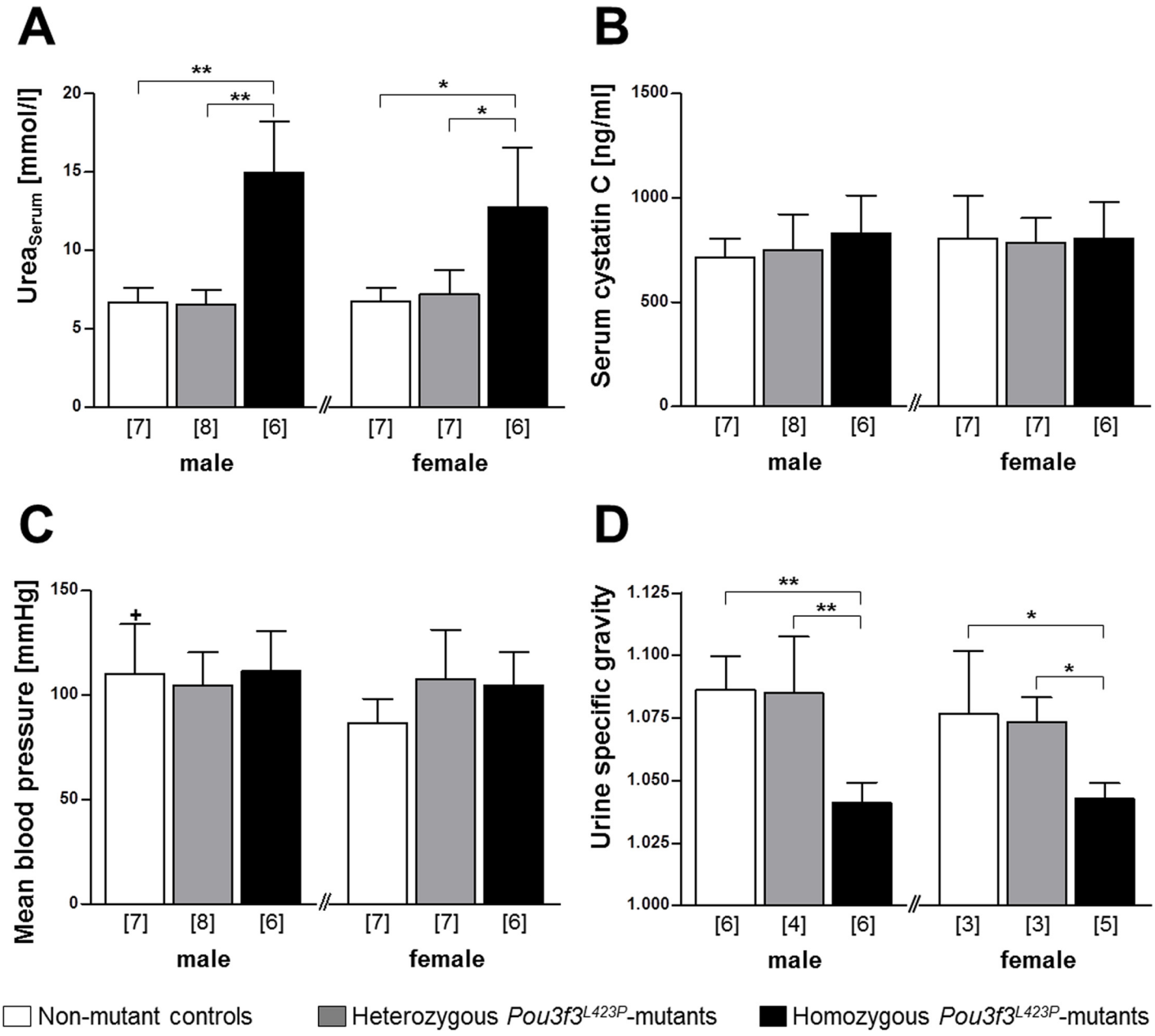

Fig 2. Serum urea concentration (A), serum cystatin C concentration (B), mean blood pressure (C), and urine specific gravity of 60-week-old *Pou3f3*^{L423P} mutant mice and non-mutant control mice (D). The numbers of animals examined are given in parentheses. Data are means ± SD. Significant differences between homozygous and heterozygous mutants and non-mutant control mice are indicated by asterisks. *: $p < 0.05$, **: $p < 0.01$, ***: $p < 0.001$. Significant differences between male and female mice of identical genotypes are indicated by crosses. +: $p < 0.05$, ++: $p < 0.01$, +++: $p < 0.001$.

doi:10.1371/journal.pone.0158977.g002

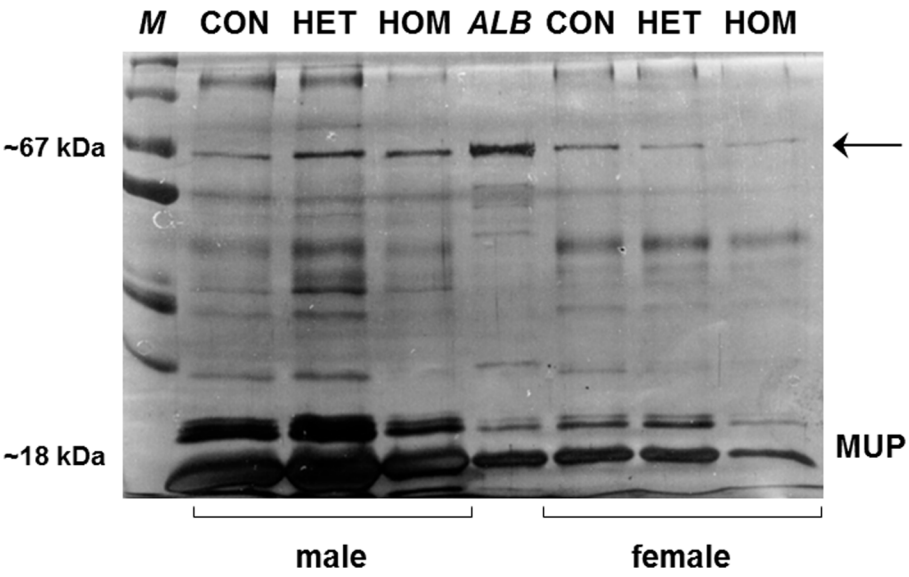

Fig 3. SDS-PAGE urine protein analysis of 60-week-old homozygous (HOM) and heterozygous (HET) *Pou3f3*^{L423P} mutant mice and non-mutant control (CON) mice. A representative gel of individual spot urine samples of three male and female HOM, HET and CON mice diluted to identical creatinine concentrations is shown. Molecular weight marker (M), murine serum albumin (ALB). Mice of all examined genotypes display discrete albumin bands (arrow) at approximately 67 kDa. The intensity of the major urinary protein (MUP) bands at approximately 18–25 kDa in male mice is stronger than in female mice.

doi:10.1371/journal.pone.0158977.g003

CD marker AQP2. In contrast, POU3F3 staining was not detectable in glomerular cells. Simultaneous detection of UMOD and POU3F3 by double-immunohistochemistry proved the co-

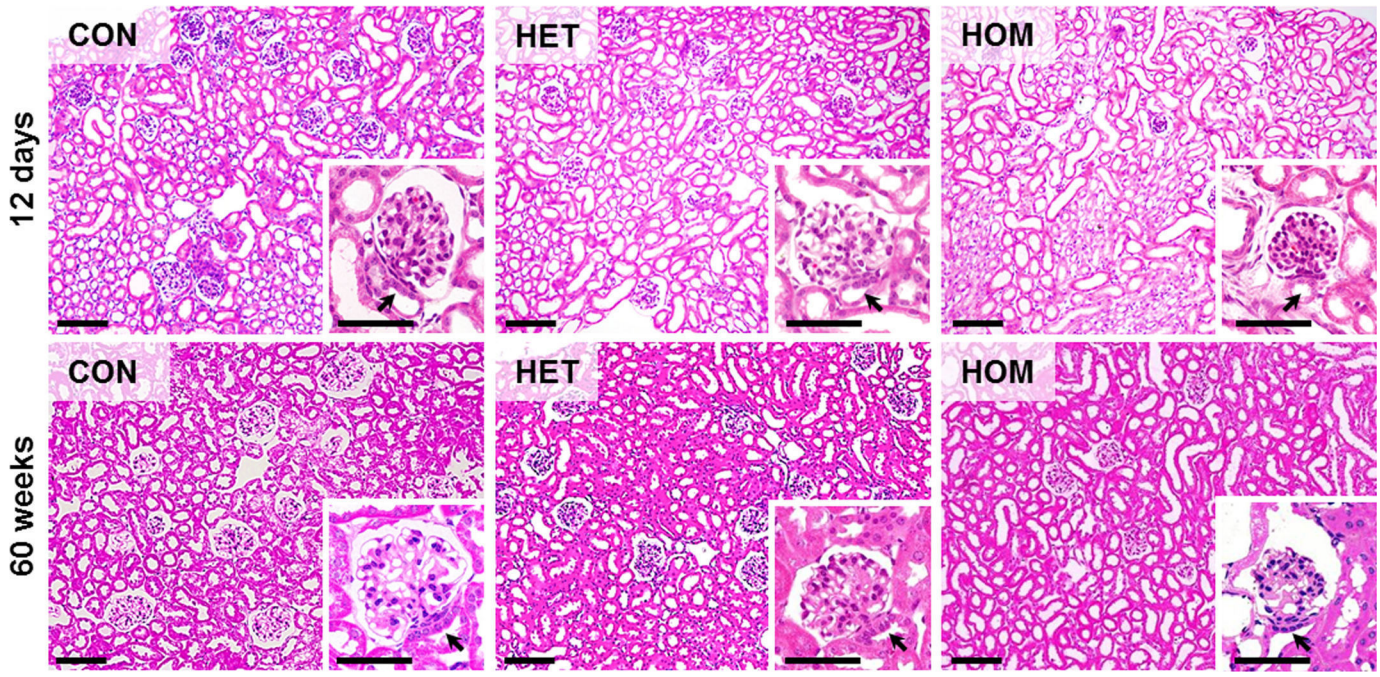

Fig 4. Kidney histology of 12-day-old and of 60-week-old homozygous (HOM) and heterozygous (HET) *Pou3f3*^{L423P} mutant mice and non-mutant control mice (CON). GMA/MMA sections, HE staining. Bars = 100 μm, in insets = 50 μm.

doi:10.1371/journal.pone.0158977.g004

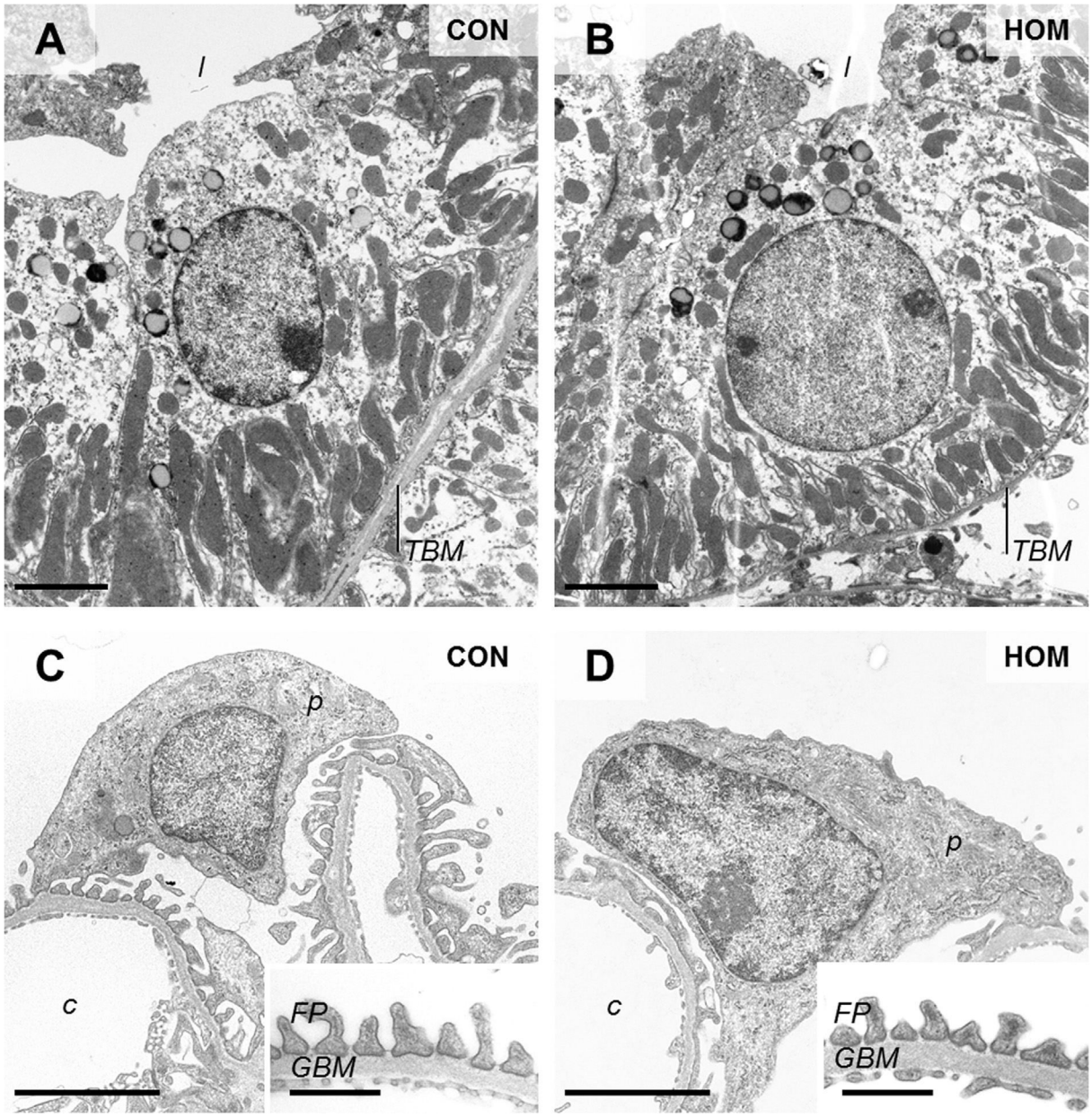

Fig 5. Ultrastructural morphology of TAL cells (A, B), podocytes and peripheral glomerular capillary walls (C, D) in 60-week-old, male, homozygous *Pou3f3*^{L423P} mutant mice (HOM) and non-mutant control mice (CON). Tubular lumen (*l*), tubular basement membrane (*TBM*), podocyte (*p*), glomerular capillary (*c*), podocyte foot processes (*FP*), glomerular basement membrane (*GBM*), Transmission electron microscopy. Bars = 2.5 μm A-D, and = 0.5 μm in insets to C, D.

doi:10.1371/journal.pone.0158977.g005

expression of both proteins in cells of the TAL (Fig 6). Likewise, the co-expression of POU3F3 and AQP2 in CD cells was shown by immunohistochemical detection of these proteins in consecutive sections of kidney tissue (Fig 6).

Quantitative morphological findings

Quantitative morphological data of the renal cortex and the medulla. Corresponding to the significantly decreased kidney volumes, the total volumes of the renal cortex and of the

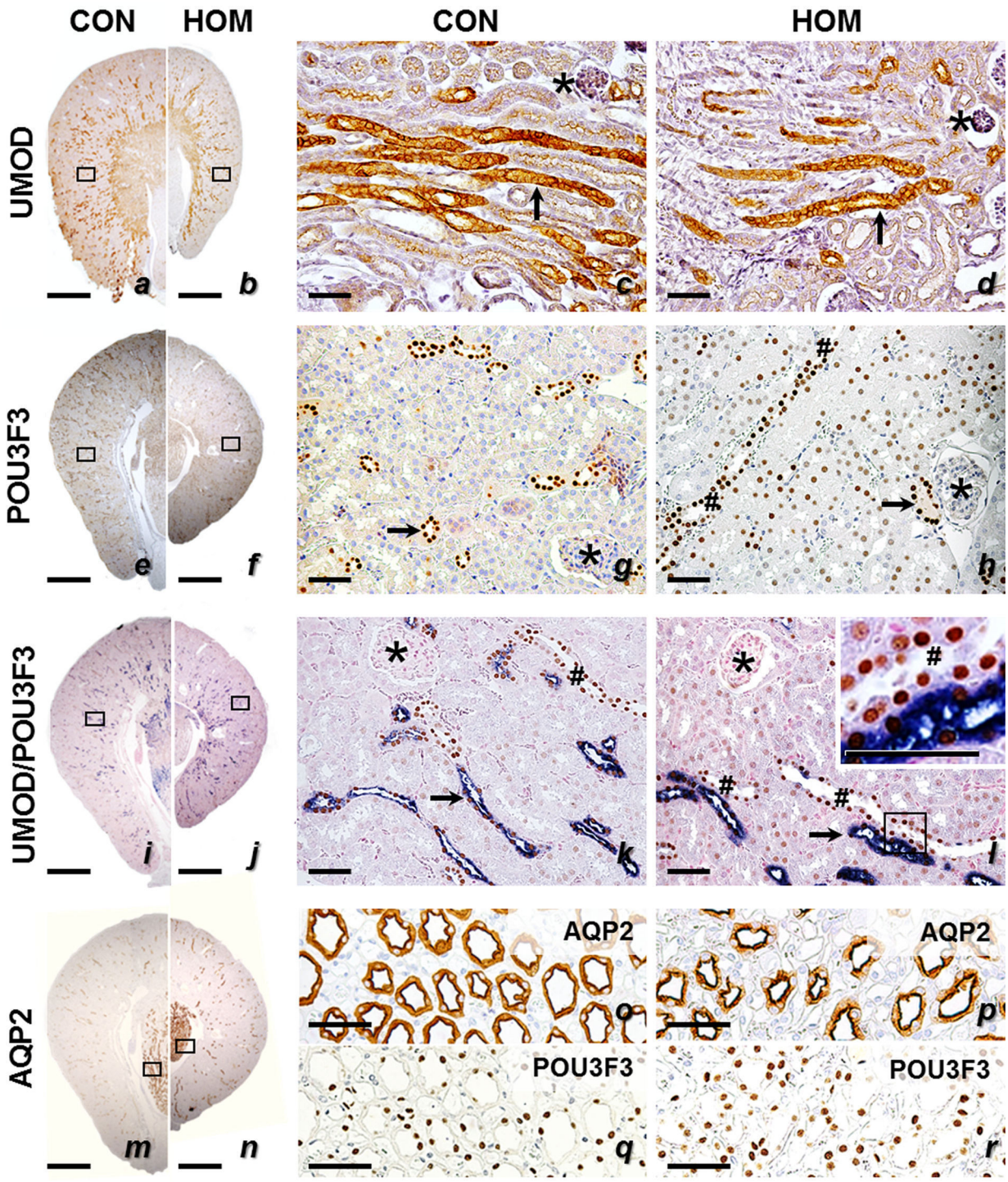

Fig 6. Immunohistochemical detection of uromodulin (UMOD, *a-d*), POU3F3 (*e-l*), and Aquaporin 2 (AQP2, *m-r*) in kidney sections of 60-week-old homozygous *Pou3f3*^{L423P} mutant mice (HOM) and non-mutant control mice (CON). Positive immunoreactivity (UMOD, POU3F3, AQP2 in a-h and m-r) is indicated by brown color (chromogen: DAB). In the double-immunohistochemical detection (i-l), UMOD immunoreactivity is indicated by blue color (chromogen: NBT/BCIP) and POU3F3 by brown color (DAB). Arrows mark the TAL and the MD, CDs are indicated by hashs, and asterisks mark glomeruli. Black rectangles indicate the positions of the detail enlargements. Positive UMOD immunoreactivity with a diffuse cytoplasmic and distinct apical membrane staining pattern is present in epithelial cells of the TAL, POU3F3 immunoreactivity is present in the TAL, the MD and the CDs (nuclear staining pattern), and CD cells display a cytoplasmic staining pattern for the CD marker AQP2. Paraffin sections. Nuclear counterstain: Hemalum. Bars = 1 mm (left row), = 50 μm (middle and right row).

doi:10.1371/journal.pone.0158977.g006

Table 3. Fractional and absolute volumes of cortex and medulla in the kidney of homozygous (HOM) and heterozygous (HET) *Pou3f3*^{L423P} mutant mice and control (CON) mice at 12 days of age.

Parameter	Sex	CON *(6/11)*		HET *(15/15)*		HOM *(7/5)*		*Statistical significance**		
								CON vs. HET	*CON vs. HOM*	*HET vs. HOM*
$V_{V(Cortex/Kid)}$	m	0.65	±0.05	0.66	±0.04	0.69	±0.04	*n.s.*	*n.s.*	*n.s.*
	f	0.65	±0.06	0.66	±0.04	0.71	±0.10	*n.s.*	*n.s.*	*n.s.*
$V_{(Cortex, Kid)}$ [mm^3]	m	42.9	±7.4	39.9	±8.4	29.5	±4.7	*n.s.*	*p<0.05*	*p<0.01*
	f	44.4	±10.1	40.1	±6.4	32.3	±7.2	*n.s.*	*p<0.05*	*n.s.*
$V_{V(Med/Kid)}$	m	0.35	±0.05	0.34	±0.04	0.31	±0.04	*n.s.*	*n.s.*	*n.s.*
	f	0.35	±0.06	0.34	±0.04	0.29	±0.10	*n.s.*	*n.s.*	*n.s.*
$V_{(Med, Kid)}$ [mm^3]	m	22.6	±4.2	19.9	±3.1	13.4	±2.9	*n.s.*	*p<0.01*	*p<0.01*
	f	23.8	±5.7	20.8	±5.5	13.0	±4.8	*n.s.*	*p<0.01*	*n.s.*

Numbers of animals examined are given in brackets (male/female). Data are means ± SD.

*1-way ANOVA with Gabriel's post hoc test; *n.s.* not significant. Male and female mice of the identical genotype did not display statistically significant differences in the listed parameters.

doi:10.1371/journal.pone.0158977.t003

medulla in 12-day-old and in 60-week-old homozygous *Pou3f3*^{L423P} mutant mice were consistently, on average one third, smaller than in age- and sex-matched heterozygous mutants and non-mutant control mice. In contrast, the total cortical and medullary volumes of heterozygous mutants and non-mutant control mice did not differ significantly (Tables 3 and 4). At 12 days of age, male and female mice of identical genotypes displayed approximately equal total volumes of the renal cortex and of the medulla (Table 3).

At 60 weeks of age, however, the total cortical volumes of female animals were significantly smaller than in male homozygous ($p<0.01$) and heterozygous mutants ($p<0.001$). Correspondingly they also showed consistently significantly smaller total medullary volumes ($p<0.01$) than male mice (Table 4).

Quantitative morphological data of the TAL. In juvenile and aged homozygous *Pou3f3*^{L423P} mutant mice, the total volume of the TAL of the loop of Henle ($V_{(TAL, Kid)}$), as well as the volume density of the TAL in the kidney ($V_{V(TAL/Kid)}$), were consistently significantly reduced (on average by 53% and 30% respectively), as compared to age- and sex-matched non-

Table 4. Fractional and absolute volumes of cortex and medulla in the kidney of homozygous (HOM) and heterozygous (HET) *Pou3f3*^{L423P} mutant mice and control (CON) mice at 60 weeks of age.

Parameter	Sex	CON *(7/7)*		HET *(8/7)*		HOM *(6/6)*		*Statistical significance**		
								CON vs. HET	*CON vs. HOM*	*HET vs. HOM*
$V_{V(Cortex/Kid)}$	m	0.72 [b]	±0.03	0.72	±0.04	0.71	±0.04	*n.s.*	*n.s.*	*n.s.*
	f	0.64 [b]	±0.05	0.70	±0.05	0.75	±0.07	*n.s.*	*p<0.01*	*n.s.*
$V_{(Cortex, Kid)}$ [mm^3]	m	292.9 [c]	±70.7	271.8 [c]	±44.4	184.0 [b]	±27.7	*n.s.*	*p<0.01*	*p<0.05*
	f	150.8 [c]	±30.0	155.9 [c]	±34.1	96.8 [b]	±27.7	*n.s.*	*p<0.05*	*p<0.01*
$V_{V(Med/Kid)}$	m	0.28 [a]	±0.03	0.28	±0.04	0.29	±0.04	*n.s.*	*n.s.*	*n.s.*
	f	0.36 [a]	±0.05	0.30	±0.05	0.25	±0.07	*n.s.*	*p<0.05*	*n.s.*
$V_{(Med, Kid)}$ [mm^3]	m	112.3	±25.6	106.3 [b]	±25.6	77.4 [b]	±24.6	*n.s.*	*n.s.*	*n.s.*
	f	86.3	±27.4	65.5 [b]	±18.3	30.8 [b]	±5.8	*n.s.*	*p<0.05*	*p<0.05*

Numbers of animals examined are given in brackets (male/female). Data are means ± SD.

*:1-way ANOVA with Gabriel's post hoc test.

[a,b,c]: Statistically significant differences (a: $p\leq0.05$, b: $p\leq0.01$, c: $p\leq0.001$) between male and female mice of the identical genotype; *n.s.* not significant.

doi:10.1371/journal.pone.0158977.t004

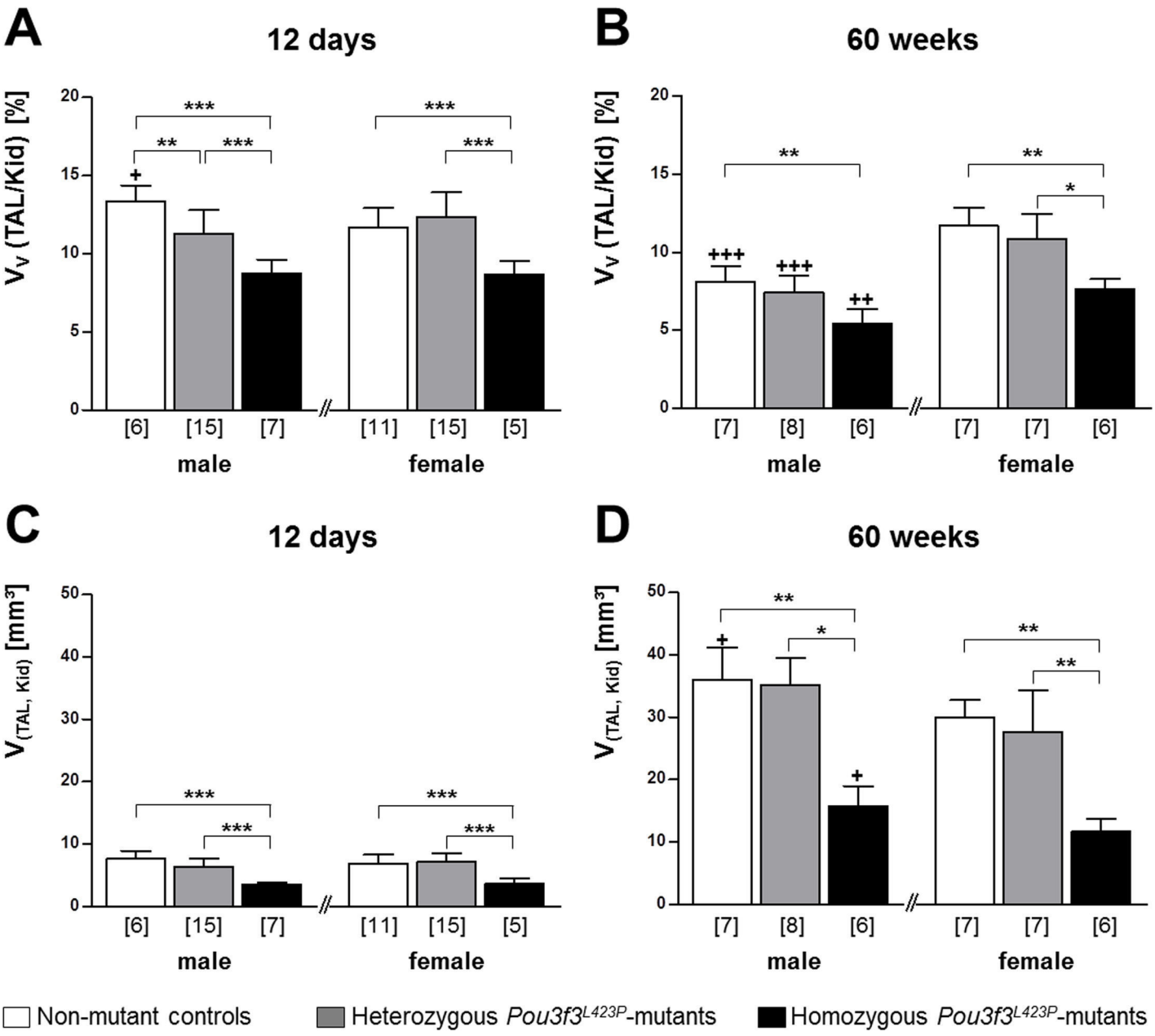

Fig 7. Volume density of TAL cells in the kidney and absolute TAL volumes in 12-day-old (A, C) and 60-week-old (B, D) *Pou3f3*^{L423P} mutant mice and non-mutant control mice. The numbers of animals examined are given in parentheses. Data are means ± SD. Significant differences between homozygous and heterozygous mutants and non-mutant control mice are indicated by asterisks. *: $p < 0.05$, **: $p < 0.01$, ***: $p < 0.001$. Significant differences between male and female mice of identical genotypes are indicated by crosses. +: $p < 0.05$, ++: $p < 0.01$, +++: $p < 0.001$.

doi:10.1371/journal.pone.0158977.g007

mutant control mice ($p<0.001$ at 12 days of age; $p<0.01$ at 60 weeks of age) (Fig 7). Compared to heterozygous mutants the $V_{(TAL, Kid)}$ as well as the $V_{V(TAL/Kid)}$ were also significantly smaller in 12-day-old homozygous mutants ($p<0.001$). In 60-week-old animals the $V_{(TAL, Kid)}$ was significantly smaller in both male ($p<0.05$) and female ($p<0.01$) homozygous *Pou3f3*^{L423P} mutants, whereas the $V_{V(TAL/Kid)}$ was only significantly reduced in female mice ($p<0.05$). In contrast, the total TAL volume and the volume density of the TAL in the kidney of

Table 5. Quantitative stereological data of glomeruli in homozygous (HOM) and heterozygous (HET) Pou3f3^{L423P} mutant mice and control (CON) mice at 12 days of age.

Parameter	Sex	CON *(6/11)*		HET *(15/15)*		HOM *(7/5)*		*Statistical significance**		
								CON vs. HET	*CON vs. HOM*	*HET vs. HOM*
$V_{V(Glom/Kid)}$	m	0.04	±0.00	0.04	±0.01	0.04	±0.01	*n.s.*	*n.s.*	*n.s.*
	f	0.04	±0.01	0.04	±0.00	0.04	±0.01	*n.s.*	*n.s.*	*n.s.*
$V_{(Glom, Kid)}$ [mm^3]	m	1.68	±0.30	1.68	±0.37	1.23	±0.25	*n.s.*	*n.s.*	*p<0.05*
	f	1.85	±0.32	1.70	±0.37	1.33	±0.32	*n.s.*	*p<0.05*	*n.s.*
$V_{(Glom, Kid)}$/body weight [10^3 x mm^3/g]	m	117	±15	117	±16	108	±18	*n.s.*	*n.s.*	*n.s.*
	f	131	±15	121	±22	110	±8	*n.s.*	*n.s.*	*n.s.*
$N_{V(Glom/Kid)}$ [n/mm^3]	m	390	±99	358	±66	306	±38	*n.s.*	*n.s.*	*n.s.*
	f	334	±78	317	±26	295	±33	*n.s.*	*p<0.05*	*n.s.*
$N_{(Glom,Kid)}$ /BW [n/g]	m	176	±33	148	±40	122	±19	*n.s.*	*p<0.05*	*n.s.*
	f	189	±40	157	±20	120	±25	*p<0.05*	*p<0.001*	*p<0.05*
$\bar{v}_{(Glom)}$/BW [10^3 µm^3/g]	m	22.6	±1.8	20.7	±4.1	20.8	±3.9	*n.s.*	*n.s.*	*n.s.*
	f	21.0	±2.6	21.2	±2.4	20.3	±4.0	*n.s.*	*n.s.*	*n.s.*

Numbers of examined animals are given in brackets (male/female). Data are means ± SD.

*:1-way ANOVA with Gabriel's post hoc test; *n.s.* not significant. Male and female mice of the identical genotype did not display statistically significant differences in the listed parameters.

doi:10.1371/journal.pone.0158977.t005

heterozygous mutants and controls were not significantly different, except for the $V_{V(TAL/Kid)}$ in male 12-day-old mice ($p<0.001$) (Fig 7).

Quantitative morphological data of the glomeruli. For quantitative characterization of glomerular alterations, the volume density of the glomeruli in the kidney ($V_{V(Glom/Kid)}$), the total volume ($V_{(Glom, Kid)}$), and the number of nephrons (glomeruli) in the kidney ($N_{(Glom, Kid)}$), and the mean glomerular volume ($\bar{v}_{(Glom)}$) were determined in both 12-day-old, and in 60-week-old mutant mice and non-mutant controls (Tables 5 and 6; Fig 8). In 60-weeks-old *Pou3f3*^{L423P} mutant mice and non-mutant controls, additional quantitative parameters of glomerular morphology were determined, including the mean mesangium volume per glomerulus ($V_{(Mes, Glom)}$), the mean capillary volume per glomerulus ($V_{(Cap, Glom)}$), the average length of the capillaries per glomerulus ($L_{(Cap, Glom)}$), the number of cells per glomerulus ($N_{(C, Glom)}$), the mean podocyte volume ($\bar{v}_{(Pod)}$), the filtration slit frequency (FSF), and the thickness of the glomerular basement membrane (GBM) (Tables 5–7; Fig 8).

Volume density of the glomeruli in the kidney, total and relative glomerular volume. At 12 days of age, the volume densities of the glomeruli in the kidney were not significantly different between homo- and heterozygous mutants and control mice (Table 5). The total volume of the glomeruli, however, was consistently smaller in homozygous mutants *vs*. control mice, as well as in homo- *vs*. heterozygous mutants, with statistically significant differences in female homozygous mutants *vs*. controls and in male homo- *vs*. heterozygous mutants ($p<0.05$). The total glomerular volumes of heterozygous mutants and control mice were not significantly different (Table 5).

The relative total glomerular volume (total glomerular volume in the kidney in relation to body weight, $V_{(Glom, Kid)}$/BW) was not significantly different between 12-day-old homo- and heterozygous *Pou3f3*^{L423P} mutant mice and non-mutant controls of both sexes (Table 5).

At 60 weeks of age, however, both the volume densities of the glomeruli in the kidney ($p<0.05$) and the total volume of the glomeruli (male $p<0.01$, female $p<0.001$) in homozygous mutant mice were significantly lower as compared to non-mutant control mice. Except for the

glomerular volume density in the kidneys of female mice, the total glomerular volumes ($p<0.01$) and glomerular volume densities ($p<0.05$) in the kidney of homozygous mutants were also significantly reduced as compared to heterozygous mutant mice. In contrast, $V_{V(Glom/Kid)}$ and $V_{(Glom, Kid)}$ were not statistically significantly different between heterozygous *Pou3f3*^{L423P} mutant mice and non-mutant controls (Table 6). In contrast to 12-day-old mice, the relative total glomerular volumes in 60-week-old homozygous *Pou3f3*^{L423P} mutants were markedly reduced, as compared to heterozygous mutant mice and non-mutant control mice, with a statistically significant difference in male homozygous mutants *vs*. controls ($p<0.05$). In contrast, the relative total glomerular volumes of 60-week-old heterozygous mutants and control mice were not significantly different (Table 6).

Total and relative nephron number, mean glomerular volume, and relative mean glomerular volume. Quantitative stereological analyses revealed a marked reduction of the numbers of nephrons (glomeruli) in juvenile and aged homozygous *Pou3f3*^{L423P} mutants as compared to heterozygous mutants and non-mutant controls, being highly significant in both sexes at 12 days of age ($p<0.001$). At 60 weeks of age, nephron numbers were also significantly lower in homozygous mutants as compared to heterozygous ($p<0.05$) and non-mutant controls (male $p<0.001$, female $p<0.05$). On average, male and female homozygous mutants showed 40% lower nephron numbers than age and sex-matched, non-mutant controls. Whereas at 12 days of age, heterozygous mutants displayed also significantly lower nephron numbers than non-mutant controls ($p<0.05$), the nephron numbers in 60-week-old heterozygous mutants and controls did not differ significantly (Fig 8). There were no statistically significant differences between the number of glomeruli in 12-day-old mice and 60-week-old mice of identical genotype and gender.

In addition to the significantly lower total number of nephrons, the relative nephron numbers (total nephron number per body weight, $N_{(Glom,Kid)}/BW$) were reduced, reaching statistical significance in 12-day-old male ($p<0.05$) and female ($p<0.001$) homozygous mutants, as well as in male homozygous mutants of 60 weeks of age ($p<0.05$) compared to non-mutant control mice (Tables 5 and 6). The relative nephron numbers of homozygous *vs*. heterozygous mutants and of heterozygous mutants *vs*. control mice were only significantly reduced in female mice of 12 days of age ($p<0.05$), but not in 12-day-old male mice, or in mice of 60 weeks of age (Tables 5 and 6).

Confirming the qualitative histological findings, the stereologically determined mean glomerular volumes of homozygous *Pou3f3*^{L423P} mutants were significantly reduced as compared to control mice in both juvenile (male $p<0.01$, female $p<0.05$) and aged animals (male $p<0.01$, female $p<0.001$) (Fig 8). On average, male and female homozygous mutants of both examined age groups displayed 27% smaller mean glomerular volumes than their age- and sex-matched controls. In both examined age groups, a statistically significant difference between the lower mean glomerular volumes in homo- *vs*. heterozygous mutant mice was only present in male mice ($p<0.05$). The mean glomerular volumes in heterozygous mutants and in control mice were not significantly different between both examined stages of age (Fig 8). In contrast to the striking reduction of the mean glomerular volumes, the relative mean glomerular volumes (related to body weight) did not display statistically significant differences between homo- and heterozygous mutants and non-mutant control mice of 12 days or 60 weeks of age (Tables 5 and 6).

Additional quantitative parameters of glomerular morphology of 60-week-old mice. In 60-week-old mice, the volume densities of the mesangium in the glomeruli were similar in all examined genotype groups. Corresponding to their lower mean glomerular volume, homozygous *Pou3f3*^{L423P} mutant mice also displayed lower mean mesangial volumes per glomerulus ($V_{(Mes, Glom)}$) than heterozygous mutants and control mice, and heterozygous mutants

Table 6. Quantitative stereological data of glomeruli and glomerular subcompartments in homozygous (HOM) and heterozygous (HET) *Pou3f3*^{L423P} mutant mice and control (CON) mice at 60 weeks of age.

Parameter	Sex	CON *(7/7)*		HET *(8/7)*		HOM *(6/6)*		*Statistical significance**		
								CON vs. HET	*CON vs. HOM*	*HET vs. HOM*
$V_{V(Glom/Kid)}$	m	0.018 [c]	±0.004	0.017 [c]	±0.003	0.013 [c]	±0.002	*n.s.*	*p<0.05*	*p<0.05*
	f	0.030 [c]	±0.003	0.026 [c]	±0.005	0.023 [c]	±0.004	*n.s.*	*p<0.05*	*n.s.*
$V_{(Glom, Kid)}$ [mm^3]	m	5.35	±1.57	4.69	±0.97	2.28	±0.59	*n.s.*	*p<0.01*	*p<0.01*
	f	4.44	±0.89	4.00	±0.81	2.27	±0.82	*n.s.*	*p<0.001*	*p<0.01*
$V_{(Glom, Kid)}$/body weight [10^3 x mm^3/g]	m	136	±41	121	±21	85	±17	*n.s.*	*p<0.05*	*n.s.*
	f	120	±27	136	±61	98	±28	*n.s.*	*n.s.*	*n.s.*
$N_{V(Glom/ Kid)}$ [n/mm^3]	m	72 [b]	±20	62 [b]	±10	59 [b]	±9	*n.s.*	*n.s.*	*n.s.*
	f	114 [b]	±27	110 [b]	±38	130 [b]	±20	*n.s.*	*n.s.*	*n.s.*
$N_{(Glom, Kid)}$ /BW [n/g]	m	386	±43	341	±70	301 [a]	±38	*n.s.*	*p<0.05*	*n.s.*
	f	344	±85	409	±131	403 [a]	±75	*n.s.*	*n.s.*	*n.s.*
$\bar{v}_{(Glom)}$/BW [10^3 μm^3/g]	m	7.9	±1.9	6.6	±1.2	6.0	±0.7	*n.s.*	*p<0.05*	*n.s.*
	f	6.9	±0.9	7.9	±2.8	6.1	±1.2	*n.s.*	*n.s.*	*n.s.*
$V_{V(Mes/Glom)}$	m	0.28	±0.04	0.23	±0.02	0.26	±0.08	*n.s.*	*n.s.*	*n.s.*
	f	0.25	±0.04	0.25	±0.04	0.26	±0.07	*n.s.*	*n.s.*	*n.s.*
$V_{(Mes, Glom)}$ [$x10^3$ μm^3]	m	86 [a]	±18	58	±12	40	±8	*p<0.01*	*p<0.001*	*n.s.*
	f	66 [a]	±9	57	±11	35	±6	*n.s.*	*p<0.01*	*p<0.05*
$V_{V(Cap/Glom)}$	m	0.44[b]	±0.03	0.51	±0.02	0.47	±0.05	*p<0.01*	*n.s.*	*n.s.*
	f	0.50 [b]	±0.04	0.50	±0.06	0.44	±0.06	*n.s.*	*n.s.*	*n.s.*
$V_{(Cap, Glom)}$ [$x10^3$ μm^3]	m	137	±42	130	±30	76	±18	*n.s.*	*p<0.05*	*p<0.05*
	f	139	±37	114	±15	63	±21	*n.s.*	*p<0.01*	*n.s.*
$V_{V(Pod/Glom)}$	m	0.28	±0.02	0.26	±0.01	0.27	±0.04	*n.s.*	*n.s.*	*n.s.*
	f	0.26	±0.04	0.26	±0.04	0.29	±0.03	*n.s.*	*n.s.*	*n.s.*
$\bar{v}_{(Pod, Glom)}$ [$x10^3$ μm^3]	m	87	±23	67	±18	44	±12	*n.s.*	*p<0.01*	*n.s.*
	f	71	±22	60	±15	41	±12	*n.s.*	*p<0.05*	*n.s.*
$L_{V(Cap/Glom)}$ [mm/mm^3]	m	0.014	±0.003	0.018	±0.003	0.019	±0.004	*n.s.*	*n.s.*	*n.s.*
	f	0.017	±0.003	0.020	±0.003	0.020	±0.004	*n.s.*	*n.s.*	*n.s.*
$L_{(Cap, Glom)}$ [mm]	m	4.2	±0.5	4.3	±0.4	3.0	±0.4	*n.s.*	*p<0.001*	*p<0.001*
	f	4.5	±0.6	4.7	±0.5	2.8	±0.5	*n.s.*	*p<0.05*	*p<0.05*
$L_{(Glom-cap, Kid)}$ [m]	m	72	±12	81	±14	42	±9	*n.s.*	*p<0.05*	*p<0.01*
	f	76	±13	81	±16	45	±11	*n.s.*	*p<0.05*	*p<0.01*
$N_{V(C/Glom)}$ [$n/10^5$ μm^3]	m	95	±12	101	±11	105 [a]	±7	*n.s.*	*n.s.*	*n.s.*
	f	108	±16	111	±6	128 [a]	±16	*n.s.*	*n.s.*	*n.s.*
$N_{(C, Glom)}$	m	277	±45	258	±66	168	±20	*n.s.*	*p<0.01*	*p<0.05*
	f	295	±65	252	±24	175	±36	*n.s.*	*p<0.01*	*n.s.*
$N_{V(M-E/Glom)}$ [$n/10^5$ μm^3]	m	58	±8	61	±14	57 [a]	±4	*n.s.*	*n.s.*	*n.s.*
	f	68	±13	66	±2	74 [a]	±16	*n.s.*	*n.s.*	*n.s.*
$N_{(M-E,Glom)}$	m	173	±43	159	±63	91	±16	*n.s.*	*p<0.05*	*n.s.*
	f	189	±70	153	±22	104	±36	*n.s.*	*p<0.01*	*n.s.*
$N_{V (Pod/Glom)}$ [$n/10^5$ μm^3]	m	37	±8	41	±8	48	±6	*n.s.*	*n.s.*	*n.s.*
	f	40	±10	44	±6	54	±13	*n.s.*	*n.s.*	*n.s.*
$N_{(Pod,Glom)}$	m	104	±5	100	±9	76	±5	*n.s.*	*p<0.001*	*p<0.01*
	f	106	±7	100	±3	72	±7	*n.s.*	*p<0.001*	*p<0.01*
$\bar{v}_{(Pod)}$	m	811	±204	675	±161	574	±122	*n.s.*	*n.s.*	*n.s.*
	f	602	±141	594	±161	572	±165	*n.s.*	*n.s.*	*n.s.*

Numbers of animals examined are given in brackets (male/female). Data are means ± SD.

*:1-way ANOVA with Gabriel's post hoc test.

[a,b,c]: Statistically significant differences (a: $p \leq 0.05$, b: $p \leq 0.01$, c: $p \leq 0.001$) between male and female mice of the identical genotype; *n.s.* not significant.

doi:10.1371/journal.pone.0158977.t006

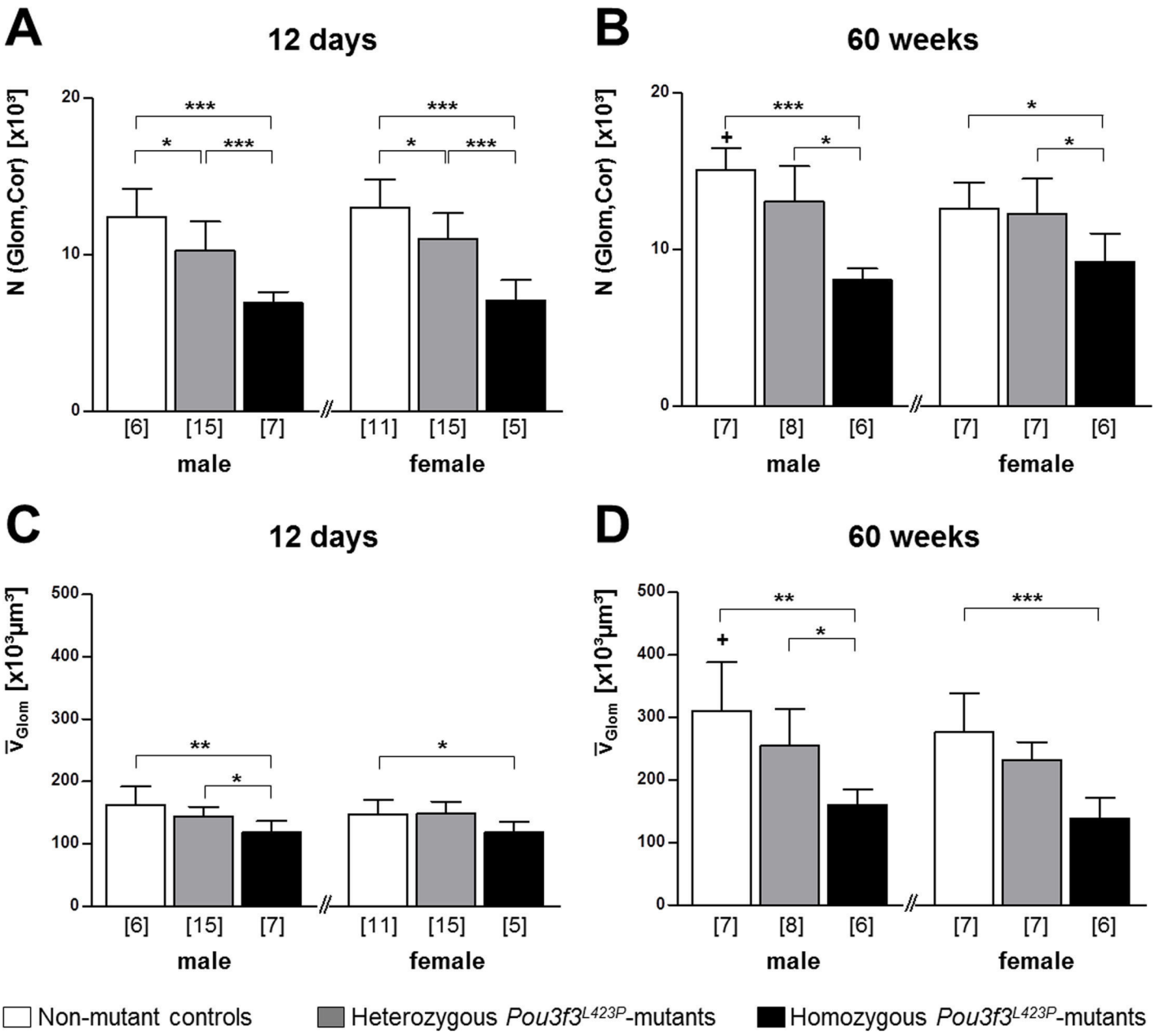

Fig 8. Number of glomeruli per kidney and mean glomerular volumes in 12-day-old (A, C) and 60-week-old (B, D) *Pou3f3*^{L423P} mutant mice and non-mutant control mice. The numbers of examined animals are given in parentheses. Data are means ± SD. Significant differences between homozygous and heterozygous mutants and non-mutant control mice are indicated by asterisks. *: $p < 0.05$, **: $p < 0.01$, ***: $p < 0.001$. Significant differences between male and female mice of identical genotypes are indicated by crosses. +: $p < 0.05$, ++: $p < 0.01$, +++: $p < 0.001$.

doi:10.1371/journal.pone.0158977.g008

displayed lower mean mesangial volumes per glomerulus than control mice (Table 6). These differences reached statistical significance in homozygous *vs*. control mice (male $p<0.001$, female $p<0.01$), female homozygous *vs*. heterozygous mutant mice ($p<0.05$), and male heterozygous mutants *vs*. control mice ($p<0.01$).

The mean capillary volume per glomerulus ($V_{(Cap,\ Glom)}$) of homozygous *Pou3f3*^{L423P} mutant mice of both sexes was significantly lower as compared to non-mutant controls ($p<0.05$). Compared to heterozygous mutants only male homozygous mutants showed a

Table 7. True harmonic mean thickness of the glomerular basement membrane (GBM) and filtration slit frequency (FSF) in homozygous (HOM) and heterozygous (HET) *Pou3f3*^{L423P} mutant mice and control (CON) mice at 60 weeks of age.

Parameter	Sex	CON *(7/7)*		HET *(8/7)*		HOM *(6/6)*		*Statistical significance**		
								CON vs. HET	*CON vs. HOM*	*HET vs. HOM*
$Th_{(GBM)}$ [nm]	m	178	±12	185	±11	156	±13	*n.s.*	*n.s.*	*p<0.05*
	f	164	±6	178	±12	146	±4	*n.s.*	*n.s.*	*p<0.05*
FSF [n/mm GBM]	m	2504	±194	2568	±179	2573	±67	*n.s.*	*n.s.*	*n.s.*
	f	2560	±189	2517	±61	2631	±158	*n.s.*	*n.s.*	*n.s.*

Numbers of animals examined are given in brackets (male/female). Data are means ± SD.

*:1-way ANOVA with Gabriel's post hoc test.

[a,b,c]: Statistically significant differences (a: p≤0.05, b: p≤0.01, c: p≤0.001) between male and female mice of the identical genotype; *n.s.* not significant.

doi:10.1371/journal.pone.0158977.t007

statistical significant reduction ($p<0.05$). The mean length of the capillaries per glomerulus ($L_{(Cap, Glom)}$) was significantly reduced in homozygous mutants as compared to both heterozygous mutants and non-mutant controls (male $p<0.001$, female 0.05). Concordingly the total length of the glomerular capillaries in the kidney ($L_{(Glom\text{-}cap, Kid)}$) in homozygous *Pou3f3*^{L423P} mutant mice was consistently significantly lower than in heterozygous mutants ($p<0.01$) and non-mutant control mice ($p<0.05$). In contrast, these parameters were not significantly different between heterozygous mutant mice and controls (Table 6).

Corresponding to their smaller mean glomerular volumes, male and female homozygous *Pou3f3*^{L423P} mutant mice exhibited significantly lower numbers of cells per glomerulus than sex-matched control mice ($p<0.01$, on average -37%). Compared to sex-matched heterozygous mutant mice, male, but not female homozygous mutant mice also displayed a significantly lower total number of cells per glomerulus ($p<0.05$). In contrast, the total number of cells per glomerulus was not significantly different between heterozygous mutants and control mice of both sexes (Table 6). Concordantly, homozygous *Pou3f3*^{L423P} mutant mice exhibited significantly reduced numbers of podocytes ($p<0.001$) and of mesangial and endothelial cells per glomerulus as compared to control mice (male $p<0.05$, female $p<0.01$). Except for the significantly reduced number of podocytes per glomerulus in male homo- *vs*. heterozygous mutants ($p<0.01$), heterozygous mutant mice did not display significantly different podocyte or mesangial and endothelial cell numbers per glomerulus as compared to homozygous mutants or non-mutant control mice (Table 6). The mean podocyte volumes were not significantly different between mice of the three examined genotypes (Table 6). The true harmonic mean thickness of the GBM of homozygous *Pou3f3*^{L423P} mutant mice of both sexes was significantly smaller (about -20%) than in heterozygous mutants ($p<0.05$), whereas there were no significant differences in GBM thickness between homozygous mutants and controls, or between heterozygous mutants and control mice (Table 7). The number of filtration slits between adjacent podocyte foot processes per length of the GBM was virtually equal in all examined groups of mice (Table 7).

Renal POU3F3 mRNA and protein abundance

Quantitative RT-real time PCR (RT-qPCR) analyses (Fig 9A and 9B) did not reveal statistically significantly different relative renal *Pou3f3* mRNA abundances (relative to *Gapdh*) in homozygous and heterozygous *Pou3f3*^{L423P} mutant mice and non-mutant control mice. The relative renal mRNA abundances of *Umod* (relative to *Gapdh*), however, were significantly lower in homozygous *Pou3f3*^{L423P} mutant mice than in non-mutant control mice ($p<0.05$), and in male homo- *vs*. heterozygous mutants ($p<0.05$). Correspondingly, homozygous *Pou3f3*^{L423P} mutant

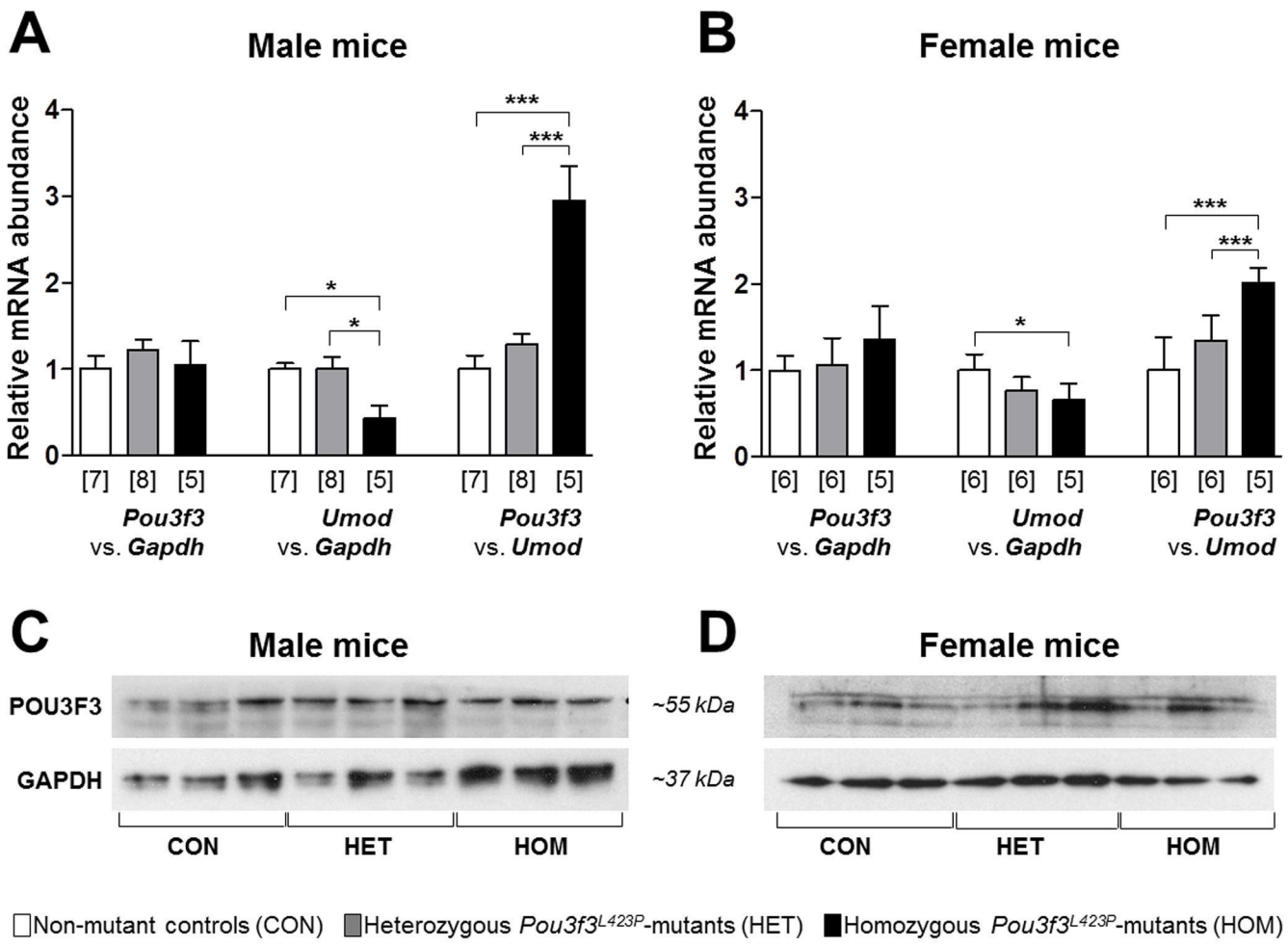

Fig 9. RT-qPCR (A, B) and Western blot analyses (C, D) of relative POU3F3 abundances in the kidneys of 60-week-old (B, D) homozygous (HOM) and heterozygous (HET) *Pou3f3*^{L423P} mutant mice and non-mutant control mice (CON). The relative mRNA abundances (*Pou3f3* vs. *Gapdh*, *Umod* vs. *Gapdh*, and *Pou3f3* vs. *Umod*) were normalized to the corresponding mean relative mRNA abundances of non-mutant control mice. The numbers of animals examined are given in parentheses. Data are means ± SD. Significant differences between homozygous and heterozygous mutants and non-mutant control mice are indicated by asterisks. *: $p < 0.05$, **: $p < 0.01$, ***: $p < 0.001$.

doi:10.1371/journal.pone.0158977.g009

mice displayed significantly higher relative renal *Pou3f3* mRNA abundances (relative to *Umod*) than heterozygous mutants ($p<0.001$) and non-mutant control mice ($p<0.001$). By Western-blot analysis, renal POU3F3 protein was detectable in total kidney protein lysates of homozygous and heterozygous *Pou3f3*^{L423P} mutant mice, as well as in non-mutant control mice (Fig 9C and 9D).

Discussion

In the mammalian kidney, development of functioning nephrons in adequate numbers (*i.e.*, nephron endowment) depends on the proper induction of nephrons in the embryonic metanephros, the subsequent transition of the renal vesicles into segmented nephrons (nephron patterning), and the maturation of the different nephron segments. These processes are

controlled by complex, temporally and spatially coordinated interaction networks of several different transcription- and growth factors, receptors, and signaling molecules/cascades that regulate nephro-nephronogenesis by activation or repression of genes in specific cell types [4,6,7]. The early fetal induction of ureteric bud branching, the accurate signaling between the tips of the developing ureteric bud and the surrounding metanephric mesenchyme leading to formation the renal vesicle (nephron induction), the subsequent metanephric mesenchymal to epithelial transformation in the renal vesicle and its conversion to primitive nephrons (comma- and S-shaped bodies) is controlled by transcriptional pathways, *inter alia* involving the glial-derived neurotrophic factor (GDNF) and CRET (ret proto-oncogene) signaling pathway, the WNT-beta-catenin cascade, and transcription- and inducing factors as EYA1 (eyes absent homolog 1 transcriptional coactivator and phosphatase 1), LIF (leukemia inhibitory factor), FGF2 (fibroblast growth factor 2), and TGFB2 (transforming growth factor beta 2) [4,6,7]. The subsequent patterning of the nephron, *i.e*., the formation of distinct differentiated tubular segments along the proximal–distal nephron axis, and the invasion of capillaries and further differentiation to immature glomeruli is governed by transcription factors such as WT1 (Wilms' tumor 1), LHX1 (LIM homeobox 1), POU3F3, and DLL1 (delta-like 1). Here, Notch–Delta pathway signaling particularly determines the patterning of proximal tubular nephron segments, whereas the fate of the distal nephron is specified by POU3F3 and IRX (iroquois homeobox) transcription factors [4,6,7]. However, the exact functions, the manifold interactions, and the regulatory hierarchies of all different factors involved in nephro-nephronogenesis are not yet fully clarified. In mice, the final maturation of the glomeruli, different tubular nephron segments, and the CDs is completed around postnatal day 7–10 [42].

The putative functions of several nephrogenetic factors were discovered and studied in genetically modified rodent models, where the complete or partial loss of function of a single growth or transcription factor led to a distinct phenotype, as, *e.g*., a typical malformation of the entire kidney, or of a distinct nephron segment [43–45]. Likewise, the important role of POU3F3 in nephron patterning during nephrogenesis, particularly for formation, differentiation, elongation, and maturation of the thick ascending limb (TAL) of the loop of Henle and the differentiation of the macula densa (MD) was discovered in *Pou3f3* knock-out mice and reported by Nakai *et al*. in 2003 [5]. In the developing nephron, *Pou3f3* expression was detected in distal renal vesicles, S-shaped bodies, and nephron regions that develop into the TAL, the MD, and the distal convoluted tubule, where *Pou3f3* expression also persists in the mature nephron. In the kidneys of homozygous *Pou3f3* knock-out mice, the TAL is largely absent at birth [5]. New-born homozygous *Pou3f3* knock-out mice exhibit increased plasma urea and potassium levels and die from renal failure within 24 hours after birth [5].

Possible mechanisms how POU3F3 deficiency triggers underdevelopment of the TAL include reduced cell proliferation and early onset of apoptosis in the primitive nephron loops of homozygous *Pou3f3* knock-out embryos [5].

Indicating a gene-dosage dependent role of POU3F3 in regulation of gene expression in the TAL, adult heterozygous *Pou3f3* knock-out mice display reduced expression levels of genes normally expressed in the TAL (including *Umod*, *Nkcc2*, and different K^+ and Cl^- channels). However, there is no evidence for an altered cellular morphology or limitation of normal TAL function heterozygous knock-out mice, as shown by histological and ultrastructural analyses and by unaltered blood/serum levels of urea, creatinine, Na^+, K^+, Cl^-, and normal urine osmolality and volumes [5].

The present study analyzed *Pou3f3*^{L423P}-mice, a mutant mouse line that was recently generated in the Munich ENU-Mouse-Mutagenesis project [15,16]. The point mutation in the *Pou3f3* gene is not lethal and, in contrast to homozygous *Pou3f3*-knock-out mice, homozygous *Pou3f3*^{L423P} mutant mice are viable and fertile [16] and thus can be used to study the effects of

the POU3F3 mutation on renal development, morphology, and function in the postnatal life. Adult homozygous *Pou3f3*^{L423P} mutant mice have previously been shown to display increased plasma urea levels, along with several other metabolic changes, including increased creatinine, chloride, and potassium serum levels, as well as a decreased bone mineral density and bone mineral content, indicative for impaired renal function, [5,16].

To analyze both immediate developmental effects on the nephronogenesis as well as long-term consequences of the *Pou3f3*^{L423P} mutation on renal function and morphology, homo- and heterozygous mutant mice and non-mutant controls were examined at 12 days, around completion of nephronogenesis [12], and at 60 weeks of age. For a comprehensive morphological analysis of the development, growth and cellular composition of distinct nephron segments, such as the TAL and the glomeruli, qualitative histological and ultrastructural examinations, as well as unbiased, design-based quantitative stereological methods were applied [46–48]. The results of these analyses confirmed the significant role of POU3F3 in nephrogenesis, and particularly in the development of the TAL, which is in line with the findings in *Pou3f3* knock-out mice reported by Nakai *et al.* [5]. Both 12-day-old and 60-week-old homozygous *Pou3f3*^{L423P} mutant mice displayed significantly smaller kidney weights and volumes than non-mutant controls, as well as significantly lower total TAL volumes and volume densities of the TAL in the kidney. Given the important function of the TAL in renal nitrogen metabolism [8,49], the incomplete formation of the TAL might provide an explanation for the increased serum urea concentrations detected in homozygous *Pou3f3*^{L423P} mutants [5,16].

In further accordance with the findings by Nakai *et al*., the present study immunohistochemically detected POU3F3 in the TAL and the MD of both juvenile and aged, mutant and non-mutant mice, confirming the importance of POU3F3 in fetal development of the TAL, and providing additional evidence for its putative role in maintenance of the function of the TAL in the developed kidney [5]. Additionally, the present study detected a positive POU3F3 immunostaining in CD cell nuclei of the mature kidney, which has not been described in the developing kidney [5].

Basically, a meaningful quantitative comparison of the effects of a complete POU3F3 deficiency in *Pou3f3* knock-out mice with the consequences of the *Pou3f3*^{L423P} mutation on the extent of TAL under-development is not possible, since mice of different ages and different genetic backgrounds were investigated, and since the extent of TAL under-development was only semiquantitatively assessed in the study of Nakai *et al.* [5]. However, marked alterations of the cellular morphology and the ultrastructure of TAL cells, as observed in *Pou3f3* knock-out mice [5], were not present in homozygous *Pou3f3*^{L423P} mutants examined in the present study. In addition to the underdevelopment of the TAL, quantitative stereological analyses revealed a striking, significant reduction of the absolute nephron numbers and the relative numbers of nephrons per body weight, as well as a significant decrease of the mean glomerular volume (but not of the relative mean glomerular volume per body weight) in the kidneys of homozygous *Pou3f3*^{L423P} mutants, present at 12 days of age. The same findings were also present in aged, 60-week-old homozygous *Pou3f3*^{L423P} mutant mice, except for the relative nephron number, which was only significantly reduced in male, but not in female homozygous mutants *vs*. control mice. In *Pou3f3* knock-out mice, a comparable effect of abolished POU3F3 function on reduction of the numbers and sizes of glomeruli has not been reported, probably because nephronogenesis and glomerular development are still in progress in newborn mice [12], or due to application of a less accurate method for quantification and sizing of glomeruli. Therefore, in addition to its known role in nephron patterning (*i.e*., development of the TAL), the results of the present study show that POU3F3 is also involved in determination of the final nephron number (nephron endowment) of the mature mouse kidney. In this context, the reduction of the absolute nephron number in homozygous mutants vs. control mice actually

appears to represent the decisive parameter, rather than alterations of the relative nephron number. Studies in different mouse strains did reveal a correlation between kidney- and body weight at birth and at adulthood, but not between the number of nephrons and body weight or between nephron number and kidney size [50]. Therefore, the finding that a significant reduction of the relative nephron number, as observed in male and female 12-day-old homozygous *Pou3f3*^{L423P} mutants, was only present in male, but not in female homozygous mutants of 60 weeks of age does not contradict a role of POU3F3 for nephron endowment of the kidney.

Long-term consequences of the quantitative reduction of the TAL were essentially restricted to functional alterations of the tubular system, like alterations in serum and urine parameters (i.e., elevation of serum urea concentrations and decreased specific urine gravities), whereas no further pathomorphological alterations of the tubular system were detected in the kidneys of aged homozygous *Pou3f3*^{L423P} mutants. In these mice, the *Pou3f3* mutation and the altered TAL did also not exert detectable effects on glomerular function, as the serum cystatin C concentration, urine albumin excretion, and blood pressure were unaffected in aged mutant mice. Apart from the reduced nephron number and the diminished size of the glomeruli, no functional, qualitative or quantitative morphological alterations were detected in aged, 60-week-old *Pou3f3*^{L423P} mutant mice. Protein analyses of spot urine samples did not reveal any evidence for an increased urinary albumin excretion in *Pou3f3*^{L423P} mutant mice as compared to non-mutant controls. These findings are in line with previously reported results of analyses of 24-hour urine samples, where the urinary albumin and total protein excretion per day was not significantly different between homozygous *Pou3f3*^{L423P} mutants and control mice of 15 weeks of age [16]. Moreover, no evidence of histological or ultrastructural glomerular lesions was present in *Pou3f3*^{L423P} mutants, and quantitative morphological parameters, such as the GBM thickness, or the mean podocyte volume, representing sensitive and early indicators of glomerular damage [17,27,32] were similar in mutant mice and non-mutant controls. Thus, the reduced nephron endowment in mutant mice did obviously not cause functionally relevant alterations of the glomerular morphology.

In the present study, RT-qPCR and Western-blot analyses did not reveal evidence for a reduced mRNA or protein abundance of POU3f3 in the kidneys of homozygous or heterozygous *Pou3f3*^{L423P} mutant mice, as compared to non-mutant control mice. A possible explanation for the observed differences in *Pou3f3* knock-out and *Pou3f3*^{L423P} mutant mice, such as the neonatal death in *Pou3f3* knock-out mice, might lie in an altered, but not completely abolished activity of the mutant POU3F3 protein. The *Pou3f3*^{L423P} mutation is located in the conserved homeobox domain of the protein and might therefore alter the transcriptional regulation of all or a subset of POU3F3 target genes. Additionally, lack of distinct POU3F3 functions in homozygous mutant mice might partially be compensated by unknown other, synergistically acting factors. Finally, the milder phenotype of heterozygous *Pou3f3* knock-out mice and of heterozygous *Pou3f3*^{L423P} mutants can also be interpreted as a gene-dose dependent effect [5]. However, further studies are necessary to clear the exact molecular mechanisms, how POU3F3 participates in regulation of nephrogenesis and maintenance of TAL function in the mature kidney, including the timely and spatially coordinated transcriptional control of its target-genes, interaction with other factors, and potential modulation of different signaling pathways regulating cell proliferation, differentiation, and apoptosis [5]. In these studies, *Pou3f3*^{L423P} mutant mice might prove a useful model system.

Finally, the observed reduction in the nephron number in homozygous *Pou3f3*^{L423P} mutant mice is of particular interest, since a low nephron endowment is considered as an important individual risk factor for development of diverse chronic kidney diseases in humans [51–53]. Several studies in human beings and animal models have shown that low nephron numbers are often associated with glomerular hypertrophy [43,54,55], a pathogenetic key lesion for

development of glomerulosclerosis [56,57], and with hypertension [52,58–60]. In this context, the *a priori* low number of nephrons is seen as a "first hit", predisposing the kidney to a facilitated development of glomerular hypertrophy, promoting subsequent establishment of glomerulosclerotic lesions, progressive loss of nephrons and renal function, and establishment of hypertension, if challenged by a "second hit", as e.g., a primary nephropathy, diabetes mellitus, or obesity [53,61–63]. The exact pathomechanisms how a low nephron endowment may favor the development of glomerular hypertrophy (e.g., by induction of compensatory glomerular growth [43] mediated by glomerular growth factors [56,64]) or hypertension (e.g., by inappropriate activation of the renin angiotensin system, impaired tubular salt excretion causing salt and volume retention, or by structural alterations of peritubular vessels) are, however, not completely understood yet [43]. There are currently only few murine models of genetically determined low nephron numbers, such as heterozygous *Gdnf* knock-out mice [43,65]. Compared to non-mutant controls, these mice display approximately 33% lower nephron numbers, while their body- and kidney weights are not altered [43,65]. However, apart from a higher occurrence of unilateral renal agenesis in heterozygous *Gdnf* knock-out mice, the reduction of nephron numbers also leads to development of a specific pattern of glomerular alterations, such as glomerular hypertrophy with hyperplasia of endothelial and mesangial glomerular cells and thickening of the glomerular basement membrane (GBM), predisposing the mice to development of glomerular sclerosis [43]. In contrast, a comparable reduction of nephron numbers in homozygous *Pou3f3*^{L423P} mutant mice by 37% on the average was not associated with an "own" pattern of pathological alterations of glomerular morphology and function, such as glomerular hypertrophy, glomerular mesangial and endothelial cell hyperplasia, thickening of the GBM, or albuminuria. Correspondingly, the aged *Pou3f3*^{L423P} mutant mice examined in the present study, did also not display significantly elevated blood pressures or serum sodium concentrations, as compared to sex-matched non-mutant control mice. These findings are in line with the results of a previous study [16], where the 24-hrs-urine-volumes, as well as the daily urinary sodium excretion in homozygous *Pou3f3*^{L423P} mutant mice were not significantly lower than in non-mutant control mice. The lack of pathogenetically relevant morphological glomerular alterations and the absence of evidence for altered renal sodium homeostasis or volume retention explain why *Pou3f3*^{L423P} mutant mice do not display systemic hypertension despite their significantly reduced nephron endowment. The lack of primary pathomorphological glomerular lesions and hypertension in homozygous *Pou3f3*^{L423P} mutant mice might actually be advantageous, since it might allow for examination of the effects of reduced nephron numbers independent of concomitant glomerular lesion patterns. This might be particularly important, if *Pou3f3*^{L423P} mutant mice are used as a model for a low nephron endowment in experiments analyzing the role of reduced nephron numbers as a predisposing factor for development of aggravated renal/glomerular lesions. Such an experimental approach could comprise the comparison of a group of homozygous *Pou3f3*^{L423P} mutant mice and a group of mice with "normal" nephron numbers, both being challenged with an additional renal insult.

In summary, the results of the present study confirm the important function of POU3F3 in nephron patterning, especially in development of the TAL. Additionally, we provide strong evidence that POU3F3 is also involved in nephron induction, the determination of nephron numbers, and in nephron size in the murine kidney. The detailed characterization of the renal morphology and function of *Pou3f3*^{L423P} mutants provides the basis for their use as an experimental animal model of low nephron numbers in nephrological research, as well as in further studies examining the molecular and cellular functions of POU3F3 during nephrogenesis.

Supporting Information

S1 Table. Exact p values of statistically analyzed* parameters of homozygous (HOM) and heterozygous (HET) *Pou3f3*^{L423P} mutant mice and control (CON) mice at 12 days of age. *Statistically significant differences between genotypes were determined by using a 1-way ANOVA with Gabriel's post hoc test, differences between male and female mice of the identical genotype by Student's t-test.
(DOCX)

S2 Table. Exact p values of statistically analyzed* parameters of homozygous (HOM) and heterozygous (HET) *Pou3f3*^{L423P} mutant mice and control (CON) mice at 60 weeks of age. UACR: Urine albumin-to-creatinine ratio. *Statistically significant differences between genotypes were determined by using a 1-way ANOVA with Gabriel's post hoc test, differences between male and female mice of the identical genotype by Student's t-test.
(DOCX)

Acknowledgments

The authors thank Prof. Dr. Wegener (Institute of Biochemistry, Emil Fischer Center, University Erlangen-Nuremberg, Germany) for providing the BRN1 antibody, Lisa Pichl, Heike Sperling, Claudia Mair and Heidrun Schöl (Institute of Veterinary Pathology at the Centre for Clinical Veterinary Medicine, Ludwig-Maximilians-Universität München, Munich, Germany), and Tatjana Schröter, Kathrin Hedegger, Christine Hösl, and Franziska Kreß (Chair for Molecular Animal Breeding and Biotechnology and Laboratory for Functional Genome Analysis, Gene Center, Ludwig-Maximilians-Universität München, Munich, Germany) for excellent technical support.

Author Contributions

Conceived and designed the experiments: AR EK SK BP BA EW RW AB. Performed the experiments: AR EK BP AB. Analyzed the data: AR EK BP RW AB. Contributed reagents/materials/analysis tools: AR EK SK BP BA EW RW AB. Wrote the paper: AR EK SK BP BA EW RW AB.

References

1. Ryan AK, Rosenfeld MG. POU domain family values: flexibility, partnerships, and developmental codes. Genes Dev. 1997; 11: 1207–1225. PMID: 9171367
2. McEvilly RJ, de Diaz MO, Schonemann MD, Hooshmand F, Rosenfeld MG. Transcriptional regulation of cortical neuron migration by POU domain factors. Science. 2002; 295: 1528–1532. PMID: 11859196
3. Sugitani Y, Nakai S, Minowa O, Nishi M, Jishage K, Kawano H, et al. Brn-1 and Brn-2 share crucial roles in the production and positioning of mouse neocortical neurons. Genes Dev. 2002; 16: 1760–1765. PMID: 12130536
4. El-Dahr SS, Aboudehen K, Saifudeen Z. Transcriptional control of terminal nephron differentiation. Am J Physiol Renal Physiol. 2008; 294: F1273–1278. doi: 10.1152/ajprenal.00562.2007 PMID: 18287399
5. Nakai S, Sugitani Y, Sato H, Ito S, Miura Y, Ogawa M, et al. Crucial roles of Brn1 in distal tubule formation and function in mouse kidney. Development. 2003; 130: 4751–4759. PMID: 12925600
6. O'Brien LL, McMahon AP. Induction and patterning of the metanephric nephron. Semin Cell Dev Biol. 2014; 36: 31–38. doi: 10.1016/j.semcdb.2014.08.014 PMID: 25194660
7. Schedl A. Renal abnormalities and their developmental origin. Nat Rev Genet. 2007; 8: 791–802. PMID: 17878895
8. Mount DB. Thick ascending limb of the loop of Henle. Clin J Am Soc Nephrol. 2014; 9: 1974–1986. doi: 10.2215/CJN.04480413 PMID: 25318757
9. Pennica D, Kohr WJ, Kuang WJ, Glaister D, Aggarwal BB, Chen EY, et al. Identification of human uromodulin as the Tamm-Horsfall urinary glycoprotein. Science. 1987; 236: 83–88. PMID: 3453112

10. Tamm I, Horsfall FL Jr. Characterization and separation of an inhibitor of viral hemagglutination present in urine. Proc Soc Exp Biol Med. 1950; 74: 106–108. PMID: 15430405
11. Burg MB. Thick ascending limb of Henle's loop. Kidney Int. 1982; 22: 454–464. PMID: 6296522
12. Lechner MS, Dressler GR. The molecular basis of embryonic kidney development. Mech Dev. 1997; 62: 105–120. PMID: 9152004
13. Little MH. Improving our resolution of kidney morphogenesis across time and space. Curr Opin Genet Dev. 2015; 32: 135–143. doi: 10.1016/j.gde.2015.03.001 PMID: 25819979
14. Cullen-McEwen L, Sutherland MR, Black MJ (2016) The Human Kidney: Parallels in Structure, Spatial Development, and Timing of Nephrogenesis. Kidney Development, Disease, Repair and Regeneration: Elsevier. pp. 27–40.
15. Aigner B, Rathkolb B, Herbach N, Kemter E, Schessl C, Klaften M, et al. Screening for increased plasma urea levels in a large-scale ENU mouse mutagenesis project reveals kidney disease models. Am J Physiol Renal Physiol. 2007; 292: F1560–1567. PMID: 17264314
16. Kumar S, Rathkolb B, Kemter E, Sabrautzki S, Michel D, Adler T, et al.Generation and Standardized, Systemic Phenotypic Analysis of Pou3f3L423P Mutant Mice. PLoS One. 2016; 11: e0150472. doi: 10.1371/journal.pone.0150472 PMID: 27003440
17. Herbach N, Schairer I, Blutke A, Kautz S, Siebert A, Goke B, et al.Diabetic kidney lesions of GIPR^{dn} transgenic mice: podocyte hypertrophy and thickening of the GBM precede glomerular hypertrophy and glomerulosclerosis. Am J Physiol Renal Physiol. 2009; 296: F819–829. doi: 10.1152/ajprenal.90665.2008 PMID: 19211686
18. Wanke R, Wolf E, Brem G, Hermanns W. [Role of podocyte damage in the pathogenesis of glomerulosclerosis and tubulointerstitial lesions: findings in the growth hormone transgenic mouse model of progressive nephropathy]. Verh Dtsch Ges Pathol. 2001; 85: 250–256. PMID: 11894406
19. Albl B, Haesner S, Braun-Reichhart C, Streckel E, Renner S, Seeliger F, et al. Tissue Sampling Guides for Porcine Biomedical Models. Toxicol Pathol. 2016; 44: 414–420. doi: 10.1177/0192623316631023 PMID: 26883152
20. Hermanns W, Liebig K, Schulz LC. Postembedding immunohistochemical demonstration of antigen in experimental polyarthritis using plastic embedded whole joints. Histochemistry. 1981; 73: 439–446. PMID: 7035413
21. Hoeflich A, Weber MM, Fisch T, Nedbal S, Fottner C, Elmlinger MW, et al. Insulin-like growth factor binding protein 2 (IGFBP-2) separates hypertrophic and hyperplastic effects of growth hormone (GH)/IGF-I excess on adrenocortical cells in vivo. FASEB J. 2002; 16: 1721–1731. PMID: 12409314
22. Nyengaard JR. Stereologic methods and their application in kidney research. J Am Soc Nephrol. 1999; 10: 1100–1123. PMID: 10232698
23. Kemter E, Prueckl P, Sklenak S, Rathkolb B, Habermann FA, Hans W, et al. Type of uromodulin mutation and allelic status influence onset and severity of uromodulin-associated kidney disease in mice. Hum Mol Genet. 2013; 22: 4148–4163. doi: 10.1093/hmg/ddt263 PMID: 23748428
24. Howard V, Reed MG. Unbiased stereology. New York: Garland Science/BIOS Scientific Publishers; 2004.
25. Sterio DC. The unbiased estimation of number and sizes of arbitrary particles using the disector. J Microsc. 1984: 127–136. PMID: 6737468
26. Blutke A, Schneider MR, Wolf E, Wanke R. Growth hormone (GH)-transgenic insulin-like growth factor 1 (IGF1)-deficient mice allow dissociation of excess GH and IGF1 effects on glomerular and tubular growth. Physiol Rep. 2016;4.
27. Blutke A, Schneider MR, Renner-Muller I, Herbach N, Wanke R, Wolf E. Genetic dissection of IGF1-dependent and -independent effects of permanent GH excess on postnatal growth and organ pathology of mice. Mol Cell Endocrinol. 2014; 394: 88–98. doi: 10.1016/j.mce.2014.07.002 PMID: 25017732
28. Kriz W, Bankir L. A standard nomenclature for structure of the kidney. The Renal Commission of the International Union of Physiological Sciences(IUPS). Anat Embryol (Berl). 1988; 178: N1–8.
29. Kriz W, Koepsell H. The structural organization of the mouse kidney. Z Anat Entwicklungsgesch. 1974; 144: 137–163. PMID: 4472393
30. Weibel ER. Stereological methods I. Practical methods for biological morphometry. London: Academic press; 1979.
31. Herbach N, Bergmayr M, Goke B, Wolf E, Wanke R. Postnatal development of numbers and mean sizes of pancreatic islets and beta-cells in healthy mice and GIPR(dn) transgenic diabetic mice. PLoS One. 2011; 6: e22814. doi: 10.1371/journal.pone.0022814 PMID: 21818396

32. El-Aouni C, Herbach N, Blattner SM, Henger A, Rastaldi MP, Jarad G, et al. Podocyte-specific deletion of integrin-linked kinase results in severe glomerular basement membrane alterations and progressive glomerulosclerosis. J Am Soc Nephrol. 2006; 17: 1334–1344. PMID: 16611717

33. Ramage IJ, Howatson AG, McColl JH, Maxwell H, Murphy AV, Beattie TJ. Glomerular basement membrane thickness in children: a stereologic assessment. Kidney Int. 2002; 62: 895–900. PMID: 12164871

34. Nyengaard JR, Rasch R. The impact of experimental diabetes mellitus in rats on glomerular capillary number and sizes. Diabetologia. 1993; 36: 189–194. PMID: 8462766

35. Massa F, Garbay S, Bouvier R, Sugitani Y, Noda T, Gubler MC, et al. Hepatocyte nuclear factor 1beta controls nephron tubular development. Development. 2013; 140: 886–896. doi: 10.1242/dev.086546 PMID: 23362349

36. Graham LA, Padmanabhan S, Fraser NJ, Kumar S, Bates JM, Raffi HS, et al. Validation of uromodulin as a candidate gene for human essential hypertension. Hypertension. 2014; 63: 551–558. doi: 10.1161/HYPERTENSIONAHA.113.01423 PMID: 24324041

37. Siner JM, Jiang G, Cohen ZI, Shan P, Zhang X, Lee CG, et al.VEGF-induced heme oxygenase-1 confers cytoprotection from lethal hyperoxia in vivo. FASEB J. 2007; 21: 1422–1432. PMID: 17264168

38. Cohen CD, Kretzler M (2003) Gene-Expression Analysis of Microdissected Renal Biopsies. In: Goligorsky MS, editor. Renal disease: Techniques and Protokols. Totowa, New Jersey: Humana Press Inc. pp. 285–293.

39. Smith PK, Krohn RI, Hermanson GT, Mallia AK, Gartner FH, Provenzano MD, et al. Measurement of protein using bicinchoninic acid. Anal Biochem. 1985; 150: 76–85. PMID: 3843705

40. Friedrich RP, Schlierf B, Tamm ER, Bosl MR, Wegner M. The class III POU domain protein Brn-1 can fully replace the related Oct-6 during schwann cell development and myelination. Mol Cell Biol. 2005; 25: 1821–1829. PMID: 15713637

41. Song S, Meyer M, Turk TR, Wilde B, Feldkamp T, Assert R, et al. Serum cystatin C in mouse models: a reliable and precise marker for renal function and superior to serum creatinine. Nephrol Dial Transplant. 2009; 24: 1157–1161. doi: 10.1093/ndt/gfn626 PMID: 19004848

42. Zhong J, Perrien DS, Yang HC, Kon V, Fogo AB, Ichikawa I, et al. Maturational regression of glomeruli determines the nephron population in normal mice. Pediatr Res. 2012; 72: 241–248. doi: 10.1038/pr.2012.81 PMID: 22717689

43. Benz K, Campean V, Cordasic N, Karpe B, Neuhuber W, Mall G, et al. Early glomerular alterations in genetically determined low nephron number. Am J Physiol Renal Physiol. 2011; 300: F521–530. doi: 10.1152/ajprenal.00490.2009 PMID: 20943767

44. Wang Q, Lan Y, Cho ES, Maltby KM, Jiang R. Odd-skipped related 1 (Odd 1) is an essential regulator of heart and urogenital development. Dev Biol. 2005; 288: 582–594. PMID: 16223478

45. Majumdar A, Vainio S, Kispert A, McMahon J, McMahon AP. Wnt11 and Ret/Gdnf pathways cooperate in regulating ureteric branching during metanephric kidney development. Development. 2003; 130: 3175–3185. PMID: 12783789

46. Boyce RW, Dorph-Petersen KA, Lyck L, Gundersen HJ. Design-based stereology: introduction to basic concepts and practical approaches for estimation of cell number. Toxicol Pathol. 2010; 38: 1011–1025. doi: 10.1177/0192623310385140 PMID: 21030683

47. Dorph-Petersen KA, Nyengaard JR, Gundersen HJ. Tissue shrinkage and unbiased stereological estimation of particle number and size. J Microsc. 2001; 204: 232–246. PMID: 11903800

48. Gundersen HJ. Stereology of arbitrary particles. A review of unbiased number and size estimators and the presentation of some new ones, in memory of William R. Thompson. J Microsc. 1986; 143: 3–45. PMID: 3761363

49. Weiner ID, Mitch WE, Sands JM. Urea and Ammonia Metabolism and the Control of Renal Nitrogen Excretion. Clin J Am Soc Nephrol. 2015; 10: 1444–1458. doi: 10.2215/CJN.10311013 PMID: 25078422

50. Murawski IJ, Maina RW, Gupta IR. The relationship between nephron number, kidney size and body weight in two inbred mouse strains. Organogenesis. 2010; 6: 189–194. PMID: 21197222

51. Amann K, Benz K. [Clinical relevance of reduced nephron count]. Klin Padiatr. 2011; 223 Suppl 1: S18–26. doi: 10.1055/s-0030-1255880 PMID: 21472673

52. Brenner BM, Lawler EV, Mackenzie HS. The hyperfiltration theory: a paradigm shift in nephrology. Kidney Int. 1996; 49: 1774–1777. PMID: 8743495

53. Bertram JF, Douglas-Denton RN, Diouf B, Hughson MD, Hoy WE. Human nephron number: implications for health and disease. Pediatr Nephrol. 2011; 26: 1529–1533. doi: 10.1007/s00467-011-1843-8 PMID: 21604189

54. Hoy WE, Hughson MD, Singh GR, Douglas-Denton R, Bertram JF. Reduced nephron number and glomerulomegaly in Australian Aborigines: a group at high risk for renal disease and hypertension. Kidney Int. 2006; 70: 104–110. PMID: 16723986

55. Keller G, Zimmer G, Mall G, Ritz E, Amann K. Nephron number in patients with primary hypertension. N Engl J Med. 2003; 348: 101–108. PMID: 12519920

56. Fogo A, Ichikawa I. Evidence for a pathogenic linkage between glomerular hypertrophy and sclerosis. Am J Kidney Dis. 1991; 17: 666–669. PMID: 2042646

57. Fogo AB. Glomerular hypertension, abnormal glomerular growth, and progression of renal diseases. Kidney Int Suppl. 2000; 75: S15–21. PMID: 10828756

58. Brenner BM, Garcia DL, Anderson S. Glomeruli and blood pressure. Less of one, more the other? Am J Hypertens. 1988; 1: 335–347. PMID: 3063284

59. Hoy WE, Hughson MD, Bertram JF, Douglas-Denton R, Amann K. Nephron number, hypertension, renal disease, and renal failure. J Am Soc Nephrol. 2005; 16: 2557–2564. PMID: 16049069

60. Hughson MD, Douglas-Denton R, Bertram JF, Hoy WE. Hypertension, glomerular number, and birth weight in African Americans and white subjects in the southeastern United States. Kidney Int. 2006; 69: 671–678. PMID: 16395270

61. Douglas-Denton RN, McNamara BJ, Hoy WE, Hughson MD, Bertram JF. Does nephron number matter in the development of kidney disease? Ethn Dis. 2006; 16: S2–40-45.

62. Hoy WE, Bertram JF, Denton RD, Zimanyi M, Samuel T, Hughson MD. Nephron number, glomerular volume, renal disease and hypertension. Curr Opin Nephrol Hypertens. 2008; 17: 258–265. doi: 10.1097/MNH.0b013e3282f9b1a5 PMID: 18408476

63. Luyckx VA, Brenner BM. The clinical importance of nephron mass. J Am Soc Nephrol. 2010; 21: 898–910. doi: 10.1681/ASN.2009121248 PMID: 20150537

64. Fogo A, Ichikawa I. Evidence for the central role of glomerular growth promoters in the development of sclerosis. Semin Nephrol. 1989; 9: 329–342. PMID: 2688009

65. Cullen-McEwen LA, Kett MM, Dowling J, Anderson WP, Bertram JF. Nephron number, renal function, and arterial pressure in aged GDNF heterozygous mice. Hypertension. 2003; 41: 335–340. PMID: 12574104

Supporting Information

S1 Table.

Exact p values of statistically analyzed* parameters of homozygous (HOM) and heterozygous (HET) *Pou3f3*^{L423P} mutant mice and control (CON) mice at 12 days of age.

Parameter	sex	overall	CON vs. HET	CON vs. HOM	HOM vs. HET	*male vs. female*		
						CON	HET	HOM
Body weight	m	0.025	0.999	0.074	0.028	0.5458	0.3519	0.7445
	f	0.086	0.998	0.104	0.097			
Kidney weight	m	0.001	0.924	0.003	0.001	0.9625	0.7076	0.3208
	f	0.006	0.992	0.007	0.006			
Relative kidney weight	m	0.003	0.623	0.040	0.019	0.6509	0.4061	0.8708
	f	0.110	0.999	0.014	0.010			
Urine albumin concentration	m	0.333	0.196	0.212	0.959	0.2085	0.4325	0.4849
	f	0.212	0.431	0.309	0.085			
$V_{(Kidney)}$	m	0.001	0.993	0.004	0.009	0.7104	0.6529	0.5682
	f	0.002	0.961	0.002	0.002			
$V_{V\ (Cortex/Kid)}$	m	0.277	0.942	0.340	0.464	0.9057	0.6368	0.5407
	f	0.106	0.980	0.113	0.142			
$V_{(Cortex,\ Kid)}$	m	0.006	0.789	0.014	0.001	0.7458	0.9556	0.4353
	f	0.028	0.426	0.021	0.154			
$V_{V\ (Med/Kid)}$	m	0.277	0.924	0.340	0.464	0.9057	0.9861	0.5407
	f	0.131	0.901	0.124	0.232			
$V_{(Med,\ Kid)}$	m	0.000	0.260	0.001	0.005	0.8016	0.9527	0.8763
	f	0.004	0.437	0.003	0.202			
$V_{V\ (TAL/Kid)}$	m	0.000	0.007	0.000004	0.000785	0.0128	0.0551	0.9149
	f	0.000	0.503	0.00086	0.000023			
$V_{(TAL,\ Kid)}$	m	0.000	0.085	0.000005	0.000059	0.3168	0.1097	0.6494
	f	0.000	0.949	0.000299	0.000041			
$V_{V\ (Glom/Kid)}$	m	0.558	0.615	0.808	0.997	0.2478	0.9311	0.9329
	f	0.964	1.000	0.990	0.993			
$V_{(Glom,\ Kid)}$	m	0.018	1.000	0.700	0.018	0.2938	0.8865	0.5625
	f	0.032	0.616	0.024	0.107			
$V_{(Glom,\ Kid)}$/body weight	m	0.403	1.000	0.629	0.470	0.7057	0.0315	0.7707
	f	0.100	0.399	0.102	0.537			
$N_{V\ (Glom/Kid)}$	m	0.187	0.533	0.190	0.650	0.8016	0.4646	0.4318
	f	0.036	0.464	0.027	0.174			
$N_{(Glom,\ Kid)}$	m	0.000	0.031	0.000009	0.000397	0.5073	0.2454	0.7768
	f	0.000	0.012	0.000006	0.000139			
$N_{(Glom,\ Kid)}$/body weight	m	0.032	0.241	0.027	0.296	0.5241	0.3856	0.8866
	f	0.000	0.028	0.000324	0.041			
$\bar{V}_{(Glom)}$	m	0.002	0.167	0.001486	0.023	0.2478	0.6494	1.000
	f	0.028	1.000	0.044	0.054			
$\bar{V}_{(Glom)}$/body weight	m	0.565	0.632	0.786	1.000	0.2134	0.6581	0.8185
	f	0.811	0.996	0.949	0.874			

*Statistically significant differences between genotypes were determined by using a 1-way ANOVA with Gabriel's post hoc test, differences between male and female mice of the identical genotype by Student's t-test.

S2 Table.

Exact p values of statistically analyzed* parameters of homozygous (HOM) and heterozygous (HET) *Pou3f3*^{L423P} mutant mice and control (CON) mice at 60 weeks of age.

Parameter	sex	overall	CON *vs.* HET	CON *vs.* HOM	HOM *vs.* HET	male *vs.* female		
						CON	HET	HOM
Body weight	m	0.001	0.989	0.0040	0.0040	0.6200	0.1079	0.0152
	f	0.002	0.269	0.01511	0.065			
Kidney weight	m	0.000	0.484	0.000065	0.000004	0.0006	0.0014	0.0022
	f	0.000	0.999	0.000039	0.000048			
Relative kidney weight	m	0.005	0.054	0.109	0.013	0.0006	0.0200	0.0022
	f	0.009	0.112	0.530	0.040			
Mean blood pressure	m	0.775	0.923	0.999	0.882	0.0369	0.7490	0.5264
	f	0.087	0.113	0.228	0.985			
Serum urea	m	0.002	0.997	0.0081	0.00412	0.9487	0.4757	0.4848
	f	0.014	0.241	0.0415	0.0295			
Serum cystatin c	m	0.474	0.975	0.545	0.776	0.4020	1.000	0.6905
	f	0.977	0.997	1.000	0.996			
Serum sodium	m	0.822	0.998	0.905	0.948	0.1098	0.0607	0.3358
	f	0.454	0.994	0.536	0.668			
Urine albumin concentration	m	0.041	0.578	0.062	0.015	0.1320	0.1709	0.1320
	f	0.006	0.116	0.005	0.246			
Urine creatinine concentration	m	0.181	0.408	0.217	0.925	0.7009	1.000	1.000
	f	0.012	0.676	0.013	0.132			
UACR	m	0.067	0.378	0.575	0.066	0.1905	0.3929	0.1143
	f	0.026	0.191	0.024	0.799			
Urine specific gravity	m	0.002	0.999	0.00417	0.00817	0.1373	0.5089	0.3341
	f	0.014	0.596	0.0141	0.0463			
$V_{(Kidney)}$	m	0.000	0.484	0.000065	0.000004	0.0001	0.0001	0.0001
	f	0.000	0.999	0.000039	0.000048			
$V_{V\ (Cortex/Kid)}$	m	0.833	1.000	0.921	0.94	0.0038	0.4484	0.3471
	f	0.013	0.170	0.009	0.419			
$V_{(Cortex, Kid)}$	m	0.003	0.813	0.004	0.016	0.0006	0.0006	0.0043
	f	0.006	0.985	0.017	0.009			
$V_{V\ (Med/Kid)}$	m	0.833	1.000	0.921	0.940	0.0279	0.5212	0.1474
	f	0.013	0.170	0.010	0.419			
$V_{(Med, Kid)}$	m	0.530	0.955	0.066	0.133	0.0913	0.0040	0.0011
	f	0.000	0.183	0.014	0.041			
$V_{V\ (TAL/Kid)}$	m	0.009	0.494	0.00798	0.07602	0.0006	0.0003	0.0087
	f	0.003	0.498	0.0040	0.0376			
$V_{(TAL, Kid)}$	m	0.006	0.981	0.0020	0.0247	0.0379	0.0541	0.0303
	f	0.002	0.691	0.0030	0.0015			
$V_{V\ (Glom/Kid)}$	m	0.013	0.884	0.014	0.041	0.0001	0.0001	0.0003
	f	0.020	0.177	0.019	0.551			
$V_{(Glom, Kid)}$	m	0.002	0.638	0.001576	0.009923	0.2911	0.1993	0.9829
	f	0.001	0.549	0.000614	0.001013			
$V_{(Glom, Kid)}$/body weight	m	0.029	0.302	0.025	0.351	0.7104	0.4908	0.6623
	f	0.343	0.677	0.387	0.934			
$N_{V\ (Glom/Kid)}$	m	0.295	0.351	0.126	0.471	0.0070	0.0022	0.0022
	f	0.621	1.000	0.726	0.679			
$N_{(Glom, Kid)}$	m	0.000	0.0885	0.0001	0.0167	0.0111	0.1893	0.1320
	f	0.000	0.620	0.027	0.0179			
$N_{(Glom, Kid)}$/body weight	m	0.036	0.320	0.033	0.453	0.2086	0.4136	0.0411
	f	0.044	0.575	0.642	0.999			
$\bar{V}_{(Glom)}$	m	0.002	0.257	0.001771	0.0150	0.0420	0.7789	0.1775
	f	0.002	0.215	0.000117	0.40877			
$\bar{V}_{(Glom)}$/body weight	m	0.023	0.657	0.020	0.116	0.7104	0.4908	0.6623
	f	0.250	0.944	0.525	0.289			
$V_{V\ (Mes/Glom)}$	m	0.101	0.104	0.850	0.481	0.1231	0.4107	0.7827
	f	0.908	0.961	0.999	0.992			
$V_{(Mes, Glom)}$	m	0.000	0.0033	0.000089	0.110	0.0263	0.9426	0.2381
	f	0.001	0.140	0.0011	0.0478			
$V_{V\ (Cap/Glom)}$	m	0.003	0.0025	0.409	0.116	0.0054	0.5478	0.5658
	f	0.470	0.915	0.519	0.825			
$V_{(Cap, Glom)}$	m	0.012	0.959	0.015	0.029	0.9015	0.3969	0.1775
	f	0.005	0.122	0.0039	0.177			
$V_{V\ (Pod/Glom)}$	m	0.458	0.517	0.966	0.848	0.1764	0.9069	0.5787
	f	0.205	0.988	0.249	0.346			

$\bar{v}_{(Pod, Glom)}$	m	0.005	0.164	0.0037	0.129	0.2136	0.4319	0.6534
	f	0.061	0.303	0.042	0.622			
$L_{V (Cap/Glom)}$	m	0.458	0.517	0.966	0.848	0.1137	0.0552	0.4422
	f	0.205	0.988	0.249	0.346			
$L_{(Cap, Glom)}$	m	0.000	0.939	0.00096	0.000268	0.4098	0.2021	0.5368
	f	0.010	0.980	0.0136	0.0213			
$L_{(Glom-cap, Kid)}$	m	0.000	0.486	0.0197	0.00121	0.7308	0.8665	0.7922
	f	0.019	0.896	0.0206	0.0066			
$N_{V (C/Glom)}$	m	0.288	0.588	0.330	0.904	0.2343	0.2180	0.0173
	f	0.206	0.742	0.212	0.664			
$N_{(C, Glom)}$	m	0.006	0.876	0.0082	0.0189	1.000	0.7546	0.7922
	f	0.01	0.132	0.0088	0.363			
$N_{V (M-E/Glom)}$	m	0.777	0.950	0.994	0.867	0.2824	0.1375	0.303
	f	0.518	1.000	0.689	0.632			
$N_{(M-E, Glom)}$	m	0.032	0.933	0.0403	0.075	1.000	0.7546	0.7922
	f	0.057	0.244	0.00631	0.754			
$N_{V (Pod/Glom)}$	m	0.071	0.721	0.069	0.259	0.5338	0.4908	0.4286
	f	0.249	0.428	0.349	0.991			
$N_{(Pod, Glom)}$	m	0.000	0.543	0.000016	0.0060	0.6116	0.8972	0.2722
	f	0.000	0.130	0.000165	0.0095			
$\bar{v}_{(Pod)}$	m	0.091	0.376	0.092	0.647	0.1320	0.4136	0.5368
	f	0.869	0.963	1.000	0.950			
$Th_{(GBM)}$	m	0.022	0.821	0.109	0.024	0.4000	0.4000	0.6286
	f	0.007	0.079	0.129	0.030			
FSF	m	0.814	0.922	0.907	1.000	1.000	1.000	0.8571
	f	0.648	0.734	0.571	0.376			
RT-qPCR: Pou3f3 vs.Gapdh relative to CON	m	0.589	0.684	0.995	0.865	0.9930	0.3649	0.3853
	f	0.158	0.937	0.172	0.323			
RT-qPCR: Umod vs. Gapdh relative to CON	m	0.009	1.000	0.018	0.014	0.9894	0.1750	0.2204
	f	0.027	0.066	0.046	0.925			
RT-qPCR: Pou3f3 vs. Umod relative to CON	m	0.000	0.673	0.00003	0.00014	1.000	0.7244	0.0488
	f	0.002	0.095	0.00133	0.058			

UACR: Urine albumin-to-creatinine ratio. *Statistically significant differences between genotypes were determined by using a 1-way ANOVA with Gabriel's post hoc test, differences between male and female mice of the identical genotype by Student's t-test.

4. Discussion

4.1. Experimental design, general and methodological aspects of the study

The aim of the present study was to analyze the renal phenotype of *Pou3f3*^{L423P} mice, a mutant mouse line recently derived from the Munich ENU Mouse Mutagenesis project (Aigner et al., 2007, Kumar et al., 2016). Mutant *Pou3f3*^{L423P} mice harbor a non-lethal point mutation in the *Pou3f3* gene, and, in contrast to homozygous *Pou3f3* knock-out mice, homozygous *Pou3f3*^{L423P} mutants are viable and fertile (Kumar et al., 2016). Therefore they allow to investigate not only the impact of the POU3F3 mutation on renal development in newborn animals but also to study the consequences of the mutation on morphology and function of the kidneys in the postnatal life. On initial establishment adult homozygous *Pou3f3*^{L423P} mutant mice have been demonstrated to display elevated plasma urea levels, together with several other metabolic changes that were pointing at an impaired renal function. These changes include increased creatinine, chloride, and potassium serum levels, as well as decreased bone mineral density and bone mineral content (Nakai et al., 2003, Kumar et al., 2016).

For a comprehensive analysis, the present study examined homo- and heterozygous mutant mice together with wildtype controls of both sexes were at 12 days and 60 weeks of age. The first age group thereby allowed to study immediate developmental effects of the *Pou3f3*^{L423P} mutation, since 12 days marks the completion of nephron(no)genesis in mice (Dressler, 2006), while the second age group made it possible to evaluate long-term ramifications on renal morphology and function. Analyses to assess renal function comprised blood pressure measurements, as well as determination of several relevant biochemical parameters in serum and urine. By applying qualitative histological and ultrastructural examinations, in combination with state-of-the-art, unbiased, design-based quantitative stereological methods (Gundersen, 1986, Dorph-Petersen et al., 2001, Weiner et al., 2015) a thorough morphological analysis of the development, growth and cellular structure of different nephron segments, such as the thick ascending limb of the loop of Henle (TAL) was facilitated. At last, renal *Pou3f3* mRNA levels and protein abundances were determined in order to gain more insight into *Pou3f3* gene expression in the mature kidney.

4.2. Renal morphology of *Pou3f3*^{L423P} mutant mice

In both 12-day-old and 60-week-old homozygous *Pou3f3*^{L423P} mutant mice kidney weights and volumes were significantly smaller than in non-mutant controls. Absolute TAL volumes as well as volume densities of the TAL in the kidney were also significantly lower. These findings are corresponding to those previously reported in *Pou3f3* knock-out mice by Nakai et al. (2003), and confirm the important role of POU3F3 in nephronogenesis, and in the development of the TAL in particular. Given the fact that the TAL occupies an important role for the renal nitrogen metabolism (Zhong et al., 2012, Mount, 2014), its incomplete development in homozygous *Pou3f3*^{L423P} mutants might provide a possible explanation for the raised serum urea levels detected in these animals (Nakai et al., 2003, Kumar et al., 2016). Equally in line with the findings by Nakai *et al.*, immunohistochemical investigation showed the presence of POU3F3 in the TAL and the MD of both 12-day-old and 60-week-old, mutant and non-mutant mice. This not only confirms the pivotal role of POU3F3 in the fetal development of the TAL, but also strengthens its presumed significance in maintaining TAL function in the mature kidney throughout adult life (Nakai et al., 2003). Moreover, the present study also found a positive signal for POU3F3 immunostaining within CD cell nuclei in the kidneys of 60-week-old animals, which has not been reported in the kidneys of neonates (Nakai et al., 2003).

Fundamentally, since Nakai et al. (2003) used mice with a different age and another genetic background and only semiquantitatively evaluated the severity of the underdevelopment of the TAL, it is not feasible to compare the effects of a total POU3F3 absence in *Pou3f3* knock-out mice with the effects of the *Pou3f3*^{L423P} mutation. Albeit, *Pou3f3* knock-out mice also showed severe morphological alterations of the TAL cells on light and electron microscopical level (Nakai et al., 2003), which were not detectable in homozygous *Pou3f3*^{L423P} mutants that were examined in the study at hand. Apart from the developmental deficits of the TAL, the kidneys of homozygous *Pou3f3*^{L423P} mutants presented with several other altered parameters regarding quantitative stereological analyses, which were already observable in the 12-day-old animals.

Probably the most striking feature of homozygously *Pou3f3*^{L423P} mutant mice is the significant reduction of the total nephron numbers. Additionally, the relative numbers of nephrons per body weight and the mean glomerular volume were significantly de-

creased in 12-day-old homozygous mutants, while the mean glomerular volume-to–body weight ratio remained unchanged, as compared to control mice. The kidneys of the aged, 60-week-old homozygous *Pou3f3*^{L423P} mutants basically presented with identical findings, whereas in these animals the relative nephron number just showed a significant reduction in male, but not in female homozygous mutant mice as compared to wildtype controls. This difference, however, can be due to the reduced body weights of aged female homozygous *Pou3f3*^{L423P} mutants as compared to the male homozygous *Pou3f3*^{L423P} mutants.

Absent POU3f3 function in *Pou3f3* knock-out mice has not been reported to yield a similar effect on glomerular number or size. This is likely due to the fact that in mice the development of the nephron and differentiation of its segments is still in progress at the time of birth and continues until several days postnatally (Dressler, 2006). Likewise, not as accurate methods might have been applied for the determination of number and size of glomeruli in the study of Nakai et al. (2003). The results of the present study therefore, revealed novel functions of POU3F3: in addition to the already known importance in differentiation of distinct nephron segments like the TAL (nephron patterning), POU3F3 also seems to be one of the factors influencing the nephron endowment, i.e., the absolute nephron number present in the matured mouse kidney. Importantly, rather than changes of the nephron number in relation to the body weight, the decrease of the absolute number of nephrons in homozygous *Pou3f3*^{L423P} mutants compared to wildtype littermates embodies the representative parameter since several studies carried out in various mouse strains show that kidney and body weight are correlated at birth and at adult age, but so far no link between nephron number and body weight or size of the kidney has been revealed (Benz et al., 2011). For this reason, although 12-day-old male and female homozygous *Pou3f3*^{L423P} mutant mice showed a significantly reduced relative nephron number, which was also observed in male, yet not in female 60-week-old homozygous mutants, does not disagree with the presumed importance of POU3F3 in determination of the kidneys endowment with nephrons. Except for slightly altered serum and urine parameters regarding the function of the tubular system, the Pou3f3 mutation with the decrease of TAL did not yield any long-term implications in terms of pathomorphologic changes of the tubular system that were detectable by light- or electron microscopy in the kidneys of 60-week-old *Pou3f3*^{L423P} mutants. The functional capacity of the glomerular compartment was virtually unaltered in these animals either,

since neither glomerular filtration rate nor urine albumin excretion or blood pressure showed any differences between *Pou3f3*^{L423P} mutants vs. non-mutant controls.
Correspondingly, besides the reduced number of nephrons and a decrease in glomerular size, qualitative as well as quantitative morphological analyses did not reveal any pathomorphological glomerular alterations in kidneys of 60-week-old *Pou3f3*^{L423P} mutants. Urine protein analyses furthermore did not display any evidence of albuminuria in homo-, or heterozygous *Pou3f3*^{L423P} mutants of both sexes.
Even on ultrastructural level no glomerular lesions were observed in *Pou3f3*^{L423P} mutants. Hereby, quantitative morphological parameters, like the thickness of the GBM, or the mean podocyte volume, represent sensitive indicators able to detect even early stages of glomerular damage (Herbach et al., 2009, Blutke et al., 2016, Herbach et al., 2011). As these parameters presented similar in mutants and non-mutant controls, the reduction in nephron numbers in Pou3f3^{L423P} mutant mice does not have any effect on the glomerular ultrastructure.

4.3. Role of POU3F3 in kidney development

Embryonic development of the mammalian kidney and, in this context, development of nephrons in sufficient numbers, is important to guarantee a fully operative functional capacity of the kidneys. After the appropriate induction of the developing nephron in the metanephric mesenchyme, it comprises the subsequent transformative processes that lead to formation of a renal vesicle and the following differentiation of the renal vesicle into the early nephron and its already distinct segments, a process also termed nephron patterning. At last, the final maturation of each segment concludes the developmental processes. Each one of these steps requires the highly complex network interactions of a plethora of transcription factors as well as growth factors, receptors and several other signaling molecules that orchestrate the nephron(no)genesis by activating or repressing specific genes in different cell types (Schedl, 2007, El-Dahr et al., 2008, O'Brien and McMahon, 2014).
Early steps in the development of the ureteric bud involve coordinated signaling between the sprouting tip and the metanephric mesenchyme it is surrounded by. This leads to branching of the ureteric bud and subsequent formation of a renal vesicle that undergoes mesenchymal to epithelial transformation in the process and is converted to a primitive nephron via the stages of comma- and S-shaped bodies. Hereby, several transcriptional pathways play important roles in governing these accurate-

ly timely and spatially coordinated processes, including the glial-derived neurotrophic factor (GDNF) and CRET (ret proto-oncogene) signaling pathway, the WNT-beta-catenin cascade, and many other transcription- and transcription inducing factors such as EYA1 (eyes absent homolog 1 transcriptional coactivator and phosphatase 1), LIF (leukemia inhibitory factor), FGF2 (fibroblast growth factor 2), and TGFB2 (transforming growth factor beta 2) (Schedl, 2007, El-Dahr et al., 2008, O'Brien and McMahon, 2014).

The following process, which is also termed nephron patterning and leads to the differentiation of the distinct morphologically and functionally unique tubular segments that the nephron exhibits along its proximal to distal axis, and along with the formation of a capillary cleft, its invasion by endothelial cell primordia and the further maturation of early glomerular structures is accomplished by transcription factors including WT1 (Wilms' tumor 1) , LHX1 (LIM homeobox 1), POU3F3, and DLL1 (delta-like 1). In particular Notch–Delta pathway signaling plays an important role for determination of proximal tubular segments, while the distal tubular segments are specified by transcription factors POU3F3 and IRX (iroquois homeobox) (Schedl, 2007, El-Dahr et al., 2008, O'Brien and McMahon, 2014). Although many pathways have been unraveled so far, there are still plenty of interactions and regulatory hierarchies of all in nephron(no)genesis involved factors, whose exact functions need to be elucidated.

Many of those factors important for nephron(no)genesis and their presumed functions have been detected and studied in genetically modified animal models, preferably rodents. By altering gene expression and thereby generating total or partial loss of a single transcription or growth factor, the presumed function of the molecule in question can be studied, as this results in a distinct phenotype that lacks the actions of the products of the modified genes, leading to e.g., typical malformations of either the entire kidney, or of a specific nephron segment (Cohen and Kretzler, 2003, Siner et al., 2007, Graham et al., 2014). Similarly, by using *Pou3f3* knock-out mice Nakai et al. in 2003 discovered and described the vital function of POU3F3 in the development of the nephron, more precisely in nephron patterning, especially the development of the thick ascending limb (TAL) of the loop of Henle and the macula densa (MD) (Nakai et al., 2003). In the developing nephron, Nakai et al. detected POU3F3 expression in distal renal vesicles, S-shaped bodies, and in distinct nephron regions that set out to differentiate into TAL and MD, as well as the distal convoluted tubule. Here, POU3F3 expression continues throughout adult life. Furthermore, the striking

absence of the TAL in kidneys of homozygous *Pou3f3* knock-out mice at the time of birth was shown (Nakai et al., 2003). A circumstance that probably contributes largely to the fact that neonatal homozygous *Pou3f3* knock-out mice display increased levels of plasma urea and potassium, and ultimately die due to renal failure within 24 hours after birth (Nakai et al., 2003).

The underlying mechanism of POU3F3 deficiency triggering TAL underdevelopment potentially include a reduced proliferation of TAL cells or an early occurrence of apoptotic process in the primitive nephron stages of homozygous *Pou3f3* knock-out embryos (Nakai et al., 2003). Since heterozygous *Pou3f3* knock-out mice exhibit decreased expression levels of several genes that are typically expressed in the TAL, such as *Umod, Nkcc2*, and certain K+ and Cl- channels, a gene-dosage dependent function of POU3F3 in terms of gene expression in the TAL has been suggested (Nakai et al., 2003). Albeit, no evidence for pathologic alterations regarding cell morphology or TAL function has been found in these mice, and neither histological and/or electron microscopical analyses nor determination of plasma levels of urea, creatinine, several electrolytes including Na^+, K^+, Cl^-, and measurement of urine osmolality and volume showed any abnormalities (Nakai et al., 2003). The observed differences between *Pou3f3* knock-out and the *Pou3f3*^{L423P} mutants, like the early postnatal death of homozygous Pou3f3 knock-out mice due to kidney failure, might originate from a remaining activity of the mutated POU3F3 transcription factor in contrast to a complete loss of function in Pou3f3 knock-out mice. In *Pou3f3*^{L423P} mutant mice the locus of the mutation has been determined to be in the highly conserved homeodomain of the protein. It is possible that this alters the transcriptional regulation of several, if not all POU3F3 target genes. In addition, a compensation of a lack of specific functions of POU3F3 in homozygous *Pou3f3*^{L423P} mutants by other, yet unknown, but in synergy acting factors is indeed thinkable, since this has been shown to be true for POU3F3 actions in the brain (Sugitani et al., 2002).

Eventually, the less pronounced phenotypes in heterozygous *Pou3f3* knock-out mice and heterozygous *Pou3f3*^{L423P} mutant mice can be construed as gene-dose dependent effect (Nakai et al., 2003).

In summary it can be stated that further studies are needed to clarify the molecular mechanisms and exact actions of POU3F3, in particular how it participates in nephro(no)genesis and how it helps to maintain TAL function once the kidney matured. This entails the transcriptional control of its target-genes, its interactions with

other factors, and the involvement and influence on other important regulatory signaling pathways. Hereby, *Pou3f3*^{L423P} mutant mice might serve as a useful model system.

4.4. Pou3f3^{L423P} mutant mice as an animal model for low nephron numbers

The striking reduction of nephron numbers observed in homozygous *Pou3f3*^{L423P} mutant mice is particular interesting, as a low nephron endowment in humans is thought to be a crucial risk factor for development of different chronic kidney diseases (Amann and Benz, 2011, Brenner et al., 1996, Bertram et al., 2011). The low nephron numbers are considered a “first hit” rendering the kidney of the affected individual susceptible to the emergence of glomerular hypertrophy, which is seen as a pathogenic key lesion in the development of glomerulosclerotic lesions and therefore ultimately to an accelerated decline in renal function in case a “second hit”, as e.g., a primary nephropathy, hypertension, obesity or diabetes mellitus challenges the renal reserve capacity (Douglas-Denton et al., 2006, Hoy et al., 2008, Luyckx et al., 2013, Bertram et al., 2011). How low nephron numbers exactly contribute to the development of glomerular hypertrophy has not been fully elucidated yet. There is evidence that the glomerular growth serves as a compensatory mechanism that is mediated by different glomerular growth factors or hypertensive changes (Fogo and Ichikawa, 1989, Fogo and Ichikawa, 1991, Benz et al., 2011). Hypertension in turn might develop due to misguided renin angiotensin system activation, alterations in the structure of peritubular vessels, or an impaired salt excretion of the tubular system leading to salt and as a consequence thereof volume retention.

Currently, there are only very few existing mouse models of a genetically determined low nephron endowment, *inter alia* heterozygous *Gdnf* knock-out mice (Cullen-McEwen et al., 2001, Benz et al., 2011). These mice show an approximate reduction of 33% in nephron numbers as compared to wildtype controls, whereby displaying similar kidney and body weights (Cullen-McEwen et al., 2001, Benz et al., 2011). However, heterozygous *Gdnf* knock-out mice show a higher occurrence of unilateral renal agenesia and the reduction in nephron endowment is associated with a distinct set of glomerular alterations, including glomerular hypertrophy with accompanying endothelial and mesangial cell hyperplasia and thickening of the glomerular basement membrane, changes that have been shown to predispose mice for the development of glomerulosclerosis and hypertension (Fogo and Ichikawa, 1991, Fogo,

2000, Benz et al., 2011). Therefore it is difficult to evaluate the sole impact of the reduced nephron numbers in development of renal lesions. Contrary to that, homozygous *Pou3f3*^{L423P} mutant mice that show a comparable average reduction in nephron numbers of 37% and do not exhibit an “own” pattern of primary glomerular pathologies. The lack thereof is particularly advantageous for the use of *Pou3f3*^{L423P} mutant mice as a model system for low nephron numbers, because it allows for experiments that study the sole impact of a reduced nephron endowment and their role as predisposing factor in the development of renal lesions.

Furthermore, using genetically modified animal models reduces the intra- and inter-experimental variability related to technical differences in models with surgically reduced nephron numbers, such as unilateral nephrectomy (Woods, 1999, Moritz et al., 2005).

4.5. Perspectives

The present study confirmed not only the important role of POU3F3 in development of the distal nephron parts, in particular the thick ascending limb of the loop of Henle, but also showed the potential of *Pou3f3*^{L423P} mutant mice as an experimental mouse model for low nephron numbers in nephrological research. These animal models are urgently required nowadays, since *a priori* low nephron numbers are seen as a trigger for the facilitated development of chronic kidney diseases later in life in case a second hit such as diabetes follows. Therefore, to study possible implications of a reduced nephron endowment, challenging homo- as well as heterozygous *Pou3f3*^{L423P} mutant mice with additional renal insults seems an appealing approach. This could entail evaluating cardiovascular and renal effects after exposure to a diet high in salt, or, crossing *Pou3f3*^{L423P} mutant mice with another established genetically modified murine model of progressive renal disease, such as DN. We are currently considering such a study by crossing *Pou3f3*^{L423P} mutant mice with GIPRdn transgenic mice. GIPRdn transgenic mice express a dominant negative receptor for the glucose-dependent insulinotropic polypeptide and represent a well characterised mouse model of diabetic nephropathy (Herbach et al., 2009, Herbach et al., 2011). Crossing these two lines creates an animal collective consisting of diabetic and non-diabetic individuals with “normal” as well as reduced absolute nephron numbers respectively. Therefore, the in depth characterization of the renal alterations in the different obtained genotypes will allow to study the impact of *a priori* low nephron numbers on onset, development and severity of diabetes associated kidney lesions.

5. Summary

Mammalian nephrogenesis is a complex process that involves the precise timely and spatially coordinated interaction of a plethora of signaling molecules. During terminal nephron segmentation, POU3F3 (aka BRN1), a POU domain class 3 transcription factor, plays a critical role in the differentiation of the distal tubule, in particular the thick ascending limb of the loop of Henle (TAL). In knock-out mice, deficiency of POU3F3 leads to underdevelopment of the TAL, lack of differentiation of TAL and macula densa cells, and perinatal death due to renal failure.

Pou3f3^{L423P} mutant mice were established in the phenotype-driven Munich ENU Mouse Mutagenesis Project within a special screen for increased plasma urea levels to detect novel mouse models for kidney diseases. These mice carry a recessive point mutation in the highly conserved homeodomain of POU3F3. In contrast to *Pou3f3* knock-out mice, homozygous *Pou3f3*^{L423P} mutants are viable and fertile.

The present study used functional, as well as qualitative and quantitative morphological analyses to characterize the renal phenotype of juvenile (12 days) and aged (60 weeks) homo- and heterozygous *Pou3f3*^{L423P} mutant mice and age-matched wild-type littermates of both sexes. In both age groups, homozygous mutants vs. control mice displayed significantly smaller kidney volumes, decreased nephron numbers and smaller mean glomerular volumes. Besides, the absolute TAL volumes and the volume densities of TAL in the kidney were significantly reduced in *Pou3f3*^{L423P} mutants. There were no histologically or ultrastructurally detectable lesions of TAL or glomerular cells. Aged homozygous mutants displayed increased serum urea concentrations and reduced specific urine gravity, but no evidence of glomerular dysfunction. These results confirm the important function of POU3F3 during nephron patterning, especially in development of the TAL. Furthermore they provide strong evidence that POU3F3 is also involved in the regulation of nephron induction, nephron endowment, and nephron size in the murine kidney, while the mutation is not associated with a distinct pattern of morphological glomerular lesions.

The detailed characterization of the renal morphology of *Pou3f3*^{L423P} mutants provided the basis for further analyses of POU3F3 actions, and showed that *Pou3f3*^{L423P} mutant mice represent a valuable research model for nephrological studies examining the role of congenital low nephron numbers in kidney disease development and progression.

6. Zusammenfassung

Bei Säugetieren stellt die Nephrogenese einen hochkomplexen Prozess dar, der ein präzises, örtlich und zeitlich koordiniertes Zusammenspiel einer Vielzahl verschiedener Signalmoleküle erfordert. Während der schlussendlichen Segmentierung des Nephrons spielt POU3F3 (aka BRN1), ein POU Domäne Klasse 3 Transkriptionsfaktor, eine kritische Rolle in der Ausdifferenzierung der distalen Tubulusabschnitte, insbesondere in der des dicken aufsteigenden Schenkels der Henle'schen Schleife (TAL). Homozygote *Pou3f3* knock-out Mäuse versterben kurz nach der Geburt an Nierenversagen. Bei diesen Tieren bleibt die Entwicklung des TAL beinahe vollständig aus. Des Weiteren ist eine Abgrenzung der TAL- und der benachbarten Macula densa-Zellen aufgrund einer fehlenden Differenzierung nicht möglich. Die Mauslinie Pou3f3^{L423P} stammt aus dem Phänotyp-basierten Münchner ENU-Mausmutagenese-Projekt und wurde im Rahmen eines Screenings auf erhöhte Plasmaharnstoffwerte zur Identifikation neuer Mausmodelle für Nierenerkrankungen entdeckt. *Pou3f3^{L423P}* mutante Mäuse besitzen eine rezessiv vererbte Punktmutation in der Homeodomäne, einer hochkonservierten DNA-Bindungsdomäne von POU3F3. Im Gegensatz zu *Pou3f3* knock-out Mäusen sind homozygote *Pou3f3^{L423P}* Mutanten lebensfähig und fruchtbar. In der hier vorliegenden Studie wurde anhand von funktionellen, sowie qualitativ und quantitativ morphologischen Untersuchungen der renale Phänotyp von juvenilen (12 Tage alten) sowie adulten (60 Wochen alten) homo- und heterozygoten *Pou3f3^{L423P}* Mutanten beider Geschlechter im Vergleich zu nicht-mutanten Wurfgeschwistern gleichen Alters und Geschlechts charakterisiert. In beiden Altersgruppen zeigten homozygote *Pou3f3^{L423P}* mutante Mäuse gegenüber den Kontrolltieren ein signifikant geringeres Nierenvolumen, verminderte Nephronzahlen und kleinere mittlere Glomerulusvolumina. Überdies waren das absolute TAL Volumen und die Volumenanteile von TAL in den Nieren von *Pou3f3^{L423P}* Mutanten signifikant reduziert. Es konnten weder mittels Licht- noch Elektronenmikroskopie Veränderungen der TAL-Zellen oder der Glomeruli festgestellt werden. Als Ausdruck einer eingeschränkten Nierenfunktion wiesen einzig adulte, homozygote *Pou3f3^{L423P}* Mutanten erhöhte Serumharnstoffwerte und eine reduziertes spezifisches Uringewicht auf. Anzeichen einer glomerulären Dysfunktion im Sinne einer Proteinurie fanden sich jedoch nicht. Die vorliegenden Ergebnisse belegen somit die zentrale Funktion von POU3F3 während der embryonalen Differenzierung des Nephrons, insbesondere im Rahmen der Entwicklung des TAL. Überdies fanden sich überzeugende Indizien darauf, dass

POU3F3 auch an der Regulation von Induktion, Anzahl und Ausprägung der Nephrone in der Mäuseniere beteiligt ist.

Die detaillierte Charakterisierung der renalen Morphologie von *Pou3f3*^{L423P} Mutanten schafft damit die Basis für weiterführende funktionelle Analysen von POU3F3 und zeigt, dass *Pou3f3*^{L423P} mutante Mäuse ein vielversprechendes Modell für die nephrologische Forschung darstellen, da sie es ermöglichen, die Auswirkungen einer *a priori* niedrigen Anzahl an Nephronen für die Entwicklung und den Verlauf von chronischen Nierenerkrankungen zu untersuchen.

7. References

2001. The Laboratory mouse. *Times Higher Education Supplement*, 10.

ACEVEDO-AROZENA, A., WELLS, S., POTTER, P., KELLY, M., COX, R. D. & BROWN, S. D. 2008. ENU mutagenesis, a way forward to understand gene function. *Annu Rev Genomics Hum Genet,* 9**,** 49-69.

AIGNER, B., RATHKOLB, B., HERBACH, N., HRABÉ DE ANGELIS, M., WANKE, R. & WOLF, E. 2008. Diabetes models by screen for hyperglycemia in phenotype-driven ENU mouse mutagenesis projects. *Am J Physiol Endocrinol Metab,* 294**,** E232-40.

AIGNER, B., RATHKOLB, B., HERBACH, N., KEMTER, E., SCHESSL, C., KLAFTEN, M., KLEMPT, M., DE ANGELIS, M. H., WANKE, R. & WOLF, E. 2007. Screening for increased plasma urea levels in a large-scale ENU mouse mutagenesis project reveals kidney disease models. *Am J Physiol Renal Physiol,* 292**,** F1560-7.

ALBL, B., HAESNER, S., BRAUN-REICHHART, C., STRECKEL, E., RENNER, S., SEELIGER, F., WOLF, E., WANKE, R. & BLUTKE, A. 2016. Tissue Sampling Guides for Porcine Biomedical Models. *Toxicol Pathol,* 44**,** 414-20.

AMANN, K. & BENZ, K. 2011. [Clinical relevance of reduced nephron count]. *Klin Padiatr,* 223 Suppl 1**,** S18-26.

AUERBACH, A. B. 2004. Production of functional transgenic mice by DNA pronuclear microinjection. *Acta Biochim Pol,* 51**,** 9-31.

AUGUSTIN, M., SEDLMEIER, R., PETERS, T., HUFFSTADT, U., KOCHMANN, E., SIMON, D., SCHONIGER, M., GARKE-MAYERTHALER, S., LAUFS, J., MAYHAUS, M., FRANKE, S., KLOSE, M., GRAUPNER, A., KURZMANN, M., ZINSER, C., WOLF, A., VOELKEL, M., KELLNER, M., KILIAN, M., SEELIG, S., KOPPIUS, A., TEUBNER, A., KORTHAUS, D., NEHLS, M. & WATTLER, S. 2005. Efficient and fast targeted production of murine models based on ENU mutagenesis. *Mamm Genome,* 16**,** 405-13.

AZARIPOUR, A., LAGERWEIJ, T., SCHARFBILLIG, C., JADCZAK, A. E., WILLERSHAUSEN, B. & VAN NOORDEN, C. J. 2016. A survey of clearing techniques for 3D imaging of tissues with special reference to connective tissue. *Prog Histochem Cytochem,* 51**,** 9-23.

BADDELEY, A. & JENSEN, E. B. V. 2005. *Stereology for statisticians,* Boca Raton, FL, Chapman & Hall/CRC.

BAINS, R. K., SIBBONS, P. D., MURRAY, R. D., HOWARD, C. V. & VAN VELZEN, D. 1996. Stereological estimation of the absolute number of glomeruli in the kidneys of lambs. *Res Vet Sci,* 60**,** 122-5.

BALLING, R. 2001. ENU mutagenesis: analyzing gene function in mice. *Annu Rev Genomics Hum Genet,* 2**,** 463-92.

BARASCH, J., YANG, J., WARE, C. B., TAGA, T., YOSHIDA, K., ERDJUMENT-BROMAGE, H., TEMPST, P., PARRAVICINI, E., MALACH, S., ARANOFF, T. & OLIVER, J. A. 1999. Mesenchymal to epithelial conversion in rat metanephros is induced by LIF. *Cell,* 99**,** 377-86.

BARBARIC, I. & DEAR, T. N. 2007. Optimizing screening and mating strategies for phenotype-driven recessive N-ethyl-N-nitrosourea screens in mice. *J Am Assoc Lab Anim Sci,* 46**,** 44-9.

BARD, J. B., GORDON, A., SHARP, L. & SELLERS, W. I. 2001. Early nephron formation in the developing mouse kidney. *J Anat,* 199**,** 385-92.

BASSON, M. A., AKBULUT, S., WATSON-JOHNSON, J., SIMON, R., CARROLL, T. J., SHAKYA, R., GROSS, I., MARTIN, G. R., LUFKIN, T., MCMAHON, A. P., WILSON, P. D., COSTANTINI, F. D., MASON, I. J. & LICHT, J. D. 2005. Sprouty1 is a critical regulator of GDNF/RET-mediated kidney induction. *Dev Cell,* 8**,** 229-39.

BASSON, M. A., WATSON-JOHNSON, J., SHAKYA, R., AKBULUT, S., HYINK, D., COSTANTINI, F. D., WILSON, P. D., MASON, I. J. & LICHT, J. D. 2006. Branching morphogenesis of the ureteric epithelium during kidney development is coordinated by the opposing functions of GDNF and Sprouty1. *Dev Biol,* 299**,** 466-77.

BATOURINA, E., GIM, S., BELLO, N., SHY, M., CLAGETT-DAME, M., SRINIVAS, S., COSTANTINI, F. & MENDELSOHN, C. 2001. Vitamin A controls epithelial/mesenchymal interactions through Ret expression. *Nat Genet,* 27**,** 74-8.

BENZ, K., CAMPEAN, V., CORDASIC, N., KARPE, B., NEUHUBER, W., MALL, G., HARTNER, A., HILGERS, K. F. & AMANN, K. 2011. Early glomerular alterations in genetically determined low nephron number. *Am J Physiol Renal Physiol,* 300**,** F521-30.

BERNARDINI, N., MATTII, L., BIANCHI, F., DA PRATO, I. & DOLFI, A. 2001. TGF-alpha mRNA expression in renal organogenesis: a study in rat and human embryos. *Exp Nephrol,* 9**,** 90-8.

BERTRAM, J. F., DOUGLAS-DENTON, R. N., DIOUF, B., HUGHSON, M. D. & HOY, W. E. 2011. Human nephron number: implications for health and disease. *Pediatr Nephrol,* 26**,** 1529-33.

BERTRAM, J. F., SOOSAIPILLAI, M. C., RICARDO, S. D. & RYAN, G. B. 1992. Total numbers of glomeruli and individual glomerular cell types in the normal rat kidney. *Cell Tissue Res,* 270**,** 37-45.

BLACK, M. J., WANG, Y. & BERTRAM, J. F. 2002. Nephron endowment and renal filtration surface area in young spontaneously hypertensive rats. *Kidney Blood Press Res,* 25**,** 20-6.

BLUTKE, A., SCHNEIDER, M. R., WOLF, E. & WANKE, R. 2016. Growth hormone (GH)-transgenic insulin-like growth factor 1 (IGF1)-deficient mice allow dissociation of excess GH and IGF1 effects on glomerular and tubular growth. *Physiol Rep,* 4.

BOCKAMP, E., MARINGER, M., SPANGENBERG, C., FEES, S., FRASER, S., ESHKIND, L., OESCH, F. & ZABEL, B. 2002. Of mice and models: improved animal models for biomedical research. *Physiol Genomics,* 11**,** 115-32.

BOUCHARD, M., SOUABNI, A., MANDLER, M., NEUBUSER, A. & BUSSLINGER, M. 2002. Nephric lineage specification by Pax2 and Pax8. *Genes Dev,* 16**,** 2958-70.

BOYCE, J. T., BOYCE, R. W. & GUNDERSEN, H. J. 2010. Choice of morphometric methods and consequences in the regulatory environment. *Toxicol Pathol,* 38**,** 1128-33.

BRENNER, B. M., GARCIA, D. L. & ANDERSON, S. 1988. Glomeruli and blood pressure. Less of one, more the other? *Am J Hypertens,* 1**,** 335-47.

BRENNER, B. M., LAWLER, E. V. & MACKENZIE, H. S. 1996. The hyperfiltration theory: a paradigm shift in nephrology. *Kidney Int,* 49**,** 1774-7.

BRODBECK, S. & ENGLERT, C. 2004. Genetic determination of nephrogenesis: the Pax/Eya/Six gene network. *Pediatr Nephrol,* 19**,** 249-55.

BROWN, S. D. & PETERS, J. 1996. Combining mutagenesis and genomics in the mouse--closing the phenotype gap. *Trends Genet,* 12**,** 433-5.

BURG, M. B. 1982. Thick ascending limb of Henle's loop. *Kidney Int,* 22**,** 454-64.

CARROLL, T. J., PARK, J. S., HAYASHI, S., MAJUMDAR, A. & MCMAHON, A. P. 2005. Wnt9b plays a central role in the regulation of mesenchymal to epithelial transitions underlying organogenesis of the mammalian urogenital system. *Dev Cell,* 9**,** 283-92.

CHENG, P., NEFEDOVA, Y., CORZO, C. A. & GABRILOVICH, D. I. 2007. Regulation of dendritic-cell differentiation by bone marrow stroma via different Notch ligands. *Blood,* 109**,** 507-15.

CHUNG, K., WALLACE, J., KIM, S. Y., KALYANASUNDARAM, S., ANDALMAN, A. S., DAVIDSON, T. J., MIRZABEKOV, J. J., ZALOCUSKY, K. A., MATTIS, J., DENISIN, A. K., PAK, S., BERNSTEIN, H., RAMAKRISHNAN, C., GROSENICK, L., GRADINARU, V. & DEISSEROTH, K. 2013. Structural and molecular interrogation of intact biological systems. *Nature,* 497**,** 332-7.

COHEN, C. D. & KRETZLER, M. 2003. Gene-expression analysis of microdissected renal biopsies. *Methods Mol Med,* 86**,** 285-93.

COLES, H. S., BURNE, J. F. & RAFF, M. C. 1993. Large-scale normal cell death in the developing rat kidney and its reduction by epidermal growth factor. *Development,* 118**,** 777-84.

CORDES, S. P. 2005. N-ethyl-N-nitrosourea mutagenesis: boarding the mouse mutant express. *Microbiol Mol Biol Rev,* 69**,** 426-39.

COSTANTINI, F. 2010. GDNF/Ret signaling and renal branching morphogenesis: From mesenchymal signals to epithelial cell behaviors. *Organogenesis,* 6**,** 252-62.

COSTANTINI, F. & SHAKYA, R. 2006. GDNF/Ret signaling and the development of the kidney. *Bioessays,* 28**,** 117-27.

COUTTS, J. C. & GALLAGHER, J. T. 1995. Receptors for fibroblast growth factors. *Immunol Cell Biol,* 73**,** 584-9.

CULLEN-MCEWEN, L., SUTHERLAND, M. R. & BLACK, M. J. 2016. The Human Kidney: Parallels in Structure, Spatial Development, and Timing of Nephrogenesis. *Kidney Development, Disease, Repair and Regeneration.* Elsevier.

CULLEN-MCEWEN, L. A., ARMITAGE, J. A., NYENGAARD, J. R., MORITZ, K. M. & BERTRAM, J. F. 2011. A design-based method for estimating glomerular number in the developing kidney. *Am J Physiol Renal Physiol,* 300**,** F1448-53.

CULLEN-MCEWEN, L. A., DRAGO, J. & BERTRAM, J. F. 2001. Nephron endowment in glial cell line-derived neurotrophic factor (GDNF) heterozygous mice. *Kidney Int,* 60**,** 31-6.

CUNNINGHAM, J. G. & KLEIN, B. G. 2013. *Cunningham's textbook of veterinary physiology,* St. Louis, Mo., Elsevier/Saunders.

DAVID, F. S., CULLEN-MCEWEN, L., WU, X. S., ZINS, S. R., LIN, J., BERTRAM, J. F. & NEEL, B. G. 2010. Regulation of kidney development by Shp2: an unbiased stereological analysis. *Anat Rec (Hoboken),* 293**,** 2147-53.

DAVIDSON, A. J. 2008. Mouse kidney development. *StemBook.* Cambridge (MA).

DAVIES, J. A. & FISHER, C. E. 2002. Genes and proteins in renal development. *Exp Nephrol,* 10**,** 102-13.

DE GROOT, D. M., HARTGRING, S., VAN DE HORST, L., MOERKENS, M., OTTO, M., BOS-KUIJPERS, M. H., KAUFMANN, W. S., LAMMERS, J. H., O'CALLAGHAN J, P., WAALKENS-BERENDSEN, I. D., PAKKENBERG, B. & GUNDERSEN, H. G. 2005. 2D and 3D assessment of neuropathology in rat brain after prenatal exposure to methylazoxymethanol, a model for developmental neurotoxicty. *Reprod Toxicol,* 20**,** 417-32.

DESGRANGE, A. & CEREGHINI, S. 2015. Nephron Patterning: Lessons from Xenopus, Zebrafish, and Mouse Studies. *Cells,* 4**,** 483-99.

DI MARCO, E., PIERCE, J. H., FLEMING, T. P., KRAUS, M. H., MOLLOY, C. J., AARONSON, S. A. & DI FIORE, P. P. 1989. Autocrine interaction between TGF alpha and the EGF-receptor: quantitative requirements for induction of the malignant phenotype. *Oncogene,* 4**,** 831-8.

DICKINSON, H., WALKER, D. W., CULLEN-MCEWEN, L., WINTOUR, E. M. & MORITZ, K. 2005. The spiny mouse (Acomys cahirinus) completes nephrogenesis before birth. *Am J Physiol Renal Physiol,* 289**,** F273-9.

DONOVAN, M. J., NATOLI, T. A., SAINIO, K., AMSTUTZ, A., JAENISCH, R., SARIOLA, H. & KREIDBERG, J. A. 1999. Initial differentiation of the metanephric mesenchyme is independent of WT1 and the ureteric bud. *Dev Genet,* 24**,** 252-62.

DORPH-PETERSEN, K. A., NYENGAARD, J. R. & GUNDERSEN, H. J. 2001. Tissue shrinkage and unbiased stereological estimation of particle number and size. *J Microsc,* 204**,** 232-46.

DOUGLAS-DENTON, R. N., MCNAMARA, B. J., HOY, W. E., HUGHSON, M. D. & BERTRAM, J. F. 2006. Does nephron number matter in the development of kidney disease? *Ethn Dis,* 16**,** S2-40-5.

DRESSLER, G. R. 2006. The cellular basis of kidney development. *Annu Rev Cell Dev Biol,* 22**,** 509-29.

DRESSLER, G. R., DEUTSCH, U., CHOWDHURY, K., NORNES, H. O. & GRUSS, P. 1990. Pax2, a new murine paired-box-containing gene and its expression in the developing excretory system. *Development,* 109**,** 787-95.

DUDLEY, A. T., GODIN, R. E. & ROBERTSON, E. J. 1999. Interaction between FGF and BMP signaling pathways regulates development of metanephric mesenchyme. *Genes Dev,* 13**,** 1601-13.

DUDLEY, A. T., LYONS, K. M. & ROBERTSON, E. J. 1995. A requirement for bone morphogenetic protein-7 during development of the mammalian kidney and eye. *Genes Dev,* 9**,** 2795-807.

EKBLOM, M., KLEIN, G., MUGRAUER, G., FECKER, L., DEUTZMANN, R., TIMPL, R. & EKBLOM, P. 1990. Transient and locally restricted expression of laminin A chain mRNA by developing epithelial cells during kidney organogenesis. *Cell,* 60**,** 337-46.

EL-DAHR, S. S., ABOUDEHEN, K. & SAIFUDEEN, Z. 2008. Transcriptional control of terminal nephron differentiation. *Am J Physiol Renal Physiol,* 294**,** F1273-8.

EREMINA, V., SOOD, M., HAIGH, J., NAGY, A., LAJOIE, G., FERRARA, N., GERBER, H. P., KIKKAWA, Y., MINER, J. H. & QUAGGIN, S. E. 2003. Glomerular-specific alterations of VEGF-A expression lead to distinct congenital and acquired renal diseases. *J Clin Invest,* 111**,** 707-16.

ERICSSON, A. C., CRIM, M. J. & FRANKLIN, C. L. 2013. A brief history of animal modeling. *Mo Med,* 110**,** 201-5.

EVANS, M. J., CARLTON, M. B. & RUSS, A. P. 1997. Gene trapping and functional genomics. *Trends Genet,* 13**,** 370-4.

FISHER, C. E., MICHAEL, L., BARNETT, M. W. & DAVIES, J. A. 2001. Erk MAP kinase regulates branching morphogenesis in the developing mouse kidney. *Development,* 128**,** 4329-38.

FOGO, A. & ICHIKAWA, I. 1989. Evidence for the central role of glomerular growth promoters in the development of sclerosis. *Semin Nephrol,* 9**,** 329-42.

FOGO, A. & ICHIKAWA, I. 1991. Evidence for a pathogenic linkage between glomerular hypertrophy and sclerosis. *Am J Kidney Dis,* 17**,** 666-9.

FOGO, A., YOSHIDA, Y., GLICK, A. D., HOMMA, T. & ICHIKAWA, I. 1988. Serial micropuncture analysis of glomerular function in two rat models of glomerular sclerosis. *J Clin Invest,* 82**,** 322-30.

FOGO, A. B. 2000. Glomerular hypertension, abnormal glomerular growth, and progression of renal diseases. *Kidney Int Suppl,* 75**,** S15-21.

FOGO, A. B. 2006. Progression versus regression of chronic kidney disease. *Nephrol Dial Transplant,* 21**,** 281-4.

FOX, J. G. 2007. *The mouse in biomedical research,* Amsterdam ; Boston, Elsevier, AP.

GAJ, T., GERSBACH, C. A. & BARBAS, C. F., 3RD 2013. ZFN, TALEN, and CRISPR/Cas-based methods for genome engineering. *Trends Biotechnol,* 31**,** 397-405.

GALINSKY, R., MOSS, T. J., GUBHAJU, L., HOOPER, S. B., BLACK, M. J. & POLGLASE, G. R. 2011. Effect of intra-amniotic lipopolysaccharide on nephron number in preterm fetal sheep. *Am J Physiol Renal Physiol,* 301**,** F280-5.

GAO, X., CHEN, X., TAGLIENTI, M., RUMBALLE, B., LITTLE, M. H. & KREIDBERG, J. A. 2005. Angioblast-mesenchyme induction of early kidney development is mediated by Wt1 and Vegfa. *Development,* 132**,** 5437-49.

GEHRING, W. J., AFFOLTER, M. & BURGLIN, T. 1994. Homeodomain proteins. *Annu Rev Biochem,* 63**,** 487-526.

GONG, K. Q., YALLOWITZ, A. R., SUN, H., DRESSLER, G. R. & WELLIK, D. M. 2007. A Hox-Eya-Pax complex regulates early kidney developmental gene expression. *Mol Cell Biol,* 27**,** 7661-8.

GRAHAM, L. A., PADMANABHAN, S., FRASER, N. J., KUMAR, S., BATES, J. M., RAFFI, H. S., WELSH, P., BEATTIE, W., HAO, S., LEH, S., HULTSTROM, M., FERRERI, N. R., DOMINICZAK, A. F., GRAHAM, D. & MCBRIDE, M. W. 2014. Validation of uromodulin as a candidate gene for human essential hypertension. *Hypertension,* 63**,** 551-8.

GREEN, E. D. 1997. *Genome analysis : a laboratory manual,* Plainview, N.Y., Cold Spring Harbor Laboratory Press.

GRIESHAMMER, U., CEBRIAN, C., ILAGAN, R., MEYERS, E., HERZLINGER, D. & MARTIN, G. R. 2005. FGF8 is required for cell survival at distinct stages of nephrogenesis and for regulation of gene expression in nascent nephrons. *Development,* 132**,** 3847-57.

GRIESHAMMER, U., LE, M., PLUMP, A. S., WANG, F., TESSIER-LAVIGNE, M. & MARTIN, G. R. 2004. SLIT2-mediated ROBO2 signaling restricts kidney induction to a single site. *Dev Cell,* 6**,** 709-17.

GUNDERSEN, H. J. 1986. Stereology of arbitrary particles. A review of unbiased number and size estimators and the presentation of some new ones, in memory of William R. Thompson. *J Microsc,* 143**,** 3-45.

GUNDERSEN, H. J., BAGGER, P., BENDTSEN, T. F., EVANS, S. M., KORBO, L., MARCUSSEN, N., MOLLER, A., NIELSEN, K., NYENGAARD, J. R., PAKKENBERG, B. & ET AL. 1988a. The new stereological tools: disector, fractionator, nucleator and point sampled intercepts and their use in pathological research and diagnosis. *APMIS,* 96**,** 857-81.

GUNDERSEN, H. J., BENDTSEN, T. F., KORBO, L., MARCUSSEN, N., MOLLER, A., NIELSEN, K., NYENGAARD, J. R., PAKKENBERG, B., SORENSEN, F. B., VESTERBY, A. & ET AL. 1988b. Some new, simple and efficient stereological methods and their use in pathological research and diagnosis. *APMIS,* 96**,** 379-94.

GUNDERSEN, H. J. & JENSEN, E. B. 1987. The efficiency of systematic sampling in stereology and its prediction. *J Microsc,* 147**,** 229-63.

HALES, C. N. & BARKER, D. J. 1992. Type 2 (non-insulin-dependent) diabetes mellitus: the thrifty phenotype hypothesis. *Diabetologia,* 35**,** 595-601.

HARA, Y., ROVESCALLI, A. C., KIM, Y. & NIRENBERG, M. 1992. Structure and evolution of four POU domain genes expressed in mouse brain. *Proc Natl Acad Sci U S A,* 89**,** 3280-4.

HASCHEK, W. M., ROUSSEAUX, C. G., WALLIG, M. A., BOLON, B., OCHOA, R. & MAHLER, B. W. 2013. *Haschek and Rousseaux's handbook of toxicologic pathology,* Amsterdam ; Boston, Academic Press.

HATINI, V., HUH, S. O., HERZLINGER, D., SOARES, V. C. & LAI, E. 1996. Essential role of stromal mesenchyme in kidney morphogenesis revealed by targeted disruption of Winged Helix transcription factor BF-2. *Genes Dev,* 10**,** 1467-78.

HE, X., TREACY, M. N., SIMMONS, D. M., INGRAHAM, H. A., SWANSON, L. W. & ROSENFELD, M. G. 1989. Expression of a large family of POU-domain regulatory genes in mammalian brain development. *Nature,* 340**,** 35-41.

HELIOT, C., DESGRANGE, A., BUISSON, I., PRUNSKAITE-HYYRYLAINEN, R., SHAN, J., VAINIO, S., UMBHAUER, M. & CEREGHINI, S. 2013. HNF1B controls proximal-intermediate nephron segment identity in vertebrates by regulating Notch signalling components and Irx1/2. *Development,* 140**,** 873-85.

HERBACH, N., BERGMAYR, M., GOKE, B., WOLF, E. & WANKE, R. 2011. Postnatal development of numbers and mean sizes of pancreatic islets and beta-cells in healthy mice and GIPR(dn) transgenic diabetic mice. *PLoS One,* 6**,** e22814.

HERBACH, N., SCHAIRER, I., BLUTKE, A., KAUTZ, S., SIEBERT, A., GOKE, B., WOLF, E. & WANKE, R. 2009. Diabetic kidney lesions of GIPRdn transgenic mice: podocyte hypertrophy and thickening of the GBM precede glomerular hypertrophy and glomerulosclerosis. *Am J Physiol Renal Physiol,* 296**,** F819-29.

HERR, W., STURM, R. A., CLERC, R. G., CORCORAN, L. M., BALTIMORE, D., SHARP, P. A., INGRAHAM, H. A., ROSENFELD, M. G., FINNEY, M., RUVKUN, G. & ET AL. 1988. The POU domain: a large conserved region in the mammalian pit-1, oct-1, oct-2, and Caenorhabditis elegans unc-86 gene products. *Genes Dev,* 2**,** 1513-6.

HINCHLIFFE, S. A., LYNCH, M. R., SARGENT, P. H., HOWARD, C. V. & VAN VELZEN, D. 1992. The effect of intrauterine growth retardation on the development of renal nephrons. *Br J Obstet Gynaecol,* 99**,** 296-301.

HITOTSUMACHI, S., CARPENTER, D. A. & RUSSELL, W. L. 1985. Dose-repetition increases the mutagenic effectiveness of N-ethyl-N-nitrosourea in mouse spermatogonia. *Proc Natl Acad Sci U S A,* 82**,** 6619-21.

HOAR, R. M. 1976. Comparative developmental aspects of selected organ systems. II. Gastrointestinal and urogenital systems. *Environ Health Perspect,* 18**,** 61-6.

HOHENSTEIN, P. & HASTIE, N. D. 2006. The many facets of the Wilms' tumour gene, WT1. *Hum Mol Genet,* 15 Spec No 2**,** R196-201.

HOPPE, C. C., EVANS, R. G., BERTRAM, J. F. & MORITZ, K. M. 2007. Effects of dietary protein restriction on nephron number in the mouse. *Am J Physiol Regul Integr Comp Physiol,* 292**,** R1768-74.

HORSTER, M. F., BRAUN, G. S. & HUBER, S. M. 1999. Embryonic renal epithelia: induction, nephrogenesis, and cell differentiation. *Physiol Rev,* 79**,** 1157-91.

HOWARD, V. & REED, M. G. 1998. *Unbiased stereology : three-dimensional measurement in microscopy,* New York, Springer.

HOWARD, V. & REED, M. G. 2004. *Unbiased stereology,* New York, Garland Science/BIOS Scientific Publishers.

HOY, W. E., BERTRAM, J. F., DENTON, R. D., ZIMANYI, M., SAMUEL, T. & HUGHSON, M. D. 2008. Nephron number, glomerular volume, renal disease and hypertension. *Curr Opin Nephrol Hypertens,* 17**,** 258-65.

HOY, W. E., HUGHSON, M. D., ZIMANYI, M., SAMUEL, T., DOUGLAS-DENTON, R., HOLDEN, L., MOTT, S. & BERTRAM, J. F. 2010a. Distribution of volumes of individual glomeruli in kidneys at autopsy: association with age, nephron number, birth weight and body mass index. *Clin Nephrol,* 74 Suppl 1**,** S105-12.

HOY, W. E., INGELFINGER, J. R., HALLAN, S., HUGHSON, M. D., MOTT, S. A. & BERTRAM, J. F. 2010b. The early development of the kidney and implications for future health. *J Dev Orig Health Dis,* 1**,** 216-33.

HRABÉ DE ANGELIS, M. & BALLING, R. 1998. Large scale ENU screens in the mouse: genetics meets genomics. *Mutat Res,* 400**,** 25-32.

HRABÉ DE ANGELIS, M. H., FLASWINKEL, H., FUCHS, H., RATHKOLB, B., SOEWARTO, D., MARSCHALL, S., HEFFNER, S., PARGENT, W., WUENSCH, K., JUNG, M., REIS, A., RICHTER, T., ALESSANDRINI, F., JAKOB, T., FUCHS, E., KOLB, H., KREMMER, E., SCHAEBLE, K., ROLLINSKI, B., ROSCHER, A., PETERS, C., MEITINGER, T., STROM, T., STECKLER, T., HOLSBOER, F., KLOPSTOCK, T., GEKELER, F., SCHINDEWOLF, C., JUNG, T., AVRAHAM, K., BEHRENDT, H., RING, J., ZIMMER, A., SCHUGHART, K., PFEFFER, K., WOLF, E. & BALLING, R. 2000. Genome-wide, large-scale production of mutant mice by ENU mutagenesis. *Nat Genet,* 25**,** 444-7.

IHERMANN-HELLA, A., LUME, M., MIINALAINEN, I. J., PIRTTINIEMI, A., GUI, Y., PERANEN, J., CHARRON, J., SAARMA, M., COSTANTINI, F. & KUURE, S. 2014. Mitogen-activated protein kinase (MAPK) pathway regulates branching by remodeling epithelial cell adhesion. *PLoS Genet,* 10**,** e1004193.

JAMES, R. G., KAMEI, C. N., WANG, Q., JIANG, R. & SCHULTHEISS, T. M. 2006. Odd-skipped related 1 is required for development of the metanephric kidney and regulates formation and differentiation of kidney precursor cells. *Development,* 133**,** 2995-3004.

JHA, V., GARCIA-GARCIA, G., ISEKI, K., LI, Z., NAICKER, S., PLATTNER, B., SARAN, R., WANG, A. Y. & YANG, C. W. 2013. Chronic kidney disease: global dimension and perspectives. *Lancet,* 382**,** 260-72.

JUSTICE, M. J., NOVEROSKE, J. K., WEBER, J. S., ZHENG, B. & BRADLEY, A. 1999. Mouse ENU mutagenesis. *Hum Mol Genet,* 8**,** 1955-63.

KALATZIS, V., SAHLY, I., EL-AMRAOUI, A. & PETIT, C. 1998. Eya1 expression in the developing ear and kidney: towards the understanding of the pathogenesis of Branchio-Oto-Renal (BOR) syndrome. *Dev Dyn,* 213**,** 486-99.

KANDA, S., TANIGAWA, S., OHMORI, T., TAGUCHI, A., KUDO, K., SUZUKI, Y., SATO, Y., HINO, S., SANDER, M., PERANTONI, A. O., SUGANO, S., NAKAO, M. & NISHINAKAMURA, R. 2014. Sall1 maintains nephron progenitors and nascent nephrons by acting as both an activator and a repressor. *J Am Soc Nephrol,* 25**,** 2584-95.

KARNER, C. M., DAS, A., MA, Z., SELF, M., CHEN, C., LUM, L., OLIVER, G. & CARROLL, T. J. 2011. Canonical Wnt9b signaling balances progenitor cell expansion and differentiation during kidney development. *Development,* 138**,** 1247-57.

KILE, B. T. & HILTON, D. J. 2005. The art and design of genetic screens: mouse. *Nat Rev Genet,* 6**,** 557-67.

KISPERT, A., VAINIO, S. & MCMAHON, A. P. 1998. Wnt-4 is a mesenchymal signal for epithelial transformation of metanephric mesenchyme in the developing kidney. *Development,* 125**,** 4225-34.

KOBAYASHI, A., KWAN, K. M., CARROLL, T. J., MCMAHON, A. P., MENDELSOHN, C. L. & BEHRINGER, R. R. 2005. Distinct and sequential tissue-specific activities of the LIM-class homeobox gene Lim1 for tubular morphogenesis during kidney development. *Development,* 132**,** 2809-23.

KOBAYASHI, A., VALERIUS, M. T., MUGFORD, J. W., CARROLL, T. J., SELF, M., OLIVER, G. & MCMAHON, A. P. 2008. Six2 defines and regulates a multipotent self-renewing nephron progenitor population throughout mammalian kidney development. *Cell Stem Cell,* 3**,** 169-81.

KREIDBERG, J. A., SARIOLA, H., LORING, J. M., MAEDA, M., PELLETIER, J., HOUSMAN, D. & JAENISCH, R. 1993. WT-1 is required for early kidney development. *Cell,* 74**,** 679-91.

KRIZ, W. & KOEPSELL, H. 1974. The structural organization of the mouse kidney. *Z Anat Entwicklungsgesch,* 144**,** 137-63.

KUMAR, S., RATHKOLB, B., KEMTER, E., SABRAUTZKI, S., MICHEL, D., ADLER, T., BECKER, L., BECKERS, J., BUSCH, D. H., GARRETT, L., HANS, W., HOLTER, S. M., HORSCH, M., KLINGENSPOR, M., KLOPSTOCK, T., RACZ, I., ROZMAN, J., VARGAS PANESSO, I. L., VERNALEKEN, A., ZIMMER, A., FUCHS, H., GAILUS-DURNER, V., HRABÉ DE ANGELIS, M., WOLF, E. & AIGNER, B. 2016. Generation and Standardized, Systemic Phenotypic Analysis of Pou3f3L423P Mutant Mice. *PLoS One,* 11**,** e0150472.

KUME, T., DENG, K. & HOGAN, B. L. 2000. Murine forkhead/winged helix genes Foxc1 (Mf1) and Foxc2 (Mfh1) are required for the early organogenesis of the kidney and urinary tract. *Development,* 127**,** 1387-95.

LANGLEY-EVANS, S. C., WELHAM, S. J. & JACKSON, A. A. 1999. Fetal exposure to a maternal low protein diet impairs nephrogenesis and promotes hypertension in the rat. *Life Sci,* 64**,** 965-74.

LATCHMAN, D. S. 1997. Transcription factors: an overview. *Int J Biochem Cell Biol,* 29**,** 1305-12.

LAVITRANO, M., BUSNELLI, M., CERRITO, M. G., GIOVANNONI, R., MANZINI, S. & VARGIOLU, A. 2006. Sperm-mediated gene transfer. *Reprod Fertil Dev,* 18**,** 19-23.

LELIEVRE-PEGORIER, M., VILAR, J., FERRIER, M. L., MOREAU, E., FREUND, N., GILBERT, T. & MERLET-BENICHOU, C. 1998. Mild vitamin A deficiency leads to inborn nephron deficit in the rat. *Kidney Int,* 54**,** 1455-62.

LEVINSON, R. S., BATOURINA, E., CHOI, C., VORONTCHIKHINA, M., KITAJEWSKI, J. & MENDELSOHN, C. L. 2005. Foxd1-dependent signals control cellularity in the renal capsule, a structure required for normal renal development. *Development,* 132**,** 529-39.

LINDBLAD-TOH, K., WINCHESTER, E., DALY, M. J., WANG, D. G., HIRSCHHORN, J. N., LAVIOLETTE, J. P., ARDLIE, K., REICH, D. E., ROBINSON, E., SKLAR, P., SHAH, N., THOMAS, D., FAN, J. B., GINGERAS, T., WARRINGTON, J., PATIL, N., HUDSON, T. J. & LANDER, E. S. 2000. Large-scale discovery and genotyping of single-nucleotide polymorphisms in the mouse. *Nat Genet,* 24**,** 381-6.

LODRUP, A. B., KARSTOFT, K., DISSING, T. H., NYENGAARD, J. R. & PEDERSEN, M. 2008a. The association between renal function and structural parameters: a pig study. *BMC Nephrol,* 9**,** 18.

LODRUP, A. B., KARSTOFT, K., DISSING, T. H., PEDERSEN, M. & NYENGAARD, J. R. 2008b. Kidney biopsies can be used for estimations of glomerular number and volume: a pig study. *Virchows Arch,* 452**,** 393-403.

LU, B. C., CEBRIAN, C., CHI, X., KUURE, S., KUO, R., BATES, C. M., ARBER, S., HASSELL, J., MACNEIL, L., HOSHI, M., JAIN, S., ASAI, N., TAKAHASHI, M., SCHMIDT-OTT, K. M., BARASCH, J., D'AGATI, V. & COSTANTINI, F. 2009. Etv4 and Etv5 are required downstream of GDNF and Ret for kidney branching morphogenesis. *Nat Genet,* 41**,** 1295-302.

LUCOCQ, J. M. 2007. Efficient quantitative morphological phenotyping of genetically altered organisms using stereology. *Transgenic Res,* 16**,** 133-45.

LUYCKX, V. A., BERTRAM, J. F., BRENNER, B. M., FALL, C., HOY, W. E., OZANNE, S. E. & VIKSE, B. E. 2013. Effect of fetal and child health on kidney development and long-term risk of hypertension and kidney disease. *Lancet,* 382**,** 273-83.

LUYCKX, V. A. & BRENNER, B. M. 2005. Low birth weight, nephron number, and kidney disease. *Kidney Int Suppl***,** S68-77.

LYONS, K. M., HOGAN, B. L. & ROBERTSON, E. J. 1995. Colocalization of BMP 7 and BMP 2 RNAs suggests that these factors cooperatively mediate tissue interactions during murine development. *Mech Dev,* 50**,** 71-83.

MACCHIARINI, F., MANZ, M. G., PALUCKA, A. K. & SHULTZ, L. D. 2005. Humanized mice: are we there yet? *J Exp Med,* 202**,** 1307-11.

MADSEN, K. M. 1999. The art of counting. *J Am Soc Nephrol,* 10**,** 1124-5.

MAJUMDAR, A., VAINIO, S., KISPERT, A., MCMAHON, J. & MCMAHON, A. P. 2003. Wnt11 and Ret/Gdnf pathways cooperate in regulating ureteric branching during metanephric kidney development. *Development,* 130**,** 3175-85.

MAKA, N., MAKRAKIS, J., PARKINGTON, H. C., TARE, M., MORLEY, R. & BLACK, M. J. 2008. Vitamin D deficiency during pregnancy and lactation stimulates nephrogenesis in rat offspring. *Pediatr Nephrol,* 23**,** 55-61.

MANSOURI, A., CHOWDHURY, K. & GRUSS, P. 1998. Follicular cells of the thyroid gland require Pax8 gene function. *Nat Genet,* 19**,** 87-90.

MASON, J. M., MORRISON, D. J., BASSON, M. A. & LICHT, J. D. 2006. Sprouty proteins: multifaceted negative-feedback regulators of receptor tyrosine kinase signaling. *Trends Cell Biol,* 16**,** 45-54.

MATENAERS, C., POPPER, B., RIEGER, A., WANKE, R. & BLUTKE, A. 2018. Practicable methods for histological section thickness measurement in quantitative stereological analyses. *PLoS One,* 13**,** e0192879.

MCCRORY, W. W. 1972. *Developmental nephrology,* Cambridge, Mass.,, Harvard University Press.

MCEVILLY, R. J., DE DIAZ, M. O., SCHONEMANN, M. D., HOOSHMAND, F. & ROSENFELD, M. G. 2002. Transcriptional regulation of cortical neuron migration by POU domain factors. *Science,* 295**,** 1528-32.

MENDELSOHN, C., BATOURINA, E., FUNG, S., GILBERT, T. & DODD, J. 1999. Stromal cells mediate retinoid-dependent functions essential for renal development. *Development,* 126**,** 1139-48.

MERLET-BENICHOU, C., GILBERT, T., VILAR, J., MOREAU, E., FREUND, N. & LELIEVRE-PEGORIER, M. 1999. Nephron number: variability is the rule. Causes and consequences. *Lab Invest,* 79**,** 515-27.

MESROBIAN, H. G. 1998. Compensatory renal growth in the solitary kidneys of Danforth mice with genetic renal agenesis. *J Urol,* 160**,** 146-9.

MICHOS, O., GONCALVES, A., LOPEZ-RIOS, J., TIECKE, E., NAILLAT, F., BEIER, K., GALLI, A., VAINIO, S. & ZELLER, R. 2007. Reduction of BMP4 activity by gremlin 1 enables ureteric bud outgrowth and GDNF/WNT11 feedback signalling during kidney branching morphogenesis. *Development,* 134**,** 2397-405.

MITCHELL, P. J. & TJIAN, R. 1989. Transcriptional regulation in mammalian cells by sequence-specific DNA binding proteins. *Science,* 245**,** 371-8.

MIYAZAKI, Y., OSHIMA, K., FOGO, A., HOGAN, B. L. & ICHIKAWA, I. 2000. Bone morphogenetic protein 4 regulates the budding site and elongation of the mouse ureter. *J Clin Invest,* 105**,** 863-73.

MOODY, S. A. 2007. *Principles of developmental genetics,* Amsterdam ; Boston, Elsevier Academic Press.

MOORE, M. W., KLEIN, R. D., FARINAS, I., SAUER, H., ARMANINI, M., PHILLIPS, H., REICHARDT, L. F., RYAN, A. M., CARVER-MOORE, K. & ROSENTHAL, A. 1996. Renal and neuronal abnormalities in mice lacking GDNF. *Nature,* 382**,** 76-9.

MORITZ, K. M., JEFFERIES, A., WONG, J., WINTOUR, E. M. & DODIC, M. 2005. Reduced renal reserve and increased cardiac output in adult female sheep uninephrectomized as fetuses. *Kidney Int,* 67**,** 822-8.

MORITZ, K. M., MAZZUCA, M. Q., SIEBEL, A. L., MIBUS, A., ARENA, D., TARE, M., OWENS, J. A. & WLODEK, M. E. 2009. Uteroplacental insufficiency causes a nephron deficit, modest renal insufficiency but no hypertension with ageing in female rats. *J Physiol,* 587**,** 2635-46.

MORITZ, K. M., WINTOUR, E. M., BLACK, M. J., BERTRAM, J. F. & CARUANA, G. 2008. Factors influencing mammalian kidney development: implications for health in adult life. *Adv Anat Embryol Cell Biol,* 196**,** 1-78.

MOUNT, D. B. 2014. Thick ascending limb of the loop of Henle. *Clin J Am Soc Nephrol,* 9**,** 1974-86.

MULLER, U., WANG, D., DENDA, S., MENESES, J. J., PEDERSEN, R. A. & REICHARDT, L. F. 1997. Integrin alpha8beta1 is critically important for epithelial-mesenchymal interactions during kidney morphogenesis. *Cell,* 88**,** 603-13.

NAKAI, S., SUGITANI, Y., SATO, H., ITO, S., MIURA, Y., OGAWA, M., NISHI, M., JISHAGE, K., MINOWA, O. & NODA, T. 2003. Crucial roles of Brn1 in distal tubule formation and function in mouse kidney. *Development,* 130**,** 4751-9.

NARLIS, M., GROTE, D., GAITAN, Y., BOUALIA, S. K. & BOUCHARD, M. 2007. Pax2 and pax8 regulate branching morphogenesis and nephron differentiation in the developing kidney. *J Am Soc Nephrol,* 18**,** 1121-9.

NEISS, W. F. 1982. Histogenesis of the loop of Henle in the rat kidney. *Anat Embryol (Berl),* 164**,** 315-30.

NENOV, V. D., TAAL, M. W., SAKHAROVA, O. V. & BRENNER, B. M. 2000. Multi-hit nature of chronic renal disease. *Curr Opin Nephrol Hypertens,* 9**,** 85-97.

NGUYEN, N., JUDD, L. M., KALANTZIS, A., WHITTLE, B., GIRAUD, A. S. & VAN DRIEL, I. R. 2011. Random mutagenesis of the mouse genome: a strategy for discovering gene function and the molecular basis of disease. *Am J Physiol Gastrointest Liver Physiol,* 300**,** G1-11.

NISHINAKAMURA, R., MATSUMOTO, Y., NAKAO, K., NAKAMURA, K., SATO, A., COPELAND, N. G., GILBERT, D. J., JENKINS, N. A., SCULLY, S., LACEY, D. L., KATSUKI, M., ASASHIMA, M. & YOKOTA, T. 2001. Murine homolog of SALL1 is essential for ureteric bud invasion in kidney development. *Development,* 128**,** 3105-15.

NOVEROSKE, J. K., WEBER, J. S. & JUSTICE, M. J. 2000. The mutagenic action of N-ethyl-N-nitrosourea in the mouse. *Mamm Genome,* 11**,** 478-83.

NYENGAARD, J. R. 1999. Stereologic methods and their application in kidney research. *J Am Soc Nephrol,* 10**,** 1100-23.

NYENGAARD, J. R. & BENDTSEN, T. F. 1992. Glomerular number and size in relation to age, kidney weight, and body surface in normal man. *Anat Rec,* 232**,** 194-201.

O'BRIEN, L. L. & MCMAHON, A. P. 2014. Induction and patterning of the metanephric nephron. *Semin Cell Dev Biol,* 36**,** 31-8.

ORVIS, G. D. & BEHRINGER, R. R. 2007. Cellular mechanisms of Mullerian duct formation in the mouse. *Dev Biol,* 306**,** 493-504.

PENNICA, D., KOHR, W. J., KUANG, W. J., GLAISTER, D., AGGARWAL, B. B., CHEN, E. Y. & GOEDDEL, D. V. 1987. Identification of human uromodulin as the Tamm-Horsfall urinary glycoprotein. *Science,* 236**,** 83-8.

PEPICELLI, C. V., KISPERT, A., ROWITCH, D. H. & MCMAHON, A. P. 1997. GDNF induces branching and increased cell proliferation in the ureter of the mouse. *Dev Biol,* 192**,** 193-8.

PERANTONI, A. O., DOVE, L. F. & KARAVANOVA, I. 1995. Basic fibroblast growth factor can mediate the early inductive events in renal development. *Proc Natl Acad Sci U S A,* 92**,** 4696-700.

PFEIFER, A. & HOFMANN, A. 2009. Lentiviral transgenesis. *Methods Mol Biol,* 530**,** 391-405.

PHILLIPS, K. & LUISI, B. 2000. The virtuoso of versatility: POU proteins that flex to fit. *J Mol Biol,* 302**,** 1023-39.

PICHEL, J. G., SHEN, L., SHENG, H. Z., GRANHOLM, A. C., DRAGO, J., GRINBERG, A., LEE, E. J., HUANG, S. P., SAARMA, M., HOFFER, B. J., SARIOLA, H. & WESTPHAL, H. 1996a. Defects in enteric innervation and kidney development in mice lacking GDNF. *Nature,* 382**,** 73-6.

PICHEL, J. G., SHEN, L., SHENG, H. Z., GRANHOLM, A. C., DRAGO, J., GRINBERG, A., LEE, E. J., HUANG, S. P., SAARMA, M., HOFFER, B. J., SARIOLA, H. & WESTPHAL, H. 1996b. GDNF is required for kidney development and enteric innervation. *Cold Spring Harb Symp Quant Biol,* 61**,** 445-57.

PLISOV, S. Y., YOSHINO, K., DOVE, L. F., HIGINBOTHAM, K. G., RUBIN, J. S. & PERANTONI, A. O. 2001. TGF beta 2, LIF and FGF2 cooperate to induce nephrogenesis. *Development,* 128**,** 1045-57.

POLADIA, D. P., KISH, K., KUTAY, B., BAUER, J., BAUM, M. & BATES, C. M. 2006a. Link between reduced nephron number and hypertension: studies in a mutant mouse model. *Pediatr Res,* 59**,** 489-93.

POLADIA, D. P., KISH, K., KUTAY, B., HAINS, D., KEGG, H., ZHAO, H. & BATES, C. M. 2006b. Role of fibroblast growth factor receptors 1 and 2 in the metanephric mesenchyme. *Dev Biol,* 291**,** 325-39.

POLLAK, V. E. & ARBEL, C. 1969. The distribution of Tamm Horsfall mucoprotein (uromucoid) in the human nephron. *Nephron,* 6**,** 667-72.

RATHKOLB, B., FUCHS, E., KOLB, H. J., RENNER-MULLER, I., KREBS, O., BALLING, R., HRABÉ DE ANGELIS, M. & WOLF, E. 2000. Large-scale N-ethyl-N-nitrosourea mutagenesis of mice--from phenotypes to genes. *Exp Physiol,* 85**,** 635-44.

REIDY, K. J. & ROSENBLUM, N. D. 2009. Cell and molecular biology of kidney development. *Semin Nephrol,* 29**,** 321-37.

REILLY, R. F. & ELLISON, D. H. 2000. Mammalian distal tubule: physiology, pathophysiology, and molecular anatomy. *Physiol Rev,* 80**,** 277-313.

RITZ, E. 2006. Diabetic nephropathy. *Saudi J Kidney Dis Transpl,* 17**,** 481-90.

ROSENTHAL, N. & BROWN, S. 2007. The mouse ascending: perspectives for human-disease models. *Nat Cell Biol,* 9**,** 993-9.

RUSS, A., STUMM, G., AUGUSTIN, M., SEDLMEIER, R., WATTLER, S. & NEHLS, M. 2002. Random mutagenesis in the mouse as a tool in drug discovery. *Drug Discov Today,* 7**,** 1175-83.

RUSSELL, W. L., KELLY, E. M., HUNSICKER, P. R., BANGHAM, J. W., MADDUX, S. C. & PHIPPS, E. L. 1979. Specific-locus test shows ethylnitrosourea to be the most potent mutagen in the mouse. *Proc Natl Acad Sci U S A,* 76**,** 5818-9.

RYAN, A. K. & ROSENFELD, M. G. 1997. POU domain family values: flexibility, partnerships, and developmental codes. *Genes Dev,* 11**,** 1207-25.

RYAN, G., STEELE-PERKINS, V., MORRIS, J. F., RAUSCHER, F. J., 3RD & DRESSLER, G. R. 1995. Repression of Pax-2 by WT1 during normal kidney development. *Development,* 121**,** 867-75.

RYBA, N. 2011. Clinical and pathomorphological characterization of uninephrectomized GIPRdn transgenic diabetic mice. Dissertation, LMU München: Tierärztliche Fakultät.

SAINIO, K., HELLSTEDT, P., KREIDBERG, J. A., SAXEN, L. & SARIOLA, H. 1997a. Differential regulation of two sets of mesonephric tubules by WT-1. *Development,* 124**,** 1293-9.

SAINIO, K., SUVANTO, P., DAVIES, J., WARTIOVAARA, J., WARTIOVAARA, K., SAARMA, M., ARUMAE, U., MENG, X., LINDAHL, M., PACHNIS, V. & SARIOLA, H. 1997b. Glial-cell-line-derived neurotrophic factor is required for bud initiation from ureteric epithelium. *Development,* 124**,** 4077-87.

SANCHEZ, M. P., SILOS-SANTIAGO, I., FRISEN, J., HE, B., LIRA, S. A. & BARBACID, M. 1996. Renal agenesis and the absence of enteric neurons in mice lacking GDNF. *Nature,* 382**,** 70-3.

SAXÉN, L. 1987. *Organogenesis of the kidney,* Cambridge Cambridgeshire ; New York, Cambridge University Press.

SAXEN, L. & SARIOLA, H. 1987. Early organogenesis of the kidney. *Pediatr Nephrol,* 1**,** 385-92.

SCHEDL, A. 2007. Renal abnormalities and their developmental origin. *Nat Rev Genet,* 8**,** 791-802.

SCHLOTE, J., SCHRODER, A., DAHLMANN, A., KARPE, B., CORDASIC, N., DANIEL, C., HILGERS, K. F., TITZE, J., AMANN, K. & BENZ, K. 2013. Cardiovascular and renal effects of high salt diet in GDNF+/- mice with low nephron number. *Kidney Blood Press Res,* 37**,** 379-91.

SHIBUYA, T. & MORIMOTO, K. 1993. A review of the genotoxicity of 1-ethyl-1-nitrosourea. *Mutat Res,* 297**,** 3-38.

SILVER, L. M. 1995. *Mouse genetics : concepts and applications,* New York, Oxford University Press.

SIMS-LUCAS, S., CULLEN-MCEWEN, L., ESWARAKUMAR, V. P., HAINS, D., KISH, K., BECKNELL, B., ZHANG, J., BERTRAM, J. F., WANG, F. & BATES, C. M. 2009. Deletion of Frs2alpha from the ureteric epithelium causes renal hypoplasia. *Am J Physiol Renal Physiol,* 297**,** F1208-19.

SINER, J. M., JIANG, G., COHEN, Z. I., SHAN, P., ZHANG, X., LEE, C. G., ELIAS, J. A. & LEE, P. J. 2007. VEGF-induced heme oxygenase-1 confers cytoprotection from lethal hyperoxia in vivo. *FASEB J,* 21**,** 1422-32.

SINGH, R. R., CULLEN-MCEWEN, L. A., KETT, M. M., BOON, W. M., DOWLING, J., BERTRAM, J. F. & MORITZ, K. M. 2007a. Prenatal corticosterone exposure results in altered AT1/AT2, nephron deficit and hypertension in the rat offspring. *J Physiol,* 579**,** 503-13.

SINGH, R. R., MORITZ, K. M., BERTRAM, J. F. & CULLEN-MCEWEN, L. A. 2007b. Effects of dexamethasone exposure on rat metanephric development: in vitro and in vivo studies. *Am J Physiol Renal Physiol,* 293**,** F548-54.

STARK, K., VAINIO, S., VASSILEVA, G. & MCMAHON, A. P. 1994. Epithelial transformation of metanephric mesenchyme in the developing kidney regulated by Wnt-4. *Nature,* 372**,** 679-83.

STERIO, D. C. 1984. The unbiased estimation of number and sizes of arbitrary particles using the disector. *J Microsc***,** 127-136.

STURM, R. A., DAS, G. & HERR, W. 1988. The ubiquitous octamer-binding protein Oct-1 contains a POU domain with a homeo box subdomain. *Genes Dev,* 2**,** 1582-99.

STURM, R. A. & HERR, W. 1988. The POU domain is a bipartite DNA-binding structure. *Nature,* 336**,** 601-4.

SUGITANI, Y., NAKAI, S., MINOWA, O., NISHI, M., JISHAGE, K., KAWANO, H., MORI, K., OGAWA, M. & NODA, T. 2002. Brn-1 and Brn-2 share crucial roles in the production and positioning of mouse neocortical neurons. *Genes Dev,* 16**,** 1760-5.

SUMIYAMA, K., WASHIO-WATANABE, K., SAITOU, N., HAYAKAWA, T. & UEDA, S. 1996. Class III POU genes: generation of homopolymeric amino acid repeats under GC pressure in mammals. *J Mol Evol,* 43**,** 170-8.

SWEENEY, D., LINDSTROM, N. & DAVIES, J. A. 2008. Developmental plasticity and regenerative capacity in the renal ureteric bud/collecting duct system. *Development,* 135**,** 2505-10.

TAAL, M. W., BRENNER, B. M. & RECTOR, F. C. 2012. *Brenner & Rector's the kidney,* Philadelphia, PA, Elsevier/Saunders.

THOMAS, K. R. & CAPECCHI, M. R. 1987. Site-directed mutagenesis by gene targeting in mouse embryo-derived stem cells. *Cell,* 51**,** 503-12.

TORRES, M., GOMEZ-PARDO, E., DRESSLER, G. R. & GRUSS, P. 1995. Pax-2 controls multiple steps of urogenital development. *Development,* 121**,** 4057-65.

TSANG, T. E., SHAWLOT, W., KINDER, S. J., KOBAYASHI, A., KWAN, K. M., SCHUGHART, K., KANIA, A., JESSELL, T. M., BEHRINGER, R. R. & TAM, P. P. 2000. Lim1 activity is required for intermediate mesoderm differentiation in the mouse embryo. *Dev Biol,* 223**,** 77-90.

TSCHANZ, S., SCHNEIDER, J. P. & KNUDSEN, L. 2014. Design-based stereology: Planning, volumetry and sampling are crucial steps for a successful study. *Ann Anat,* 196**,** 3-11.

VAN VUUREN, S. H., SOL, C. M., BROEKHUIZEN, R., LILIEN, M. R., OOSTERVELD, M. J., NGUYEN, T. Q., GOLDSCHMEDING, R. & DE JONG, T. P. 2012. Compensatory growth of congenital solitary kidneys in pigs reflects increased nephron numbers rather than hypertrophy. *PLoS One,* 7**,** e49735.

VETTER, M. R. & GIBLEY, C. W., JR. 1966. Morphogenesis and histochemistry of the developing mouse kidney. *J Morphol,* 120**,** 135-55.

WALKER, K. A. & BERTRAM, J. F. 2011. Kidney development: core curriculum 2011. *Am J Kidney Dis,* 57**,** 948-58.

WALKER, K. A., CAI, X., CARUANA, G., THOMAS, M. C., BERTRAM, J. F. & KETT, M. M. 2012. High nephron endowment protects against salt-induced hypertension. *Am J Physiol Renal Physiol,* 303**,** F253-8.

WANG, X., JOHNSON, A. C., WILLIAMS, J. M., WHITE, T., CHADE, A. R., ZHANG, J., LIU, R., ROMAN, R. J., LEE, J. W., KYLE, P. B., SOLBERG-WOODS, L. & GARRETT, M. R. 2015. Nephron Deficiency and Predisposition to Renal Injury in a Novel One-Kidney Genetic Model. *J Am Soc Nephrol,* 26**,** 1634-46.

WANKE, R. 2002. Stereology--benefits and pitfalls. *Exp Toxicol Pathol,* 54**,** 163-4.

WANKE, R. 2017. Quantifizierung in der Morphologie – Wozu und wie? Nova Acta Leopoldina NF 121, Nr. 409, 59-84.

WATANABE, T. & COSTANTINI, F. 2004. Real-time analysis of ureteric bud branching morphogenesis in vitro. *Dev Biol,* 271**,** 98-108.

WEBER, J. S., SALINGER, A. & JUSTICE, M. J. 2000. Optimal N-ethyl-N-nitrosourea (ENU) doses for inbred mouse strains. *Genesis,* 26**,** 230-3.

WEGNER, M., DROLET, D. W. & ROSENFELD, M. G. 1993. POU-domain proteins: structure and function of developmental regulators. *Curr Opin Cell Biol,* 5**,** 488-98.

WEIBEL, E. R. 1979a. Morphometry of the human lung: the state of the art after two decades. *Bull Eur Physiopathol Respir,* 15**,** 999-1013.

WEIBEL, E. R. 1979b. *Stereological methods,* London ; New York, Academic Press.

WEIBEL, E. R. 1979c. *Stereological methods I. Practical methods for biological morphometry,* London, Academic press.

WEIBEL, E. R., ELIAS, H. & INTERNATIONAL SOCIETY FOR STEREOLOGY. 1967. *Quantitative methods in morphology. Quantitative Methoden in der Morphologie; proceedings,* Berlin, New York, Springer-Verlag.

WEIBEL, E. R., KISTLER, G. S. & SCHERLE, W. F. 1966. Practical stereological methods for morphometric cytology. *J Cell Biol,* 30**,** 23-38.

WEINER, I. D., MITCH, W. E. & SANDS, J. M. 2015. Urea and Ammonia Metabolism and the Control of Renal Nitrogen Excretion. *Clin J Am Soc Nephrol,* 10**,** 1444-58.

WELLIK, D. M., HAWKES, P. J. & CAPECCHI, M. R. 2002. Hox11 paralogous genes are essential for metanephric kidney induction. *Genes Dev,* 16**,** 1423-32.

WEST, M. J. 2012. Introduction to stereology. *Cold Spring Harb Protoc,* 2012.

WIEMANN, S., ARLT, D., HUBER, W., WELLENREUTHER, R., SCHLEEGER, S., MEHRLE, A., BECHTEL, S., SAUERMANN, M., KORF, U., PEPPERKOK, R., SULTMANN, H. & POUSTKA, A. 2004. From ORFeome to biology: a functional genomics pipeline. *Genome Res,* 14**,** 2136-44.

WILMUT, I., BAI, Y. & TAYLOR, J. 2015. Somatic cell nuclear transfer: origins, the present position and future opportunities. *Philos Trans R Soc Lond B Biol Sci,* 370**,** 20140366.

WINTOUR, E. M., MORITZ, K. M., JOHNSON, K., RICARDO, S., SAMUEL, C. S. & DODIC, M. 2003. Reduced nephron number in adult sheep, hypertensive as a result of prenatal glucocorticoid treatment. *J Physiol,* 549**,** 929-35.

WLODEK, M. E., MIBUS, A., TAN, A., SIEBEL, A. L., OWENS, J. A. & MORITZ, K. M. 2007. Normal lactational environment restores nephron endowment and prevents hypertension after placental restriction in the rat. *J Am Soc Nephrol,* 18**,** 1688-96.

WOODS, L. L. 1999. Neonatal uninephrectomy causes hypertension in adult rats. *Am J Physiol,* 276**,** R974-8.

WOODS, L. L., WEEKS, D. A. & RASCH, R. 2001. Hypertension after neonatal uninephrectomy in rats precedes glomerular damage. *Hypertension,* 38**,** 337-42.

XU, P. X., ADAMS, J., PETERS, H., BROWN, M. C., HEANEY, S. & MAAS, R. 1999. Eya1-deficient mice lack ears and kidneys and show abnormal apoptosis of organ primordia. *Nat Genet,* 23**,** 113-7.

XU, P. X., ZHENG, W., HUANG, L., MAIRE, P., LACLEF, C. & SILVIUS, D. 2003. Six1 is required for the early organogenesis of mammalian kidney. *Development,* 130**,** 3085-94.

YOSHIDA, Y., FOGO, A., SHIRAGA, H., GLICK, A. D. & ICHIKAWA, I. 1988. Serial micropuncture analysis of single nephron function in subtotal renal ablation. *Kidney Int,* 33**,** 855-67.

ZHANG, Z., QUINLAN, J., HOY, W., HUGHSON, M. D., LEMIRE, M., HUDSON, T., HUEBER, P. A., BENJAMIN, A., ROY, A., PASCUET, E., GOODYER, M., RAJU, C., HOUGHTON, F., BERTRAM, J. & GOODYER, P. 2008. A common RET variant is associated with reduced newborn kidney size and function. *J Am Soc Nephrol,* 19**,** 2027-34.

ZHONG, J., PERRIEN, D. S., YANG, H. C., KON, V., FOGO, A. B., ICHIKAWA, I. & MA, J. 2012. Maturational regression of glomeruli determines the nephron population in normal mice. *Pediatr Res,* 72**,** 241-8.

ZIMANYI, M. A., BERTRAM, J. F. & BLACK, M. J. 2002. Nephron number and blood pressure in rat offspring with maternal high-protein diet. *Pediatr Nephrol,* 17**,** 1000-4.

ZOHDI, V., MORITZ, K. M., BUBB, K. J., COCK, M. L., WREFORD, N., HARDING, R. & BLACK, M. J. 2007. Nephrogenesis and the renal renin-angiotensin system in fetal sheep: effects of intrauterine growth restriction during late gestation. *Am J Physiol Regul Integr Comp Physiol,* 293**,** R1267-73.

8. Figures and Tables

Figures

Tables

Acknowledgements

Zu Beginn möchte ich mich herzlich bei Herrn Prof. Dr. Wanke für die Überlassung des Themas, die stets gewährte Unterstützung sowie die finale Durchsicht der vorliegenden Arbeit bedanken.

Mein ganz besonderer Dank gilt meinem Betreuer, Herrn PD Dr. Andreas Parzefall, ohne dessen enormes Engagement die Anfertigung der Publikation und damit auch dieser Dissertation nicht möglich gewesen wäre.

Bei Herrn Prof. Dr. Bernhard Aigner möchte ich mich vielmals für die Bereitstellung der Phänotypisierungsdaten bedanken.

Herrn Prof. Dr. Eckhard Wolf danke ich ganz besonders für die Unterstützung bei Beantragung des Promotionsstipendiums.

Ein riesiges Dankeschön geht an Frau Dr. Elisabeth Kemter dafür, dass sie sich die Mühe gemacht hat mich in die Kunst der Immunhistochemie einzuweihen. In diesem Zuge möchte ich mich auch bei Simona Stüber und Tatiana Schröter für die Hilfe bei Ausführung der praktischen Arbeiten bedanken.

Vielen Dank an die Hanns-Seidl-Stiftung, die mir durch ein Promotionsstipendium nicht nur zwei Jahre lang finanzielle Unterstützung gewährt hat, sondern deren ideelle Förderung mich über den medizinischen Tellerrand blicken ließ.

Heike Bartels, Claudia Mair, Lisa Pichl und Heidrun Schöl danke ich herzlich für die hervorragende technische Assistenz, Sabine Zwirz und Adrian Ciolovan für die kompetente Versorgung der Mäuse.

Bei allen anderen aktuellen und ehemaligen Mitarbeiterinnen und Mitarbeitern des Instituts für Tierpathologie, die mich in den letzten Jahren begleitet haben, möchte ich mich ebenso von Herzen für die schöne Zeit und die Hilfestellung in unterschiedlichsten Lebenslagen bedanken, ganz besonders bei Marjam O'Gorman, Frauke Groth, Almuth Falkenau, Miriam Leipig, Martin Langenmayer, Isabelle Lutzmann, Hazal Öztürk und Beate Schmidt.

Meinen Mitstreitern am Morphomaten, Mai Le, Bastian Popper und Judith Steinmetz, sei noch einmal ganz speziell für ihre Gesellschaft beim Punkte zählen gedankt.

Abschließend geht mein größter Dank an meine Familie, insbesondere an meine Mutter und meine Großeltern, die immerzu an mich geglaubt haben, sowie an alle meine zwei- und vierbeinigen Freunde, die mir stets den notwendigen Ausgleich geboten und somit wesentlich zur Überwindung der ein oder anderen akuten Motivationsnekrose beigetragen haben.